DISS. ETH NO. 23166

NITRIFICATION OF URINE AS PRETREATMENT FOR NUTRIENT RECOVERY

A thesis submitted to attain the degree of

DOCTOR OF SCIENCES of ETH ZURICH

(Dr. sc. ETH Zurich)

presented by

ALEXANDRA FUMASOLI (-HUG)

Master of Science in Umwelt-Ing. ETH

born on *02.12.1984*

citizen of Rütschelen BE

accepted on the recommendation of

Prof. Dr. Eberhard Morgenroth, examiner

Prof. Dr. George A. Ekama, co-examiner

Prof. Dr. Zhiguo Yuan, co-examiner

Dr. Kai M. Udert, co-examiner

2016

Acknowledgement

This thesis would not have been possible without the contribution and support of many people.

First of all I would like to thank my supervisors: Kai Udert offered me the unique opportunity of being part of the VUNA team and he supported me with technical guidance and his catching enthusiasm. I thank Eberhard Morgenroth for his critical questions and for keeping the big picture in mind.

I want to express my gratitude to my co-examiners George Ekama and Zighuo Yuan for critically reviewing my thesis. It was always a pleasure to discuss nitrification related topics with George at the annual VUNA meetings in Durban and Zürich.

At this point I would also like to thank the Bill and Melinda Gates Foundation for founding the VUNA project. I very much enjoyed being part of this project.

I would like to specially acknowledge my close co-workers: Bastian Etter for his great job in the construction of the pilot-scale nitrification reactor, Michael Wächter for supporting me during my first steps with urine nitrification, and Hanspeter Zöllig for the many fruitful discussions. Many thanks also to Sarina Jenni for the support and company in the urine lab.

I also thank the Reactor Team in South Africa with Lungiswa Zuma, Maximilian Grau, Sara Rhoton, and Christopher Buckley for frequent exchanges on urine nitrification, as well as Chris Brouckaert for the inputs on modeling.

A special thank goes to Bettina Sterkele for strong support with laboratory- and pilot-scale experiments, as well as Karin Rottermann and Claudia Bänninger Werffeli for the great support in reactor operation and chemical analysis of all the samples.

The work on microbial population dynamics added a whole new dimension to my thesis and would not have been possible without the support of Helmut Bürgmann, David G. Weissbrodt, and George F. Wells. I also thank Joachim Mohn for nitrogenous off-gas measurements.

Furthermore, I enjoyed the discussions with Kris Villez, Alma Masic, Christian Thürlimann and the whole Spike group on urine nitrification modeling.

It was great to have Alexandra Florin, Corine Uhlmann and Mathias Kämpf working on urine nitrification during their Master thesis, and Patrick Rambosson during his internship.

Special thanks also go to the PhD group and assistants for critical feedback and enjoyable social events after the Wednesday's seminars, and to my long-term BU-B03 colleagues Jonathan Habermacher, Anna Chomiak and Hanspeter Zöllig.

Finally, I would like to thank my family and friends for reminding me that there are other important parts in life in addition to a PhD. But most of all, I thank Tobi for his support during the ups and downs of a PhD and for enjoying our frequent travels after international meetings and conferences.

Table of contents

Zusammenfassung

Urin enthält viele Nährstoffe, welche mit einer Kombination von Nitrifikation und Verdampfung zurückgewonnen werden können. Die Nitrifikation ist unerlässlich, um Stickstoffverluste durch die Ausgasung von Ammoniak (NH_3) zu verhindern. Da das molare Verhältnis von Alkalinität zu Ammonium ungefähr eins beträgt, kann nur 50% des Ammoniums in Nitrat umgewandelt werden. NH_3 wird aber durch die pH-Senkung während der Nitrifikation in stabiles Ammonium (NH_4^+) transformiert und Verluste werden dadurch vermieden. Aufgrund der tiefen Alkalinität in nitrifiziertem Urin ist der Prozess anfällig auf pH-Veränderungen, was wiederum die nitrifizierenden Bakterien und die Prozessstabilität beeinflusst. Das Ziel dieser Arbeit ist deshalb, den Einfluss vom pH-Wert auf die nitrifizierenden Bakterien zu verstehen, um eine hohe Prozessstabilität sicherzustellen.

Der Betrieb einer Pilotanlage bestätigte frühere Erfahrungen, dass das Zwischenprodukt Nitrit häufig akkumuliert, vor allem während des Hochfahrens des Reaktors. In Experimenten konnte ich zeigen, dass diese kritische Phase vereinfacht wird, indem der pH-Wert durch die Regulation des Zulaufs in einem engen Bereich gehalten wird. Höhere pH-Werte (zwischen 6.20 und 6.25) waren tendenziell kritischer bezüglich der Akkumulation von Nitrit, während säuretolerante ammoniumoxidierende Bakterien (AOB) bei tiefen pH-Werten (zwischen 5.80 und 5.85) selektiert wurden. Das Auftreten von säuretoleranten AOB ist erstaunlich, da gemeinhin angenommen wird, dass Nitrifikation bei pH-Werten unter 5.4 nicht möglich ist.

Diese Arbeit zeigt, dass die Säureintoleranz der Nitrifikation damit begründet werden kann, dass die Aktivität der verbreiteten AOB der *Nitrosomonas europaea* Linie bei einem minimalen pH-Wert von 5.4 stoppt. Diese pH-Grenze ist vermutlich dadurch bedingt, dass kein NADH zur Energiekonservierung hergestellt werden kann. Limitierung durch NH_3 oder Hemmung durch salpetrige Säure (HNO_2) können das Limit hingegen nicht erklären. Das pH-Limit dieser AOB kann durch einen exponentiellen pH-Term modelliert werden und die benötigten Parameter stimmen gut mir der Energiekonservierungs-Hypothese überein.

Im Gegensatz zu *Nitrosomonas europaea* können andere AOB bei tiefem pH-Wert wachsen. So war ein Wechsel zu einer möglicherweise neuen *Nitrosococcus*-Gattung der Grund für die pH-Absenkung von 6 zu 2.2 in Urinreaktoren. Während nitritoxidierende Bakterien (NOB) durch HNO_2 gehemmt wurden, wandelte sich Nitrit chemisch zu Nitrat um, wobei schädliches Stickstoffmonoxid freigesetzt wurde. Tiefe pH-Werte sollten deshalb verhindert werden.

Ein Nitrifikationsmodell bestätigte, dass eine stabile Nitratproduktion nur in einem engen pH-Bereich möglich ist. Da NOB bei hohen pH-Werten und starkem Zulauf langsamer wachsen als AOB, akkumuliert Nitrit innerhalb kurzer Zeit zu irreversibel hohen Konzentrationen. Bei noch stärkerer Beschickung stoppt die Nitrifikation gänzlich. Bei langfristig zu tiefer Beschickungsrate hingegen werden säuretolerante AOB selektiert, welche den pH-Wert senken.

Nitrifikation ist ein vielversprechender Prozess, um Urin zu stabilisieren, aber Urinreaktoren müssen sorgfältig beschickt und der Nitrit Gehalt muss regelmässig gemessen werden. Ein Nitrit Sensor würde den Betrieb vor allem in dezentralen Gebieten stark vereinfachen und sollte deshalb in einem nächsten Schritt entwickelt werden.

Summary

Source-separated urine contains most of the excreted nutrients, which can be recovered with a process combination of nitrification and distillation. Nitrification is required to prevent volatilization of ammonia (NH_3) during distillation. As the molar ratio of alkalinity to total ammonia is approximately one to one in urine, only 50% of the total ammonia is converted to non-volatile nitrate (NO_3^-). NH_3 losses are still prevented, because the pH drop during nitrification converts NH_3 into non-volatile ammonium (NH_4^+). The low remaining alkalinity in nitrified urine makes the process susceptible for pH changes, which in turn affect bacterial activity and cause process failures. The aim of this thesis is therefore to understand the effects of pH on nitrifying bacteria in order to ensure high process stability during urine nitrification.

The operation of a pilot-scale reactor confirmed previous observations that the nitrification intermediate nitrite is very likely to accumulate, particularly during reactor start-up. In laboratory experiments, I showed that the start-up can be simplified by controlling the pH within a tight interval by regulating the influent. While nitrite was more likely to accumulate by keeping the pH high (between 6.20 and 6.25), acid-tolerant ammonia oxidizing bacteria (AOB) were selected by choosing a lower pH setpoint (between 5.80 and 5.85). The presence of acid-tolerant AOB has been surprising, as nitrification is often expected to cease at minimal pH values of 5.4.

In this thesis I found that the acid-sensitivity of nitrification can be attributed to the common AOB from the *Nitrosomonas europaea* lineage, the activity of which stops at a pH of 5.4. This pH limit is most probably linked to the energy conservation in this organism by preventing NADH production. Neither limitation of the substrate NH_3 nor inhibition by the product nitrous acid (HNO_2) can explain the pH limit. To model the pH limit of this AOB, established mathematical models need to be extended with an exponential pH term. The parameters needed for the pH term agree with the energy conservation hypothesis.

In contrast to the *Nitrosomonas europaea* lineage, various other AOB can grow at low pH values. A population shift from *Nitrosomonas europaea* to a possibly novel *Nitrosococcus* genus was responsible for the pH drop from 6 to 2.2 in urine reactors. While nitrite oxidizing bacteria (NOB) were inhibited by HNO_2 during and after the pH drop, nitrite was still converted chemically to nitrate. The chemical processes released harmful volatile intermediates such as nitric oxide. Low pH values need thus to be prevented in urine applications.

A nitrification model confirmed that stable nitrate production from urine is only possible within a narrow pH range. As NOB grow more slowly than AOB at high pH values resulting from high urine dosage rates, nitrite accumulates to irreversibly high levels within days. Nitrification ceases completely at even stronger reactor overloading. A long-term underloading in turn results in the selection of acid-tolerant AOB and a drop of pH to very low values.

To conclude, nitrification is a promising process for urine stabilization, but the influent rate must be chosen carefully and nitrite should be monitored regularly. A nitrite sensor would greatly simplify reactor operation, particularly in decentralized places, and should be developed as a next step to further enhance this technology.

Abbreviations

AOA	Ammonia oxidizing archaea
AOB	Ammonia oxidizing bacteria
ATP	Adenosine triphosphate
COD	Chemical oxygen demand
CSTR	Continuous stirred tank reactor
HNO_2	Nitrous acid
MABR	Membrane aerated biofilm reactor
MBBR	Moving bed biofilm reactor
MBR	Membrane bioreactor
NADH	Nicotinamide adenine dinucleotide
NH_3	Ammonia
NH_4^+	Ammonium
$NH_4^+ + NH_3$	Total ammonia
NOB	Nitrite oxidizing bacteria
N_2O	Nitrous oxide
NO	Nitric oxide
NO_2	Nitrogen dioxide
NO_2^-	Nitrite
$NO_2^- + HNO_2$	Total nitrite
OTU	Operational taxonomic unit
PCR	Polymerase chain reaction
qPCR	Quantitative polymerase chain reaction
SBR	Sequencing batch reactor
TIC	Total inorganic carbon
TOC	Total organic carbon
WWTP	Wastewater treatment plant

Introduction

Urine source separation

Water flushing toilets, large sewage networks and centralized treatment of wastewater are the common sanitation approach in Western Europe and North America (Maurer et al. 2006). The construction of sewer networks has been an excellent way to drastically reduce water-borne diseases by separating wastewater from drinking water. However, centralized, water-based sanitation is not applicable in many regions of this world.

One of the main limitations is the large amount of water required for toilet flushing as well as for transportation in the sewer. Particularly in arid regions, water-based sanitation would be a waste of the essential resource water. The facts that an estimated 3 billion people will be living in water stressed countries by 2025 (United Nations Development Programme 2006) and that 2.5 billion people currently lack improved sanitation (United Nations 2014) imply that water-based sanitation cannot be the only option to solve all sanitation problems worldwide and that new dry sanitation systems need to be developed.

Furthermore, the mixing and dilution of feces and urine in water-based sanitation systems impede nutrient recovery. Recovery of nutrients and closing the nutrient cycle is, however, important for scarce nutrients, such as phosphorus (Scholz et al. 2014). Nutrient recovery is also economically sensible in regions where commercial fertilizers are expensive such as in Africa (Sanchez 2002).

Approximately 50% of the phosphorus and 75% of the nitrogen in wastewater originates from urine, while urine accounts for less than 1% of the total volume (Larsen and Gujer 1996). Nutrient recovery from urine is therefore in many cases energetically efficient (Maurer et al. 2003). One challenge of urine separation is, though, that it usually requires some sort of storage. During urine storage urea, the main compound in urine is decomposed quickly to ammonia (NH_3) and bicarbonate causing a pH increase to values above 9 (Udert et al. 2003b). At such high pH values, NH_3 volatilizes causing bad odor and high nitrogen losses.

Due to the risk of NH_3 losses, urine should not be transported over long distances, but a more decentralized treatment is required. Decentralized treatment could even be an economic advantage: large sewer networks are expensive installations (Maurer et al. 2006). Eggimann et al. (2015) showed in a case scenario for Switzerland that the optimal degree of centralization is substantially lower than the current level.

Decentralized treatment requires a high degree of reliability. Chemical processes are considered to be more robust than biological processes. The simple chemical precipitation of struvite ($NH_4MgPO_4 \cdot 6H_2O$) has thus been widely studied to recover phosphate from urine. Struvite precipitates spontaneously from urine, if a magnesium source is added. Struvite precipitation has been tested in the field (Etter et al. 2011), a fully automated struvite reactor has been developed (Grau et al. 2015), and an efficient magnesium dosage based on the dissolution of a magnesium sacrificial electrode has been proposed for decentralized urine treatment (Hug and Udert 2013).

Struvite precipitation, however, mainly removes phosphorus leaving behind phosphorus-depleted and nitrogen-rich urine, which needs to be treated further in order to prevent eutrophication of water bodies and pollution of drinking water resources. Additionally, only

about one-fifth of the monetary value can be recovered from urine with struvite precipitation, while the remaining fertilizer value in form of nitrogen and potassium stays in urine (Etter et al. 2011).

The combination of nitrification and distillation (Udert and Wächter 2012) provides an attractive alternative to struvite precipitation, as it allows for complete nutrient recovery as well as for the treatment of urine. In fact, the concentrated nutrient solution, distilled water, and a small amount of excess sludge are the only products.

The goal of the first process step, nitrification, is to stabilize the urine in order to prevent ammonia loss prior to the concentration with distillation. During nitrification bacteria convert half of the total ammonia (NH_4^+ and NH_3) into non-volatile nitrate (NO_3^-) and, as the pH drops to values around 6, the other half is stabilized as non-volatile ammonium (NH_4^+). Concomitantly with nitrification, 90% of the organic substances are degraded including compounds responsible for malodor (Troccaz et al. 2013) and for foaming during distillation (Tettenborn et al. 2007). The resulting stabilized solution can be concentrated without any substantial nitrogen losses in order to simplify transportation, storage or direct application as fertilizer.

The nitrification process has so far been tested under well-controlled laboratory conditions (Udert et al. 2003a, Udert and Wächter 2012). However, new challenges may occur during a more dynamic reactor operation, such as during the reactor start-up or the operation of a pilot-scale reactor with varying influent composition and temperature pattern. Explaining the causes for failures and elaborating the conditions to achieve high process stability is thus the main aim of this thesis.

Bacteria involved in nitrification

Nitrification involves two different bacterial groups: ammonia oxidizing bacteria (AOB) convert ammonia to nitrite (NO_2^-, Equation 1), which is then further transformed to nitrate by nitrite oxidizing bacteria (NOB, Equations 2). Based on stoichiometry, nitrification produces two moles of protons per mole of ammonium that is oxidized.

AOB: $$NH_4^+ + 1.5\ O_2 \rightarrow NO_2^- + 2\ H^+ + H_2O \quad (1)$$

NOB: $$NO_2^- + 0.5\ O_2 \rightarrow NO_3^- \quad (2)$$

Ammonia and nitrite oxidation is conducted by several populations of AOB and NOB, respectively. Different AOB and NOB populations have adapted to distinct environments. The substrate as well as the salt concentration is a known selection criteria between different AOB and NOB populations (Koops et al. 2006, Nowka et al. 2015).

Most of the AOB belong to the class of β-*Proteobacteria* (e.g., genus *Nitrosomonas* and genus *Nitrosospira*), while only the genus *Nitrosococcus* belongs to the class of γ-*Proteobacteria* (Purkhold et al. 2000). The species *Nitrosomonas europaea*, *eutropha*, *oligotropha*, and *mobilis* from the genus *Nitrosomonas* are most commonly found in wastewater treatment plants (Nielsen et al. 2009). The species *Nitrosomonas europaea* has also been intensively studied in

pure culture studies (e.g., Groeneweg et al. 1994, Hunik et al. 1992, and Kumar et al. 1983). The genus *Nitrosospira* is frequently observed in acidic soils (De Boer and Kowalchuk 2001) and is occasionally detected in engineered reactors (Nielsen et al. 2009). γ-proteobacterial AOB are mainly found in marine environments (Ward and O'Mullan 2002), and are not expected in engineered reactors (Nielsen et al. 2009), a perception which will, however, be challenged in this thesis.

Ammonia oxidation is not restricted to bacteria. Ammonia oxidizing archaea (AOA) were found to play a more important role in strongly acidic soils than AOB (Zhang et al. 2012). The relative abundance of AOA is, however, low compared to AOB in conventional wastewater treatment (Wells et al. 2009).

NOB are phylogenetically more scattered than AOB and belong to the class of α, β, γ and δ-*Proteobacteria*, as well as to the phylum *Nitrospirae* (genus *Nitrospira*) (Daims et al. 2011). The genus of *Nitrospira* is dominant in most wastewater treatment plants, while *Nitrobacter* (α-*Proteobacteria*) seem to play a minor role (Nielsen et al. 2009), which can be explained by the higher affinity of *Nitrospira* for nitrite compared to *Nitrobacter* (Nowka et al. 2015).

Nitrification of urine

Nitrification is a well-known process from wastewater treatment, but new challenges occur, when the process is applied to urine treatment: urine is a far more concentrated solution revealing higher total ammonia and salt concentrations (Udert et al. 2006), and urine contains a limited alkalinity to total ammonia ratio, which is usually not the case in conventional wastewaters (Tchobanoglous et al. 2003). The alkalinity to total ammonia ratio in urine accounts for one mole of alkalinity per mole of total ammonia (Udert et al. 2006), which is not sufficient for complete ammonia oxidation (Equation 1). Hence, urine can only be partially nitrified, except if a base is added.

Nitrification of human or animal urine by the addition of a base is known since ancient times: saltpeter (potassium/sodium/calcium/magnesium nitrate) was manufactured from urine for the use as gunpowder, e.g., during the American civil war (LeConte 1962). Saltpeter was produced in so-called nitre beds by adding potash or lime and by regular watering with urine (LeConte 1962). More recently, decentralized urine nitrification by addition of a base has been studied in the Netherlands (Oosterhuis and van Loosdrecht 2009) and in Hong Kong (Jiang et al. 2011). Nitrified urine can be added to pressurized sewers for in-sewer-denitrification, which minimizes upgrade requirements for nitrogen removal at wastewater treatment plants (Jiang et al. 2011) and prevents hydrogen sulfide (H_2S) formation and thereby corrosion (Oosterhuis and van Loosdrecht 2009).

The base addition is, however, costly and not required for nutrient recovery with the nitrification/distillation process: the pH drop during nitrification is sufficient to stabilize the solution and the produced ammonium-nitrate solution is well suited as fertilizer (Bonvin et al. 2015). The high remaining total ammonia concentration and the low alkalinity in nitrified urine make the process, however, susceptible for process instabilities.

While the partial ammonia oxidation to nitrate seems to be feasible (Udert et al. 2003a, Udert and Wächter 2012), the accumulation of nitrite has been identified as a major concern (Sun et al. 2012, Udert et al. 2003a, Udert and Wächter 2012). Ammonium nitrite is an unwanted nitrification product, as it leads to nearly complete nitrogen loss during distillation (Wächter et al. In prep.), but the conditions leading to nitrite production during urine treatment have not been completely understood so far.

Another concern for partial ammonia oxidation from urine is the pH drop to values below 3, which was observed in a membrane aerated biofilm reactor (MABR) after several weeks of adaptation time (Udert et al. 2005). Very low pH values need to be prevented due to harmful off-gases (see below) and corrosion issues; currently however, it is unclear why this pH drop occurred and how this could be prevented.

Importance of pH

The pH value influences the growth rates of AOB and NOB differently and therefore impedes their interplay. The growth of AOB is fast at high pH values, because NH_3, the actual substrate of AOB (Suzuki et al. 1974) occurs at high concentrations (pK_a value of 9.24, Gustafsson 2012). The fast growth of AOB at high pH values and high temperatures is frequently used for the selective wash-out of NOB in reactors designed to produce nitrite, e.g., for shortcut nitritation/denitritation in digester supernatant (Hellinga et al. 1999). In contrast, NOB must be retained during urine nitrification in order to produce nitrate.

Lower pH values may be more beneficial to operate urine nitrification reactors, as the growth rate of AOB decreases with pH and commonly stops completely at pH values slightly below 6 (Udert et al. 2003a), allowing NOB to keep up converting nitrite into nitrate. However, reactor operation at lower pH values can also be a risk, as the pH can decrease further to values below 3. At these very low pH values, around 16% of the transformed nitrogen was lost by chemical decomposition of nitrous acid (HNO_2) and volatilization, partially in the form of harmful gases (HNO_2, nitric oxide and nitrous oxide) (Udert et al. 2005). In contrast, nitrogen losses were negligible in urine reactors operated at pH values close to neutral (Udert et al. 2003a). Hence, it is of practical importance to understand (1) why ammonia oxidation commonly ceases at pH values below 6, and (2) why nitrification at lower pH values is still possible.

The growth rate of AOB decreases with pH, as AOB lack their substrate NH_3 (Hellinga et al. 1999). AOB are also known to be inhibited by HNO_2, the acid of their own product nitrite (Anthonisen et al. 1976). Furthermore, total inorganic carbon (TIC) has been reported to reduce the growth rate of AOB at low pH values (Wett and Rauch 2003). Nitrifiers use inorganic carbon for biomass growth, however, TIC concentrations decrease with pH, because the acid H_2CO_3 is formed, which volatilizes as CO_2 (pK_a value 6.35, Stumm and Morgan, 1996). Low pH values may have also a direct effect on AOB activity due to the damage of proteins (Wiesmann et al. 2006), an increased energy demand for maintenance (Van Hulle et al. 2007), or the inactivity of the rate limiting enzyme at a certain ionization state (Antoniou et al. 1990). Hence, a large variety of factors have been proposed, but it is not clear, which of the factors cause the cessation of AOB activity during urine treatment.

Nitrification at pH values around 4 has been observed in synthetic wastewaters with a limited alkalinity (Gieseke et al. 2006, Tarre et al. 2004, Tarre and Green 2004, Tarre et al. 2007), while nitrification is commonly not expected at pH values below 5.8 in municipal wastewaters (Painter and Loveless 1983, Wiesmann et al. 2006). Gieseke et al. (2006) found that nitrification at low pH values is not due to favorable microenvironments with locally enhanced pH values and it is not due to unknown nitrifying populations. In fact, AOB affiliated with *Nitrosomonas oligotropha* and *Nitrosospira* as well as NOB affiliated with *Nitrospira* were abundant at a pH of 4.5 in the synthetic wastewater (Gieseke et al. 2006). Tarre et al. (2007) further showed that the pH decrease from 6 to 4.5 was a result of a shift from AOB related with *Nitrosomonas europaea* to *Nitrosomonas oligotropha*. Prevalent AOB and possible population shifts have not been investigated in urine nitrification reactors so far.

Aim of this thesis

This thesis focuses on the use of biological nitrification to convert human urine into a stable ammonium-nitrate solution, which can be easily transported, stored and further treated with distillation. The main aim was to elaborate the conditions needed for process stability and to explain the main causes for process failures. I specifically investigated the causes for the pH drop to very low values and for the accumulation of nitrite, which I identified as the most likely process failures.

I hypothesized that pH has a very crucial influence on process stability by influencing the activity of AOB and by selecting distinct AOB populations. The pH dependency of AOB was thus investigated experimentally and by mathematical modeling. Furthermore, AOB with different pH dependencies were identified by means of amplicon pyrosequencing. The specific research questions of the four chapters are given below.

- Chapter 1: Can urine nitrification be applied at pilot-scale? Which process instabilities do we encounter? How to start-up a urine nitrification reactor?
- Chapter 2: Which AOB are commonly present in urine nitrification reactors? Why does the activity of these AOB decrease with pH and stop at a pH slightly below 6? How can we model the growth rate of this AOB?
- Chapter 3: Is a population shift to distinct AOB responsible for low pH nitrification? How does the pH drop affect reactor performance and bacterial richness?
- Chapter 4: How should we operate urine nitrification reactors? How can we prevent the accumulation of nitrite and the selection of acid-tolerant AOB?

Thesis outline

Chapter 1 summarizes the experience with a nitrification/distillation pilot plant at Eawag. This chapter addresses the nitrification rates, the energy demand and the quality of the concentrate as fertilizer based on the results from the pilot-scale installations. Possible process instabilities, i.e. the accumulation of nitrite and the selection of acid-tolerant AOB, are discussed based on start-up experiments of laboratory nitrification reactors.

In Chapter 2 we investigate the pH dependency of the AOB usually present in urine nitrification reactors as a first step towards understanding and enhancing process stability. The pH dependency of the growth rate and the pH limit of activity of this AOB are determined in batch experiments and by setting up a mechanistic model. To model the limit of activity of this AOB at pH values close to 5.4, a new pH term is proposed.

In Chapter 3, we follow the population dynamics of AOB by means of amplicon pyrosequencing, as the pH decreases from values close to neutral to very low values as a response in a decrease in the loading rate. We investigate how the selection of acid-tolerant AOB and the pH drop affect reactor performance and overall bacterial community structure.

Chapter 4 determines the conditions enabling stable nitrate formation and preventing the unfavorable system states of nitrite accumulation and low pH nitrification by the selection of acid-tolerant AOB. For this purpose the nitrification model with the acid-sensitive AOB (Chapter 2) is extended with the growth rate of acid-tolerant AOB (Chapter 3) as well as NOB.

Chapter 1

Operating a pilot-scale nitrification/distillation plant for complete nutrient recovery from urine

Alexandra Fumasoli, Bastian Etter, Bettina Sterkele, Eberhard Morgenroth and Kai M. Udert

Water Science and Technology, 2016, 73(1), 215-222

Abstract

Source-separated urine contains most of the excreted nutrients, which can be recovered by using nitrification to stabilize the urine before concentrating the nutrient solution with distillation. The aim of this study was to test this process combination at pilot-scale. The nitrification process was efficient in a moving bed biofilm reactor with maximal rates of 930 mg $N \cdot L^{-1} \cdot d^{-1}$. Rates decreased to 120 mg $N \cdot L^{-1} \cdot d^{-1}$ after switching to more concentrated urine. At high nitrification rates (640 mg $N \cdot L^{-1} \cdot d^{-1}$) and low total ammonia concentrations (1790 mg NH_4-$N \cdot L^{-1}$ in influent) distillation caused the main primary energy demand of 71 $W \cdot cap^{-1}$ (nitrification: 13 $W \cdot cap^{-1}$) assuming a nitrogen production of 8.8 $gN \cdot cap^{-1} \cdot d^{-1}$. Possible process failures include the accumulation of the nitrification intermediate nitrite and the selection of acid-tolerant ammonia oxidizing bacteria. Especially during reactor start-up, the process must therefore be carefully supervised. The concentrate produced by the nitrification/distillation process is low in heavy metals, but high in nutrients, suggesting a good suitability as an integral fertilizer.

Introduction

Separating urine at the source is an effective approach to recover nutrients from wastewater, given that urine contains most nutrients, which humans excrete (Larsen and Gujer 1996). Researchers have targeted specific nutrients (e.g. nitrogen, phosphorus) and developed technologies to reclaim them from the liquid (Larsen et al. 2013). Alternatively, our research group opted for another procedure: water is separated from urine, leaving behind a concentrate, which contains all nutrients. After extensive laboratory work (Udert et al. 2003a, Udert and Wächter 2012), a pilot plant was started up at Eawag's main building Forum Chriesbach. The plant operates in two stages: First, half of the total ammonia (NH_4^+ and NH_3) in urine is biologically converted into nitrate (NO_3^-), which is then concentrated with a distiller.

The aim of the nitrification step is to prevent ammonia (NH_3) losses and malodor. During nitrification bacteria convert half of the total ammonia into non-volatile nitrate and, as the pH drops from pH 9 to values around 6, the other half is stabilized as non-volatile ammonium (NH_4^+). About 90% of the organic substances are mineralized including compounds, which are responsible for the malodor (Troccaz et al. 2013). The resulting stabilized solution can be concentrated without any substantial nitrogen losses in order to simplify transportation, storage or direct application as fertilizer.

Four main factors determine the suitability of the pilot-scale reactor for nutrient recovery: first, nitrification rates determining the reactor size; second, the energy demand; third, stability of the biological processes; and fourth, the quality of the concentrate produced.

High urine nitrification rates of 380 mg N $L^{-1} \cdot d^{-1}$ were observed in a laboratory scale moving bed biofilm reactor (MBBR) at temperatures of 25 ± 0.3°C and over a period of 80 days (Udert et al. 2003a). However, stronger changes in temperature and urine composition have to be expected for the pilot-scale reactor, which may influence long-term performance.

The primary energy demand for the overall process (nitrification and distillation) has been calculated as 30 $W \cdot cap^{-1}$ based on laboratory results and literature data (Udert and Wächter 2012). This is two and a half times higher than for the treatment of municipal wastewater in a conventional wastewater treatment (Maurer et al. 2003). The energy consumption was estimated for the urine composition given in Udert et al. (2006). The concentrations from urine collected in urine diverting toilets may, however, not reach equally high values (Goosse et al. 2009), which will cause a higher energy demand for water removal by distillation.

The stability of the biological process is particularly challenging, as it requires the well-tuned interplay of ammonia oxidizing bacteria (AOB) and nitrite oxidizing bacteria (NOB). A simple pH control was proposed to achieve high process stability in a urine nitrification reactor (Udert and Wächter 2012). The pH value is kept in a narrow range by intermittent dosage of stored urine based on the following principle: when no urine is pumped the pH decreases due to nitrification. During urine dosage, pH increases due to the high pH value and alkalinity of stored urine. Udert and Wächter (2012) tested this strategy for the steady-state operation of a laboratory reactor, but not for reactor start-up, which is the most critical phase in reactor operation.

The nitrification process converts 50% of the total ammonia to nitrate and heterotrophic bacteria degrade 90% of the organic substances (measured as chemical oxygen demand) (Udert and Wächter 2012). Most other compounds though are not degraded or removed during nitrification and become concentrated during distillation. If the concentrate is supposed to be used as a fertilizer, its composition needs to satisfy legal standards with respect to various compounds (e.g., heavy metals; Council regulation (EEC), 1991).

This paper summarizes our previous experience with the nitrification/distillation pilot plant at Eawag. The results provide important information for further research and pilot studies. We address the nitrification rates, energy demand and the quality of the concentrate as fertilizer based on the results from the pilot-scale installations. The factors influencing process stability are discussed based on laboratory nitrification experiments.

Materials & Methods

Urine collection and composition

Urine was collected from urine-diverting flush toilets (NoMix toilets, Roediger Vacuum, Hanau, Germany) and waterless urinals through a separate piping system at Eawag's main building (Dübendorf, Switzerland). In the building, an average of 110 L of urine is collected daily (only working days). In two 1000 L tanks, women’s and men’s urine is stored separately before it is treated in the nitrification/distillation process. Urine from the women’s storage tank is less concentrated by a factor of approximately 2 with respect to all compounds compared with men’s urine (Table 1). The main reason for the lower concentration of women's urine is the collection with NoMix toilets only: leaky valves allow some flushing water to enter the collection tank.

Pilot-scale nitrification reactor and vacuum distiller

The urine treatment facilities are located in the basement of the building (Figure 1). The nitrification reactor consists of two columns with a diameter of 32 cm and a liquid volume of 120 L. The reactors are continuously fed with stored urine and contain high-density polyethylene (HDPE) biomass carriers (Kaldnes® K1) with a bulk volume of 60% of the total reactor volume and a specific surface of 500 $m^2 \cdot m^{-3}$ (Rusten et al. 2006). The reactor's aeration acts as the driving force for the mixing of the carriers and liquid. To achieve complete mixing, the aeration rate had to be set to a value of 2 $m^3 \cdot h^{-1}$ (per column). Due to the strong aeration, the dissolved oxygen concentration in the reactor is constantly above 7 $mg \cdot L^{-1}$. The urine is pumped from the storage tanks into the reactor with a membrane dosing pump (Delta 730, Prominent, Heidelberg, Germany); the flow rate can be adjusted gradually from 0 to 30 $L \cdot h^{-1}$. Initially only one reactor column was in use.

In order to reduce water loss during aeration of the biological reactor, the air from Eawag's pressured air supply is humidified in a column containing distilled water prior to injection into the reactor. In the nitrification reactor, the instrumentation comprises pH, temperature, and dissolved oxygen probes (Tophit CPS491D, Oxymax COS61D, Liquiline CM448, Endress & Hauser AG, Reinach, Switzerland). Between the nitrification reactor and the distiller, an intermediate storage tank is installed, which holds 600 L nitrified urine corresponding to the

volume of one distillation batch. The average concentration factor during distillation is between 20 and 25.

Table 1: Composition of stored urine as well as composition of concentrate (produced from women's urine) compared to threshold values for organic farming from European legislation (Council Regulation (EEC) 1991).

		Women's urine Average ± Std. Dev.[1]	Men's urine Average ± Std. Dev.[1]	Concentrate Average ± Std. Dev.[2]	Council regulation (EEC) Threshold value
pH	[-]	8.9 ± 0.1	9.0 ± 0.1	4.1	
Total ammonia-N	[mg·L^{-1}]	1990 ± 420	4140 ± 870	23100 ± 4700	
Nitrate-N	[mg·L^{-1}]	<10	<10	24400 ± 2200	
Dissolved COD	[mg·L^{-1}]	2010 ± 540	3860 ± 870	4650 ± 1030	
Total inorganic C	[mg·L^{-1}]	1020 ± 250	2080 ± 260	<5	
Total phosphate-P	[mg·L^{-1}]	106 ± 17	242 ± 23	2130 ± 180	
Potassium	[mg·L^{-1}]	854 ± 143	1470 ± 130	17400 ± 2800	
Sodium	[mg·L^{-1}]	881 ± 239	1760 ± 90	19400 ± 2700	
Sulfate	[mg·L^{-1}]	308 ± 87	708 ± 109	8620 ± 810	
Chloride	[mg·L^{-1}]	1630 ± 400	2980 ± 440	35300 ± 2900	
Calcium	[mg·L^{-1}]	13.5 ± 11.0	n/a	428 ± 37	
Magnesium	[mg·L^{-1}]	<4	n/a	<4	
Iron	[mg·L^{-1}]	n/a	n/a	0.6 ± 0.1	
Manganese	[mg·L^{-1}]	n/a	n/a	0.4 ± 0.5	
Boron	[mg·L^{-1}]	n/a	n/a	17.2 ± 0.8	
Cobalt	[mg·L^{-1}]	n/a	n/a	0.1 ± 0.1	
Copper	[mg·L^{-1}]	n/a	n/a	0.4 ± 0.3	70
Chromium	[mg·L^{-1}]	n/a	n/a	0.2 ± 0.1	70
Zinc	[mg·L^{-1}]	n/a	n/a	14.2 ± 0.9	200
Cadmium	[mg·L^{-1}]	n/a	n/a	<0.05	0.7
Nickel	[mg·L^{-1}]	n/a	n/a	<0.1	25
Lead	[mg·L^{-1}]	n/a	n/a	0.27	45

[1] sample number > 8; [2] three samples

The distiller is a commercially available industrial vapor compression vacuum distiller (KMU-Loft Cleanwater, Hausen, Germany). It is set to operate at approximately 500 mbar working pressure. The vapor compression occurring in the vacuum pump is the sole source of heating, as the heated vapor is recycled into a heat exchanger located in the distiller's sump. The distiller is operated in semi-batch mode, i.e. the liquid volume in the sump is kept constant at 20 L by compensating evaporated liquid with new influent. Thus, over a distillation batch, the concentration in the sump continuously augments up to a given level. Once a set volume of liquid has been distilled, the process is halted and the remaining concentrated liquid is drained from the distiller. In the case of our set-up, the distilled water is recycled into the toilet flush

system. In the distiller, temperature, pressure, electric conductivity (as a proxy for concentration), and electricity consumption are measured and recorded. In both, the urine supply tanks and the intermediate storage tank holding the nitrified urine, differential pressure sensors (Vegaflex 61, VEGA Grieshaber KG, Schiltach, Germany) record the liquid level.

Figure 1: The nitrification reactor (left column) and distiller (right) at Eawag (Photo: B. Etter).

Start-up experiments in laboratory reactors

Laboratory experiments were conducted to test the start-up procedure. Each of the two reactors had a volume of 7 L. The pH and oxygen concentrations were measured continuously. Data was stored in a data logger (Memograph M, RSG40, Endress & Hauser, Reinach, Switzerland), which was also used to control the influent pumps (SCi-Q 400, Watson Marlow, Falmouth, United Kingdom). The airflow was maintained at 1 $L \cdot min^{-1}$ using a flow controller (EL-FLOW, Bronkhorst, Reinach, Switzerland), resulting in dissolved oxygen concentrations above 7 $mg \cdot L^{-1}$. The reactors were stirred magnetically at 500 rpm. The temperature was maintained at 25°C with a thermostat (F32, Julabo Labortechnik GmbH, Seelbach, Germany).

For start-up, the reactors were filled with 0.7 L of activated sludge from the nitrification tank of Eawag's municipal wastewater treatment plant, 140 mL of men’s urine, and tap water. The reactors were operated with suspended biomass but no biofilm carriers. Men’s urine was added automatically according to the pH control mechanism described above (Udert and Wächter 2012). The two reactors were operated in two different pH intervals: reactor 1 (R1) between 5.80 and 5.85 and reactor 2 (R2) between 6.2 and 6.25. As the low pH setpoints were initially not reached, four and two times 50 mL of urine were added manually within the first 15 days to R1 and R2, respectively.

Analytical methods

Chloride, sulfate, phosphate, nitrate, potassium and sodium were analyzed with ion chromatography (IC, Metrohm, Herisau, Switzerland). Magnesium, calcium, iron, copper, zinc, manganese, cobalt, copper, chromium, cadmium, nickel, lead and boron were determined with inductively coupled plasma optical emission spectrometry (ICP OES, Ciros, Spectro Analytical Instruments, Kleve, Germany). The total ammonia, total nitrite (nitrite and nitrous acid) concentration as well as the chemical oxygen demand (COD) were measured photometrically with cuvette tests (LCK 303, LCK 342, LCK 614 Hach-Lange, Berlin, Germany). Total inorganic and organic carbon (TIC and TOC) were measured with a TIC/TOC analyzer (IL550 OmniTOC, Hach-Lange, Berlin, Germany).

Biomass analysis

To characterize the distribution between suspended and attached nitrifying bacteria, biomass samples of the suspended biomass and of the carrier material were taken from the pilot-scale reactor. Samples were taken at one day in month 15 and at a second day in month 29. The nitrification rates were substantially different in both cases (see Table 2). Furthermore, biomass samples were removed from each of the two laboratory reactors after 142 days of reactor operation. The biomass samples were stored at -20°C prior to analysis. DNA was extracted using the FastDNA SPIN Kit for Soil (MP Biomedicals, Santa Ana, CA, USA) and analyzed by Research and Testing Laboratory (Lubbock, TX, USA) with bacterial tag-encoded FLX amplicon pyrosequencing using the primer pair 341F (5'-CCTACGGGNGGCWGCAG-3') / 785R (5'-GACTACHVGGGTATCTAATCC-3') targeting the bacterial 16S rRNA gene pool (Herlemann et al. 2011).

Results & Discussion

Nitrification rates in the pilot-scale reactor

The nitrification reactor was fed for 3 years with women's urine, after which men's urine was dosed for another half a year of reactor operation. Nitrification rates in women's urine reached 310 mg $N \cdot L^{-1} \cdot d^{-1}$ during the months 12 to 16 (Table 2). The COD of the particulate organic matter, a measure for suspended biomass, was 2260 mg $COD \cdot L^{-1}$. The biomass fraction of the nitrifiers in the suspended biomass was very low, while AOB and NOB were predominant in the biofilm attached to the carriers (Figure 2).

AOB sequences affiliated with the *Nitrosomonas europaea* lineage and NOB sequences with the genus of *Nitrobacter* (Figure 2). The predominance of these nitrifiers was not surprising, as AOB from the *Nitrosomonas europaea* lineage are often selected in environments with high ammonia concentrations (Koops et al. 2006), while NOB of the genus *Nitrobacter* are adapted to higher nitrite concentrations than *Nitrospira* (Nowka et al. 2015).The relative abundance of all other AOB or NOB was below 0.1%.

Table 2: Performance data of the pilot-scale nitrification reactor at different time points. During the first two operational phases (month 12 to 16 and 29 to 30) the reactor was fed with women's urine, and in the third phase (month 36 to 40) with men's urine.

Time	Nitrification rate		Influent ammonia	Discharge	COD to N ratio	pH	Temperature	Particulate COD
[month]	[mg N·L^{-1}·d^{-1}]	[g·m^{-2}·d^{-1}]	[mgN·L^{-1}]	[L·d^{-1}]	[-]	[-]	[°C]	[mg·L^{-1}]
12-16	310 ± 50	1.0 ± 0.2	1800 ± 140	42 ± 5	1.3 ± 0.6	5.9 ± 0.2	23.7 ± 0.9	2260 ± 470
29-30	640 ± 160	2.1 ± 0.5	1790 ± 50	84 ± 17	1.2 ± 0.1	5.8 ± 0.1	26.3 ± 1.0	3600
36-40	120 ± 50	0.4 ± 0.1	4100 ± 450	7 ± 3	1.0 ± 0.2	6.0 ± 0.1	22.5 ± 0.6	220 ± 150

The nitrification rate increased to 640 mg N·L^{-1}·d^{-1} at higher temperatures of 26.3°C (months 29 to 30). At temperatures of 27.0°C, the maximal rate of 930 mg N·L^{-1}·d^{-1} (3.1 g N·m^{-2}·d^{-1}) was reached, corresponding to a discharge of 120 L·d^{-1} of women's urine. The high rates were maintained for only 10 days, because not sufficient urine was available from the women's urine tank. In this phase, both, the particulate COD as well as the relative abundance of nitrifying bacteria in suspension, increased (Table 2, Figure 2). Hence, the nitrification rate increased at higher temperatures, because both suspended and attached nitrifiers contributed to the overall conversion rate.

Following the switch from women's to men's urine (months 36 to 40), the nitrification rate dropped to average values of 120 mg N·L^{-1}·d^{-1}. The particulate COD concentrations decreased drastically to 220 mg·L^{-1}. In the biofilm of the carrier material, nitrifying biomass competes with heterotrophic bacteria for oxygen and space (Hem et al. 1994). The increased attachment of bacteria to the carrier material (visual observation) after the switch to men's urine further boosted this competition resulting in lower nitrification rates.

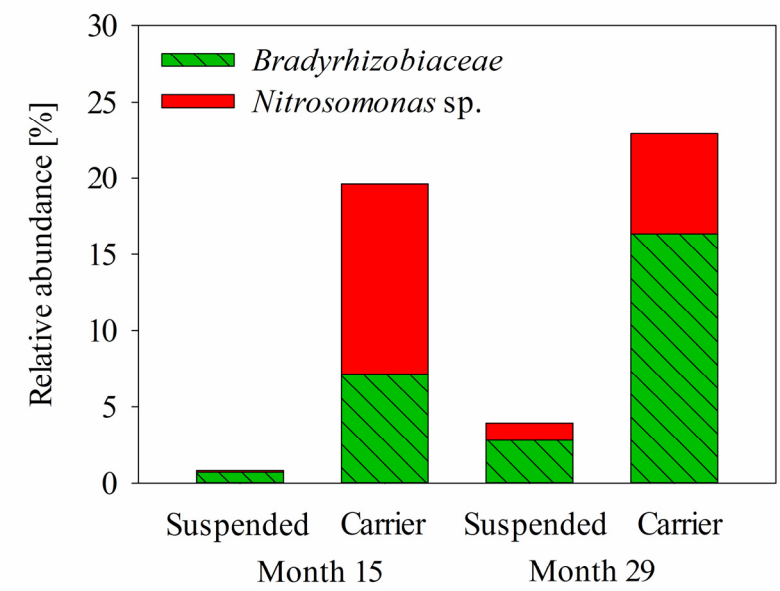

Figure 2: Relative abundance of *Nitrosomonas* sp. and sequences from the family of *Bradyrhizobiaceae* in suspension and attached to the carrier during reactor operation with women's urine. The *Bradyrhizobiaceae* sequences showed 100% identity to *Nitrobacter*, but could not be uniquely attributed to this genus. The relative abundance was determined for one day in month 15 and 29, respectively, by 16S rRNA amplicon sequencing.

Energy efficiency of the nitrification/distillation pilot plant

The average electric energy demand for distillation was 107 ± 31 $Wh \cdot L^{-1}$ of urine for 33 distiller runs. The energy required for distillation with respect to nitrogen depends on the initial degree of dilution of the urine solution represented by the total ammonia concentration (Figure 3). Hence, for the less concentrated women's urine in this study, more energy was required for distillation than for the more concentrated men's urine.

The energy demand for nitrification is mainly caused by aeration. Due to the fact that the airflow was used for mixing, the airflow was kept constant independently of the nitrification rate. The electric energy demand for nitrification is relatively low (11 $Wh \cdot gN^{-1}$) at high nitrification rates (640 mg $N \cdot L^{-1} \cdot d^{-1}$), but it increases to values of 59 $Wh \cdot gN^{-1}$ for the low rates observed in men's urine (120 mg $N \cdot L^{-1} \cdot d^{-1}$, Figure 3).

The electric energy demand for the overall process amounted to 71 $Wh \cdot gN^{-1}$ in the best case (640 mg $N \cdot L^{-1} \cdot d^{-1}$, 1790 mg NH_4-$N \cdot L^{-1}$ in influent). By assuming a conversion efficiency of 31% for electricity production (average European electricity mix, UCPTE, 1994) and a nitrogen production of 8.8 $gN \cdot cap^{-1} \cdot d^{-1}$ (Maurer et al. 2003) the primary energy demand amounted to 84 $W \cdot cap^{-1}$ (71 $W \cdot cap^{-1}$ for distillation and 13 $W \cdot cap^{-1}$ for nitrification), which corresponds to 1.9% of the overall primary energy demand in the European Union (4430 $W \cdot cap^{-1}$ in 2012, The World Bank 2015).

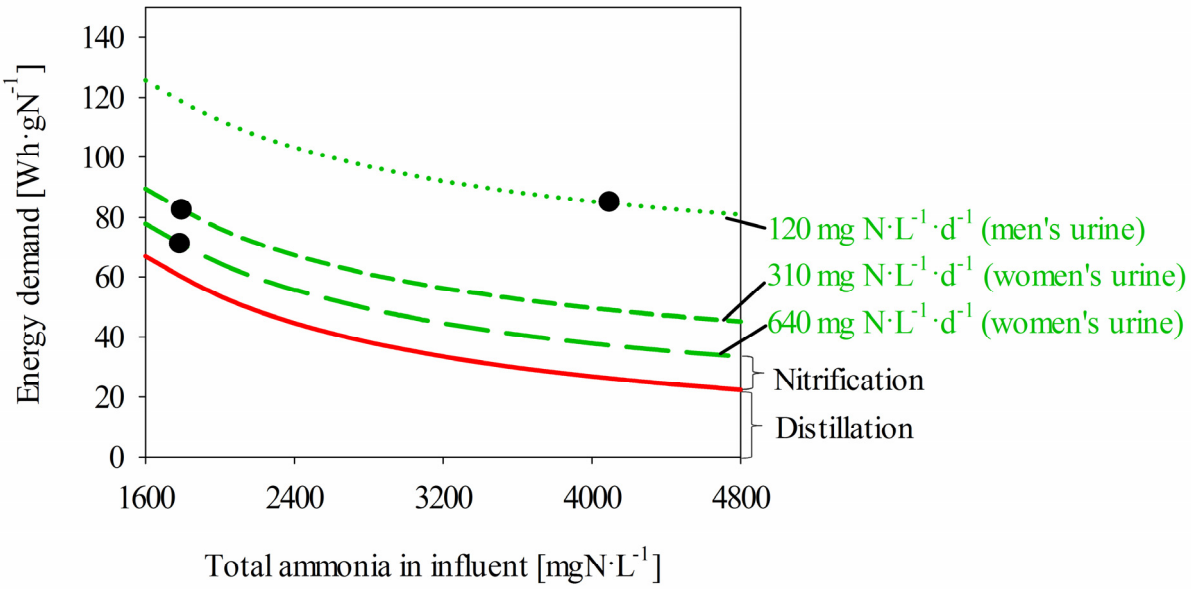

Figure 3: Energy demand for the nitrification/distillation process as a function of the total ammonia in the urine influent. The solid line represents the energy demand for distillation; the dotted lines are the sum of the nitrification/distillation process at different nitrification rates. The three large dots represent the energy demand for the evaluated operation periods as specified in Table 2.

The energy demand is clearly higher than the estimated primary energy demand of 10 $W \cdot cap^{-1}$ for the combination of conventional treatment of municipal wastewater and industrial fertilizer production (Maurer et al. 2003) (nitrification/pre-denitrification in wastewater treatment plant

(WWTP), average N- and P-fertilizer production in Europe, P-precipitation in WWTP including energy for sludge transport and incineration). However, the overall energy demand can still be reduced significantly and additional energy demands in urban water management, e.g., for flushing water provision have not been considered so far. In fact, the lower flushing water requirement for urine diverting toilets has been shown to be an important energetic advantage of urine separation (Ishii and Boyer 2015).

Collecting urine as concentrated as possible is an important requirement to save energy. If urine is collected in a more concentrated form, however, the aeration rate should be reduced due to the lower nitrification rate. Stirrers instead of the aeration could be used to provide sufficient mixing under such conditions. Alternatively, different reactor types, e.g. membrane bioreactors could achieve lower energy demands.

Process stability during reactor start-up

The start-up of the urine nitrification reactor was the main challenge during the operation of the pilot-scale reactor, mainly due to the accumulation of nitrite and the growth of acid-tolerant AOB (see below). The urine addition to the pilot plant was increased manually, and several trials were required for successful reactor start-up. To simplify the start-up procedure, a simple pH control was tested in two laboratory reactors.

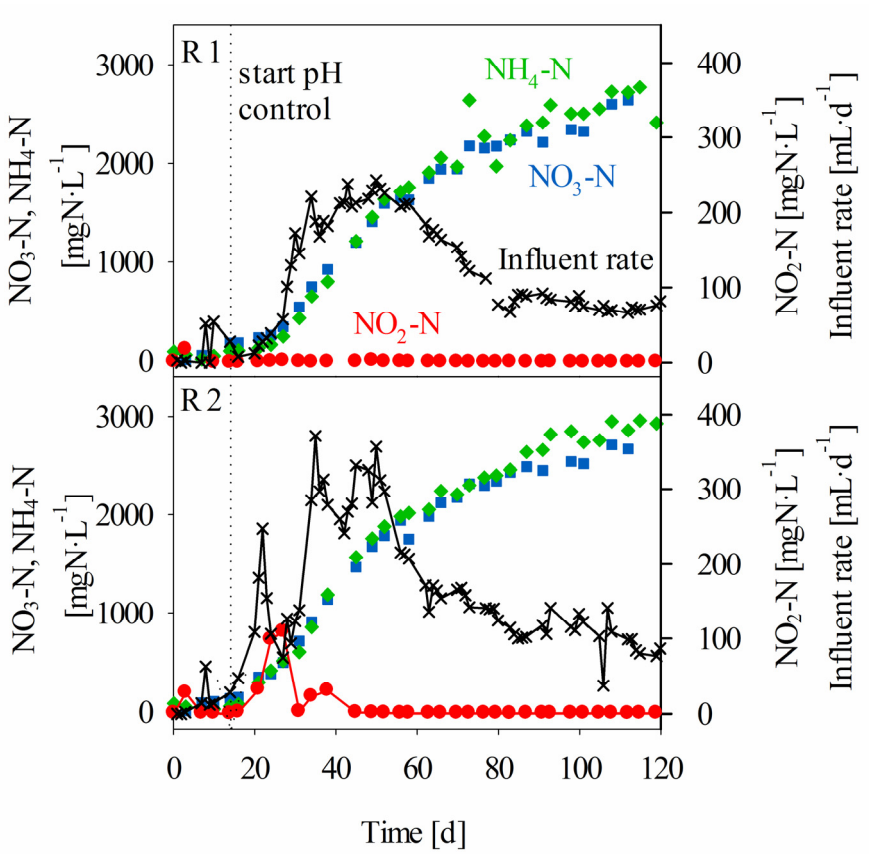

Figure 4: Concentrations of ammonium (NH_4-N, ♦), nitrate (NO_3-N, ■) and nitrite (NO_2-N, ●) as well as the influent rate during the automated start-up of two laboratory reactors with pH control. The pH is controlled between 5.80 and 5.85 in R1 and 6.20 and 6.25 in R2 by switching on and off the influent pump.

The strict pH control allowed for the automated start-up of the laboratory reactors: as the nitrification rate increased due to biomass growth, more urine was dosed automatically (Figure 4). Due to the limited alkalinity in urine, only 50% of the total ammonia in the influent was converted to nitrate. Thus, the total ammonia and nitrate concentrations increased concomitantly as more and more of the reactor content was replaced by nitrified urine.

The pH setpoints had an influence on nitrite production: nitrite increased to a maximal value of 109 $mgN \cdot L^{-1}$ in R2, while the nitrite concentrations remained below 1 $mgN \cdot L^{-1}$ at all times in R1 (Figure 4). NOB are inhibited by nitrous acid (HNO_2), but despite of this inhibition NOB were still capable of removing the excess nitrite in R2 (Anthonisen et al. 1976), which was not always the case during the start-up of the pilot-scale application.

Nitrite accumulated in R2 but not in R1, as the influent rate increased faster in R2 compared to R1 (Figure 4). The faster increase in the urine dosage can be explained by the faster growth of AOB at higher pH values (Fumasoli et al. 2015), which boosted the automated urine addition. AOB and not NOB control the influent regime, because protons are released during ammonia oxidation to nitrite.

The inflow reached a maximal rate of 240 $mL \cdot d^{-1}$ in R1 (pH 5.8) and 370 $mL \cdot d^{-1}$ in R2 (pH 6.2) corresponding to a hydraulic residence time of 28.8 d in R1 and 18.9 d in R2, respectively (Figure 4). In the course of the experiment the inflow rates decreased, which may be explained with the increasing salt concentrations; high salt concentrations are known to reduce AOB and NOB activity (Moussa et al. 2006).

By switching off the influent pump, the pH in R1 dropped to 4.6, whereas the pH in R2 decreased to a minimal value of 5.7 only (Figure 5). This strong difference in the final pH minimum indicates that different AOB populations were selected in the two reactors with different pH setpoints. Indeed, the main AOB with an abundance of 3.1% in reactor R2 (pH 6.2) affiliated with the *Nitrosomonas europaea* lineage, which is similar to the AOB population during long-term operation of the pilot-scale reactor (Figure 2). In R1 (pH 5.8), however, *Nitrosospira* sp. were selected at pH 5.8 with relative abundance of 0.8%, while hardly any *Nitrosomonas* sp. were found.

Acid-tolerant AOB are a potential risk in urine nitrification reactors, because some acid-tolerant strains can decrease the pH to values as low as 2.2 (Fumasoli et al. subm.), in case that no or only very low amounts of urine are added (e.g. during holidays), which could buffer the pH value. Low pH values can inhibit NOB and lead to chemical decomposition of nitrite (Udert et al. 2005), during which significant amounts of harmful gases, such as nitric oxide (NO), nitrogen dioxide (NO_2), nitrous oxide (N_2O) and HNO_2 are released (Fumasoli et al. subm.).

An appropriate selection of the pH setpoint is therefore important for urine nitrification. A too high pH setpoint can lead to the accumulation of nitrite and subsequent inhibition of NOB, whereas a too low setpoint can foster the selection of acid-tolerant AOB and a consequent process destabilization. Online nitrite monitoring would be a possibility to explore the maximum pH setpoint. Unfortunately, online sensors for the high concentrations to be expected in urine treatment are currently not available, but recent tests with an ultraviolet spectral probe are promising (Mašić et al. 2015).

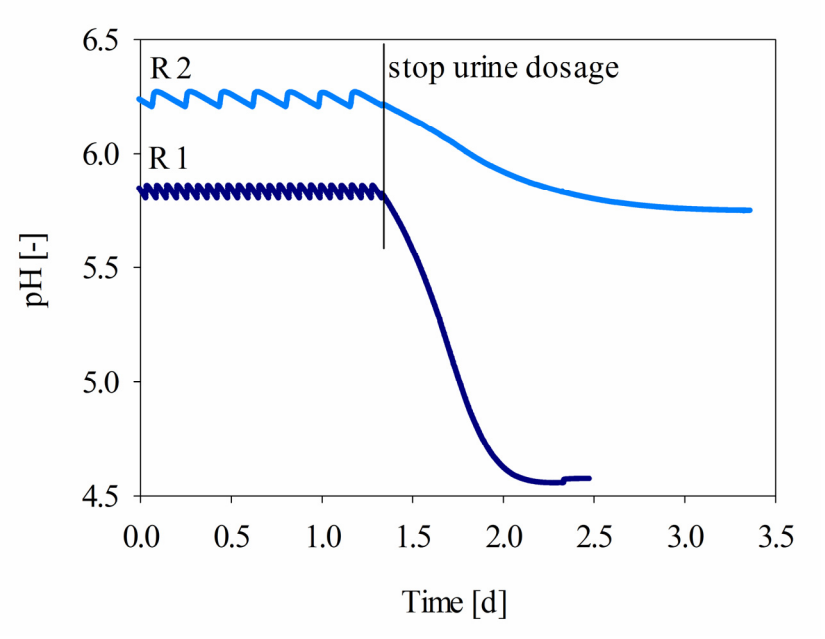

Figure 5: After switching off the influent pump, the pH decreases to the low pH limit of the particular AOB population present in the laboratory reactors.

Quality of the concentrate for fertilizer purposes

The concentrate has a high nitrogen content, but it also contains other important nutrients, such as phosphorus and potassium (Table 1). Most of the compounds from the initial influent are recovered in the final concentrate. Exceptions are the organic substances, ammonia and TIC: organic substances are oxidized during the biological treatment, about half of the ammonia is nitrified to nitrate and nearly all TIC is lost due to CO_2 volatilization, mainly during the biological treatment.

Studies on pharmaceuticals removal showed that some antiviral and antibiotic compounds were substantially degraded in the nitrification reactor. Remaining pharmaceuticals can be removed after the nitrification process by adsorption onto activated carbon (Oezel Duygan et al. in prep.).

The heavy metal content in the concentrated nutrient solution is far below the general limits for fertilizers in organic agriculture (Council regulation (EEC), 1991, Table 1). The heavy metal concentrations in the concentrate are close to the expected values taking into account the heavy metal concentrations in urine (Ronteltap et al. 2007) and a concentration factor of 20 to 25. The heavy metal content in urine is generally low, because heavy metals are mostly excreted with feces (Jönsson and Vinnerås 2013).

The greenhouse trials with synthetic solutions representing concentrated nitrified urine showed that the fertilizer performed equally or better than commercial fertilizers (Bonvin et al. 2015). The trials were conducted on Italian ryegrass (lolium multiflorum) on a growth period of 11 weeks in sandy, slightly acidic (pH = 6.5) soil with moderate phosphorus levels.

Conclusion

The nitrification/distillation process produces a concentrated nutrient solution, which could be well suited as an integral fertilizer. Current challenges of the system are the high energy demand and the possible process destabilization due to nitrite accumulation or low pH values. The inhibition by nitrite as well as the growth of acid-tolerant bacteria could be prevented by online monitoring and controlling the nitrite concentration. This should be the main focus of further research. The energy demand can be decreased by collecting urine as concentrated as possible and by energetically optimizing the nitrification reactor.

Acknowledgement

We thank the Bill and Melinda Gates Foundation for the funding received for the VUNA project (www.vuna.ch, Grant No. OPP1011603) and Eawag for infrastructure funds to construct the reactors. We also thank Karin Rottermann and Claudia Bänninger-Werffeli for their dependable laboratory analyses, and Mathias Mosberger and Corine Uhlmann for reactor operation and sampling. Furthermore, we greatly appreciated the frequent knowledge and experience exchange with our project partners in South Africa, Christopher Buckley, Maximilian Grau, Sara Rhoton, and Lungiswa Zuma, who have been operating a similar reactor combination in Durban.

Chapter 2

Modeling the low pH limit of *Nitrosomonas eutropha* in high-strength nitrogen wastewaters

Alexandra Fumasoli, Eberhard Morgenroth, Kai M. Udert

Water Research, 2015, 83, 161-170

Graphical abstract

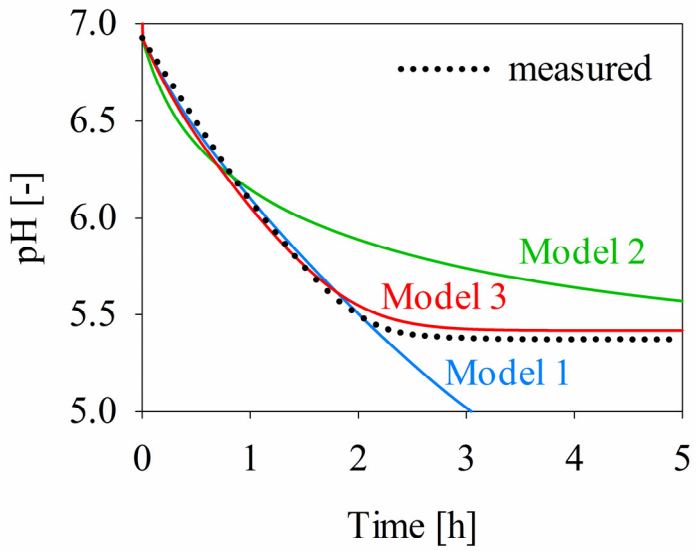

Model 1
Monod-type kinetics

Model 2
Monod-type kinetics and sigmoidal pH term

Model 3
Monod-type kinetics and exponential pH term

Abstract

In wastewater treatment, the rate of ammonia oxidation decreases with pH and stops very often slightly below a pH of 6. Free ammonia (NH_3) limitation, inhibition by nitrous acid (HNO_2), limitation by inorganic carbon or direct effect of high proton concentrations have been proposed to cause the rate decrease with pH as well as the cessation of ammonia oxidation. In this study, we compare an exponential pH term common for food microbiology with conventionally applied rate laws based on Monod-type kinetics for NH_3 limitation and non-competitive HNO_2 inhibition as well as sigmoidal pH functions to model the low pH limit of ammonia oxidizing bacteria (AOB). For this purpose we conducted well controlled batch experiments which were then simulated with a computer model. The results showed that kinetics based on NH_3 limitation and HNO_2 inhibition can explain the rate decrease of ammonia oxidation between pH 7 and 6, but fail in predicting the pH limit of *Nitrosomonas eutropha* at pH 5.4 and rates close to that limit. This is where the exponential pH term becomes important: this term decreases the rate of ammonia oxidation to zero, as the pH limit approaches. Previously proposed sigmoidal pH functions that affect large pH regions, however, led to an overestimation of the pH effect and could therefore not be applied successfully. We show that the proposed exponential pH term can be explained quantitatively with thermodynamic principles: at low pH values, the energy available from the proton motive force is too small for the NADH production in *Nitrosomonas eutropha* and related AOB causing an energy limited state of the bacterial cell. Hence, energy limitation and not inhibition or limitation of enzymes is responsible for the cessation of the AOB activity at low pH values.

Introduction

Ammonia oxidizing bacteria (AOB) release two moles of protons per mole of ammonia that is oxidized to nitrite. If the buffer capacity in the bulk solution is low, biological ammonia oxidation causes a substantial pH drop, which in turn affects the rate of ammonia oxidation. In wastewater treatment, ammonia oxidation decreases with pH and usually stops when the pH value drops below pH 6 (Painter 1986). However, the reasons for the rate decrease, but especially for the cessation of activity are not very well understood. There are also some exceptions in wastewater treatment where AOB have adapted to low pH environments and grew at pH values as low as 4 (Gieseke et al. 2006) or even below (Udert et al. 2005).

The pH dependence and the pH limit of AOB is usually not relevant for conventional wastewater treatment as most municipal wastewaters contain sufficient alkalinity to allow complete ammonia oxidation (Tchobanoglous et al. 2003). However, the pH dependence of AOB becomes important in wastewaters with a low alkalinity to ammonia ratio, such as human urine (Udert et al. 2003a) or digester supernatant (Van Hulle et al. 2007).

The pH has a crucial role during nitrification of these wastewaters, because it influences AOB and nitrite-oxidizing bacteria (NOB) differently and thereby determines whether nitrite or nitrate is the main nitrification product. The SHARON (Single reactor High activity Ammonia Removal Over Nitrite) process for instance is deliberately operated at pH values above 7 and temperatures of 30°C (Hellinga et al. 1999), because under these conditions AOB grow faster than NOB causing the wash out of the latter. In contrast, NOB should be retained in nitrification reactors with urine, when nitrified urine is further processed to a fertilizer product (Udert et al. 2015). To ensure that NOB are retained in the system, this process is operated at pH values as low as 6 or even below (Etter et al. 2013), where the growth rate of AOB is reduced strongly. Despite the low pH values, nitrite can accumulate in the system, which is a major problem for this process (Etter et al. 2013). Hence, a model that reliably predicts the rate of nitrite production by AOB at such low pH values would be of great benefit to understand and improve the process performance. Furthermore, as nitrite accumulation is usually a result of a dynamic change in the reactor pH (Etter et al. 2013), this model requires explicit pH calculations.

The growth rate of AOB decreases with pH, because at low pH values the actual substrate of AOB (Suzuki et al. 1974), NH_3 occurs only at very low concentrations even if the total ammonia (NH_4^+ and NH_3) concentration is high. AOB are also known to be inhibited by nitrous acid (HNO_2), the acid of their own product nitrite (NO_2^-) (Anthonisen et al. 1976). To account for the effects of NH_3 limitation and HNO_2 inhibition on the ammonia oxidation in digester supernatant, Hellinga et al. (1999) proposed a first kinetic expression. This rate law bases on a Monod term for NH_3 and a term for non-competitive inhibition by HNO_2.

Whereas Hellinga et al. (1999) were able to model their data by considering effects of NH_3 and HNO_2 only, Wett and Rauch (2003) found that limitation of total inorganic carbon (TIC) was the main reason for the decrease in ammonia oxidation at low pH values and that NH_3 limitation was often overestimated. TIC concentrations are generally low at low pH values, because its acid H_2CO_3 is formed, which volatilizes as CO_2 (pK_a value 6.35, Stumm and Morgan, 1996). According to their measurements, Wett and Rauch (2003) found that a

sigmoidal term for bicarbonate (HCO_3^-) was suitable to account for the effects of TIC limitation.

Besides an indirect effect of pH via the speciation of NH_3/NH_4^+ and NO_2^-/HNO_2 and H_2CO_2/HCO_3^-, pH has been suggested to influence AOB directly (Antoniou et al. 1990, Van Hulle et al. 2007, Wiesmann et al. 2006). Wiesmann et al. (2006) explained the direct pH effect for nitrifiers with protein damage, but they did not propose a model to account for this inhibition. Van Hulle et al. (2007) proposed a bell-shaped curve to model the pH dependency of AOB in the SHARON process and explained the effect by an increased demand for maintenance energy and the effect of pH on the structure and permeability of the cell membrane. Finally, Antoniou et al. (1990) attributed the direct pH effect of AOB to the pH dependence of the rate limiting enzyme. They suggested that the controlling enzyme is only active in a certain ionization state, which was expressed with a sigmoidal pH term. However, Antoniou et al. (1990) applied this model between pH 6.4 and 8.5, but not to values close to the pH limit. Furthermore, they did not consider indirect pH effects (e.g., the effect of NH_3 limitation).

Models to predict the low pH limit of bacteria, however, were the main focus of many studies from food microbiology in order to prevent microbial growth in foods and to ensure food safety. Presser et al. (1997) proposed to multiply the growth rate with an exponential pH inhibition term to model the deactivation of *Escherichia coli* under acidic conditions (e.g., after lactic acid fermentation). This exponential pH term bases on the experimental observation that the growth rate is fairly constant over a wide pH range and decreases only as the pH limit is approached.

The pH term proposed by Presser et al. (1997) is based on an empirical observation and is not built on first principles. However, the exponential pH term resembles the rate law proposed by Jin and Bethke (2002, 2007), who proposed to extend conventional Monod-type kinetics with a thermodynamic potential factor. This factor approaches 1, when the thermodynamic driving force is large, but it decreases to zero as the driving force depletes. The thermodynamic driving force is the difference between the energy available and the energy required to drive a particular reaction. The synthesis of ATP as well as of NADH are important reactions for the energy metabolism of AOB (Poughon et al. 2001). The energy required to synthesize ATP or NADH is derived from the proton motive force (Nicholls and Ferguson 1997), which is a transmembrane electrochemical gradient that results from the extrusion of protons from the cyto- to the periplasm during cellular respiration. Hence, the thermodynamic potential factor approaches zero, when the stored energy in the proton motive force is just enough to satisfy the energy requirements for ATP or NADH production.

Even though many studies focused on the pH influence on nitrifiers, only very few studies represent models that provide predictions of pH. The model by Hellinga et al. (1999) included pH calculations based on acid-base equilibria only. However, for a realistic modeling of pH in high strength wastewaters ion activity and complex formation have to be considered as well (Batstone et al. 2012). This is definitely the case for source-separated urine (Udert et al. 2003c). Accurate modeling of pH is a prerequisite for being able to predict the influence of low pH on nitrification.

In this study, we compared the exponential pH term from Presser et al. (1997) with commonly used mathematical expressions (Monod, non-competitive inhibition and sigmoidal pH dependency) to model the pH dependency and the low pH limit of AOB. The exponential pH term is explained quantitatively with bioenergetic calculations. The kinetic expressions were tested and compared with well-controlled batch experiments. To maximize the accuracy of the pH calculations, it was necessary to develop and validate a chemical speciation model, which includes ionic strength corrections and complex formation.

Experiments

Batch experiments

Batch experiments were conducted in a 2 L column reactor. The reactor was aerated with a constant air flux (1 $L \cdot min^{-1}$) controlled with a red-y GCR flowmeter (Vögtlin Instruments AG, Aesch, Switzerland). The air flux was chosen sufficiently high to enable good mixing conditions. Additionally the reactor was stirred magnetically at 500 rpm (RCT basic, Ika Labortechnik, Staufen, Germany). Shortly before the experiments, the Kaldnes® K1 biofilm carriers (0.75 L) were taken from an operating pilot-scale reactor for urine nitrification (see below). The temperature was controlled at 25 ± 0.1°C with a thermostat (F32, Julabo Labortechnik GmbH, Seelbach, Germany). The oxygen concentration remained above 6.3 $mg \cdot L^{-1}$ in all experiments.

The initial pH value of the solution was adjusted to 7 by adding a one-molar sodium hydroxide solution. During the batch experiments, pH was not adjusted, such that the lower pH limit was reached. The experiments lasted for 12 hours, except for two experiments (NH_4^+(a-b), Table 1), which lasted 22 hours. These time durations were chosen to make sure that the low pH limit was clearly reached. Experiments NH_4^+(a-b) lasted longer, because the rate of ammonia oxidation was slower, such that more time was required to reach the low pH limit. Samples were taken at constant time intervals until the pH limit was reached. Samples were immediately filtrated (0.45 µm, MN GF-5, Macherey–Nagel, Düren, Germany) and analyzed for total ammonia, total nitrite and nitrate. At the beginning and at the end of each batch experiment samples were taken to characterize the urine composition (for measured parameters see Table S1, supplementary information).

To investigate the influence of NH_3 we used five synthetic solutions (NH_4^+(a) to NH_4^+(e)) that contained initial total ammonia concentrations of 28, 42, 105, 310 and 1010 mg $N \cdot L^{-1}$. The total ammonia and total nitrite concentrations of the solutions at the beginning of the experiments are given in Table 1. The complete composition and the recipes for all synthetic solutions are given in Table S1 and S2 in the supplementary information. Nitrite was consumed by NOB during the experiments and was below the detection limit (0.1 mg $N \cdot L^{-1}$). Synthetic urine solutions were used, because this allowed us to freely vary total ammonia concentrations, which would not have been possible in real nitrified urine. We did not add nitrate to the synthetic urine solutions, as we aimed to follow the increase in nitrate during the experiments (not shown in this study) and the expected changes were too small to be detected with high background nitrate concentrations. To investigate the influence of HNO_2, we used five synthetic solutions (NO_2^-(a) to NO_2^-(e)) containing initial total nitrite concentrations of 28, 42, 105, 310 and 898 mg $N \cdot L^{-1}$

(Table 1 and Table S1, supplementary information). The total ammonia concentrations in these experiments were between 319 and 333 mg $N \cdot L^{-1}$. We also investigated the influence of nitrite in four experiments, where sodium nitrite was added to the effluent solution of a nitrification reactor operated with real urine (Etter et al. 2013). As the biodegradable organic substances are mostly degraded in the nitrification reactor, the real nitrified urine solutions contained hardly any biodegradable organic substances. The starting concentrations of total nitrite were between 50 and 208 mg $N \cdot L^{-1}$ and the total ammonia concentrations between 850 and 882 mg $N \cdot L^{-1}$, respectively (Real (a) to Real (d), Table S1, supplementary information). Furthermore, we investigated the pH limit in one experiment with suspended sludge in a real nitrified urine solution. This experiment was performed to see whether the model is directly applicable to a suspended sludge system (Suspended, Table S1, supplementary information).

Table 1: Composition of the synthetic solutions at the beginning of the batch experiments.

	NH_4-N $mg \cdot L^{-1}$	NO_2-N $mg \cdot L^{-1}$
NH_4^+(a)	35	0.7
NH_4^+(b)	69	1.0
NH_4^+(c)	145	0.8
NH_4^+(d)	333	2.1
NH_4^+(e)	1010	1.7
NO_2^-(a)	333	28.1
NO_2^-(b)	326	41.6
NO_2^-(c)	326	105
NO_2^-(d)	326	310
NO_2^-(e)	319	898

To investigate the influence of TIC, different gas mixtures were used to achieve a CO_2 partial pressure of 0, 5 and 10%. Synthetic air containing 20% O_2 and 80% N_2 was used for experiments without CO_2. Synthetic air with 10% CO_2, 18% O_2 and 72% N_2 was used for a partial CO_2 pressure of 10%. The two types of synthetic air were mixed with red-y GCR flowmeters (Vögtlin Instruments AG, Aesch, Switzerland) to obtain the CO_2 partial pressure at 5%. The synthetic and real nitrified urine solutions for the three experiment CO_2(a) to CO_2(c) contained total ammonia concentrations between 801 and 996 mg $N \cdot L^{-1}$ (Table S1, supplementary information) and total nitrite was mostly oxidized to nitrate (NO_3^-) by NOB during the experiments.

Titration

Titrations were performed to validate the chemical speciation model and to test which degree of complexity (ionic strength effects, number of complexation reactions) would be required. The pH range for titration was 4 to 8.5. We conducted the titration experiments in synthetic urine solutions (Table S1, supplementary information). The reactor contained 1 L of the solution. The initial pH of the solution was adjusted to pH 4. The pH was then increased by dosing a 1 $mol \cdot L^{-1}$ sodium hydroxide solution. The reactor was stirred magnetically at approximately 500 rpm and temperature was controlled at 25 ± 0.1°C. To prevent CO_2 uptake from ambient air due to

stirring, the headspace was flushed with N_2 gas during titrations. To investigate the influence of biomass on the buffer intensity, we added 0.375 mL of well drained Kaldnes® K1 biofilm carriers to the synthetic solution. Before adding the biofilm carriers to the reactor, they were washed three times with the same solution that was used for titration.

Analytical methods

Chloride, sulfate, phosphate, nitrate, potassium and sodium were analyzed with ion chromatography (IC, Metrohm, Herisau, Switzerland). Magnesium and calcium were determined with inductively coupled plasma optical emission spectrometry (ICP OES, Ciros, Spectro Analytical Instruments, Kleve, Germany). The total ammonia concentration was measured photometrically with cuvette tests (LCK 303, Hach-Lange, Berlin, Germany) or on a flow injection analyzer (FIA, Application Note 5220, FOSS, Hillerød, Denmark). Total nitrite was measured with FIA (Application Note 5200) or IC. TIC and total organic carbon (TOC) were measured with a TIC/TOC analyzer (IL550 OmniTOC, Hach-Lange, Berlin, Germany). The standard deviation for all measurements was below 4%.

To increase the accuracy of the pH data, we used two pH meters (pH-meter 605, Metrohm, Herisau, Switzerland) with two different pH electrodes (Sentix 41, WTW, Weilheim, Germany and 405-DXX-S8/225, Mettler-Toledo, Greifensee, Switzerland) for continuous pH measurement. The average of the two measurements was used for all calculations. The measurement of the two sensors differed maximally by 0.03 units. Both pH sensors were calibrated before each experiment in buffer solutions preheated to 25°C. O_2 was measured with a mobile WTW device (Oxi340, WTW, Weilheim, Germany). Temperature was measured with a Pt100 sensor (Pt100/4/Cl/.A, Endress & Hauser, Reinach, Switzerland). All data were recorded in 30 s intervals on a data logger (Memograph S, RSG40, Endress & Hauser, Reinach, Switzerland).

Pilot-scale reactor and characterization of ammonia-oxidizing population

The biomass for the batch experiments originated from a pilot-scale nitrification reactor (Etter et al. 2013). During the phase of batch experiments, the pH in the pilot reactor was between 5.6 and 6.2. Amplicon pyrosequencing analyses of the floc and biofilm fractions of the biomass (not shown) revealed that most of the autotrophic biomass was attached to the carriers. The biofilm carriers and not the suspended sludge were therefore used in the batch experiments. The biofilm carriers were used since the attached biomass could not be removed from the carrier material without destroying it.

To characterize the ammonia oxidizing population, a sample of two biomass carriers was taken from the reactor and stored at -20°C prior to molecular analysis. Metagenomic DNA was extracted from the carriers using the FastDNA SPIN Kit for Soil (MP Biomedicals, Santa Ana, CA, USA) with adaptation to manufacturer's protocol, and analyzed by Research and Testing Laboratory (Lubbock, TX, USA) for bacterial tag-encoded FLX amplicon pyrosequencing (bTEFAP) according to in-house protocol (Sun et al. 2011) a primer pair targeting the v1-v3 hypervariable region of the bacterial 16S rRNA gene pool (27F/518R) (Weissbrodt et al. 2012). A total number of 28145 reads was obtained in the sequencing set. The denoised sequencing datasets were processed and mapped against the Greengenes database of reference 16S rRNA

gene sequences (DeSantis et al. 2006) in the bioinformatics PyroTRF-ID workflow (Weissbrodt et al. 2012). The dominant sequences related to AOB were then retrieved out of the PyroTRF-ID annotation files and aligned against NCBI BLASTn (Altschul et al. 1997) in order to validate the taxonomic assignments at identity level. The relative abundances of AOB in the overall bacterial community covered by the primer pair were calculated as the amount of reads mapping with reference sequences of AOB compared to the total sequencing depth.

Models

Nitrification model

In the computer model biological processes and gas exchange as well as acid-base equilibria and complex formation were implemented. To calculate the chemical speciation reactions, the effect of ionic strength was considered for charged species, which means that we calculated in activities and not in concentrations. Activity coefficients were estimated from ionic strength according to the Davies approach as described in Stumm and Morgan (1996).

The biological processes growth and decay of AOB and NOB were included in the model. The growth and decay of heterotrophic bacteria were neglected in the model to decrease the complexity of the model and as the content of biodegradable organic substances was negligible low (Table 1, supplementary information). The stoichiometric matrix is given in Table 2. The main focus of this study was on the kinetic expression for AOB. To model the growth of AOB we used three kinetic approaches:

- Model 1 includes Monod terms for NH_3 and HNO_2 only (Hellinga et al. 1999):

$$r_{AOB} = \mu_{max,AOB} \cdot \frac{\{NH_3\}}{\{NH_3\}+K_{NH3,AOB}} \cdot \frac{K_{I,HNO2,AOB}}{\{HNO_2\}+K_{I,HNO2,AOB}} \cdot X_{AOB} \quad (1)$$

  where r_{AOB} is the rate of ammonia oxidation (g COD·L^{-1}·d^{-1}), μ_{max} the maximum growth rate (d^{-1}), $K_{NH3,AOB}$ the affinity constant for NH_3 (mol·L^{-1}), $K_{I,HNO2,AOB}$ the non-competitive inhibition constant for HNO_2 (mol·L^{-1}), and X_{AOB} the biomass concentration of AOB (g COD·L^{-1}). All constants are specified in Table 3.

- Model 2 is based on Monod terms for NH_3 and HNO_2 and a sigmoidal pH term (Antoniou et al. 1990, Jubany 2007):

$$r_{AOB} = \mu_{max,AOB} \cdot \frac{\{NH_3\}}{\{NH_3\}+K_{NH3,AOB}} \cdot \frac{K_{I,HNO2,AOB}}{\{HNO_2\}+K_{I,HNO2,AOB}} \cdot \frac{1}{1+\frac{10^{-pH}}{10^{-pK}}} \cdot X_{AOB} \quad (2)$$

  where pK is the lower half saturation constant for pH (Antoniou et al. 1990, Jubany 2007). The initial formula contains also an upper pK value for the enzyme inhibition at high pH values. However, for pH values below pH 7, this term can be neglected.

- Model 3 includes Monod terms for NH_3 and HNO_2 and an exponential pH term (Presser et al. 1997, Ratkowsky 2002):

$$r_{AOB} = \begin{cases} 0, & pH < pH_{min} \\ \mu_{max,AOB} \cdot \frac{\{NH_3\}}{\{NH_3\}+K_{NH3,AOB}} \cdot \frac{K_{I,HNO2,AOB}}{\{HNO_2\}+K_{I,HNO2,AOB}} \cdot (1-10^{(K_{pH}(pH_{min}-pH))}) \cdot X_{AOB}, & pH \geq pH_{min} \end{cases} \quad (3)$$

where pH_{min} is the minimal pH for growth, and K_{pH} a fitting parameter.

For the growth of NOB we used Haldane kinetics as proposed by Hellinga et al. (1999), which was also applied in Jubany (2007):

$$r_{NOB} = \mu_{max,NOB} \cdot \frac{\{HNO_2\}}{\{HNO_2\}+K_{HNO2,NOB}+\frac{\{HNO_2\}^2}{K_{I,HNO2,NOB}}} \cdot X_{NOB} \quad (4)$$

where $K_{HNO2,NOB}$ and $K_{I,HNO2,NOB}$ are the affinity and inhibition constant for HNO_2 ($mol \cdot L^{-1}$), respectively, and X_{NOB} the biomass concentration of NOB ($g\ COD \cdot L^{-1}$).

Decay of AOB and NOB was modeled according to Jubany (2007):

$$r_{Decay} = b \cdot X \quad (5)$$

where r_{Decay} is the decay rate ($g\ COD \cdot L^{-1} \cdot d^{-1}$), and b the decay coefficient (d^{-1}).

The gas exchange of CO_2 due to bubble aeration was included in the model as follows:

$$r_{CO_2} = H_{CO_2} \cdot (\{CO_2\} - \{CO_{2,Sat}\}) \cdot \frac{Q_{gas}}{V} \cdot (1 - e^{\frac{-KLa_{CO2} \cdot V}{Q_{gas} \cdot H_{CO2}}}) \quad (6)$$

where r_{CO2} is the rate of CO_2 volatilization ($mol \cdot L^{-1} \cdot d^{-1}$), H_{CO2} the Henry coefficient for CO_2 (1.2 $mol(g) \cdot mol(aq)^{-1}$, Stumm and Morgan 1996), $CO_{2,sat}$ the saturation concentration of CO_2 in the water phase in relation to the gas concentration in the inlet air ($mol \cdot L^{-1}$, section S2, supplementary information), Q_{gas} the controlled gas flow ($L \cdot d^{-1}$), V the liquid volume (L), and K_La_{CO2} the gas exchange coefficient for CO_2 (d^{-1}). K_La_{CO2} was estimated from K_La_{O2} based on the penetration theory and the assumption that the diffusion coefficient for CO_2 is 20% smaller than that for O_2 (section S2, supplementary information). The K_La_{O2} was estimated with experiments in deionized water with the same reactor configuration used for the batch experiments. NH_3 and HNO_2 volatilization were neglected, due to the low volatility and the low concentrations of both compounds.

The acid-base equilibria and complex formation reactions considered in the model are shown in Table 4. Chemical equilibria were modeled with back- and forward reactions (Udert et al. 2003c). As an example, Equation 7 shows the rate expression of the NH_3/NH_4^+ equilibrium:

$$r_{NH_3} = -r_{NH_4^+} = k_{eqNH_3} \cdot (\{NH_4^+\} - \{NH_3\} \cdot \{H^+\} \cdot 10^{pK_{NH_3}}) \quad (7)$$

where r_{NH3} and r_{NH4+} are the rate of NH_3 and NH_4^+ production ($mol \cdot L^{-1} \cdot d^{-1}$), respectively, and k_{eqNH3} the rate constant for equilibrium (d^{-1}). The value of all equilibrium rate constants was $10^6\ L \cdot mol^{-1} \cdot d^{-1}$ and thereby much larger than any other kinetic constant in the model.

Table 2: Stoichiometric matrix for bacterial growth and decay of AOB and NOB. The parameters are specified in Table 3.

Parameter	X_{AOB} g COD	X_{NOB} g COD	O_2 mol	NH_3 mol	HNO_2 mol	NO_3 mol	CO_2 mol	H^+ mol
AOB								
Aerobic growth	1		$(1-48/Y_{AOB})/32$	$-1/Y_{AOB}-i_N$	$1/Y_{AOB}$		$-i_C$	
Decay	-1		-1/32	i_N			i_C	
NOB								
Aerobic growth		1	$(1-16/Y_{NOB})/32$	$-i_N$	$-1/Y_{NOB}$	$1/Y_{NOB}$	$-i_C$	$1/Y_{NOB}$
Decay		-1	-1/32	i_N			i_C	

Table 3: Kinetic parameter for microbial growth and decay of AOB and NOB included in the computer models.

Parameter		Value	Unit	Reference
Nitrogen fraction of biomass	i_N	0.00625	mol N·g COD^{-1}	assumed composition
Carbon fraction of biomass	i_C	0.03125	mol C·g COD^{-1}	of biomass: $C_5H_7O_2N$
AOB				
Maximal growth rate	$\mu_{max,AOB}$	1.21	d^{-1}	Jubany (2007)
Decay rate	b_{AOB}	0.20	d^{-1}	Jubany (2007)
Growth yield	Y_{AOB}	2.52	g COD·mol N^{-1}	Jubany (2007)
NH_3 affinity constant	$K_{NH3,AOB}$	$5.36\cdot10^{-5}$	$mol\cdot L^{-1}$	Van Hulle et al. (2007)
HNO_2 inhibition constant	$K_{I,HNO2,AOB}$	$1.46\cdot10^{-4}$	$mol\cdot L^{-1}$	Van Hulle et al. (2007)
Constant (Model 2)	pK	6.78	-	Jubany (2007)
Constant (Model 3)	K_{pH}	2.3	-	Fitted
NOB				
Maximal growth rate	$\mu_{max,NOB}$	1.02	d^{-1}	Jubany (2007)
Decay rate	b_{NOB}	0.17	d^{-1}	Jubany (2007)
Growth yield	Y_{NOB}	1.12	g COD·mol N^{-1}	Jubany (2007)
HNO_2 affinity constant	$K_{HNO2,NOB}$	$1.70\cdot10^{-7}$	$mol\cdot L^{-1}$	Jubany (2007)
HNO_2 inhibition constant	$K_{I,HNO2,NOB}$	$9.57\cdot10^{-6}$	$mol\cdot L^{-1}$	Jubany (2007)

The computer model was implemented in the simulation environment AQUASIM (Reichert 1994). For parameter estimation, we used the secant algorithm implemented in AQUASIM. K_{pH} was the only fitted kinetic parameter. Furthermore, the initial AOB concentration (X_{AOB}) was fitted to the measured pH values and the initial NOB concentration (X_{NOB}) to the measured total nitrite concentrations for each experiment. The estimated parameters and the standard errors for K_{pH} and the initial AOB concentrations are given in Table S4 of the supplementary information. The affinity and inhibition constants for NH_3 and HNO_2 were taken from Van Hulle et al. (2007), because the biomass in our experiments was exposed to similar reactor conditions, and because it was close to the expected NH_3 affinity constant based on the analysis of the biomass (see above). All other growth parameters (Table 3) were taken from Jubany (2007) without further validating these values.

Table 4: Acid-base equilibria and complex formation included in the computer models. All values are given for 25°C and zero ionic strength.

Equation	pK_a
Acid-Base equilibria	
$HCO_3^- \rightleftharpoons CO_3^{2-} + H^+$	10.33[a]
$H_2CO_3 \rightleftharpoons HCO_3^- + H^+$	6.35[a]
$NH_4^+ \rightleftharpoons NH_3 + H^+$	9.24[a]
$HNO_2 \rightleftharpoons NO_2^- + H^+$	3.25[b]
$H_3PO_4 \rightleftharpoons H_2PO_4^- + H^+$	2.15[a]
$H_2PO_4^- \rightleftharpoons HPO_4^{2-} + H^+$	7.20[a]
$HPO_4^{2-} \rightleftharpoons PO_4^{3-} + H^+$	12.38[a]
$HSO_4^- \rightleftharpoons SO_4^{2-} + H^+$	1.99[a]
$H_2O \rightleftharpoons OH^- + H^+$	14.00[a]
Complex formation	
$K^+ + H_2PO_4^- \rightleftharpoons KH_2PO_4$	-0.30[a]
$K^+ + H_2PO_4^- \rightleftharpoons KHPO_4^- + H^+$	6.30[a]
$2\ K^+ + H_2PO_4^- \rightleftharpoons K_2HPO_4 + H^+$	6.07[a]
$K^+ + SO_4^{2-} \rightleftharpoons KSO_4^-$	-0.85[a]
$Na^+ + H_2PO_4^- \rightleftharpoons NaH_2PO_4$	-0.30[a]
$Na^+ + H_2PO_4^- \rightleftharpoons NaHPO_4^- + H^+$	6.13[a]
$2\ Na^+ + H_2PO_4^- \rightleftharpoons Na_2HPO_4 + H^+$	6.25[a]
$Na^+ + SO_4^{2-} \rightleftharpoons NaSO_4^-$	-0.74[a]
$NH_4^+ + H_2PO_4^- \rightleftharpoons NH_4H_2PO_4$	-0.10[c]
$NH_4^+ + HPO_4^{2-} \rightleftharpoons NH_4HPO_4^-$	-1.30[c]
$NH_4^+ + SO_4^{2-} \rightleftharpoons NH_4SO_4^-$	-1.03[a]

[a] thermo_minteq.dat, standard database in Visual MINTEQ (Gustafsson 2012)
[b] Lide (2009)
[c] Martell et al. (1997)

Conceptual metabolic model

Jin and Bethke (2002, 2007) proposed a rate law of the form:

$$r = r_+ \cdot F_T \tag{8}$$

with r the net rate of the overall reaction (forward minus reverse rate), r_+ the forward reaction rate, and F_T the thermodynamic potential factor. Equation 8 is based on the concept that every chemical reaction can be written as a forward and reverse reaction, and that the equilibrium (r = 0) is reached once the forward and reverse reaction rates are in balance. During the dissolution and precipitation of minerals, for instance, this equilibrium is reached when the reaction's ion activity product Q and the equilibrium constant K are equal. In the electron transfer chain of bacteria the overall reaction rate becomes zero, if the energy stored in the proton motive force just equals the energy required for ATP or NADH production.

F_T depends on the thermodynamic drive f, which can be expressed as:

$$F_T[-] = 1 - 10^{\left(-\frac{f}{\ln(10)\chi RT}\right)} \quad (9)$$

where f the thermodynamic driving force [J·mol^{-1}], χ a stoichiometric factor [-], R the universal gas constant [8.314 J·K^{-1}·mol^{-1}], and T the temperature [K]. The thermodynamic drive f can be expressed as:

$$f = mF\Delta p - \Delta G \quad (10)$$

where ΔG the Gibbs free energy change of the critical reaction in the electron transfer chain [J·mol^{-1}], m the protons translocated from the peri- to the cytoplasm [-], F the Faraday constant [96485 J·mol^{-1}·V^{-1}], Δp the proton motive force [V].

Aerobic bacteria transfer electrons from a substrate to O_2 through the electron transfer chain, during which protons are exported from the cyto- to the periplasm. The translocated protons result in a transmembrane electrochemical gradient: the proton motive force. The energy from the re-entry of protons from the peri- to the cytoplasm, (mFΔp) can then be used for the synthesis of ATP and NADH. If the energy from the re-entry of protons is far higher than the ΔG required for ATP or NADH synthesis then f is large and F_T approaches 1. However, F_T decreases to zero or to negative values as mFΔp is equal or below the ΔG required for ATP or NADH synthesis.

Results

pH limit of nitrification

Simulations of pH for all experiments are shown in Figure 1. The pH value can be used directly to quantify the activity of AOB, because protons are released during ammonia oxidation. However, to be able to interpret the pH data quantitatively, the chemical speciation model must represent the effect of proton release on the pH value accurately. The chemical speciation model is discussed in the following section.

Model 1 (Monod-type kinetics) is capable of representing pH values above pH 6, but the model completely fails to predict the course of the pH values below and the pH limit (Figure 1, first row). Whereas the decrease in pH stops in the experimental data, the modeled pH keeps decreasing. In the model, it is not possible to stop the pH decrease by increasing the decay rate. Based on the model, biomass decay increases the pH, because the base NH_3 is released (Table 2). However the sharp bend in the pH curve close to the pH limit cannot be represented, even by adapting the decay coefficient (b_{AOB}). To fit the initial biomass concentrations only pH values between 7 and pH 5.8 for NH_4^+(a-e) and between 7 and 6 for NO_2^-(a-e) were used for Model 1. Fitting the whole pH range did not improve the poor ability of this model to represent the pH limit.

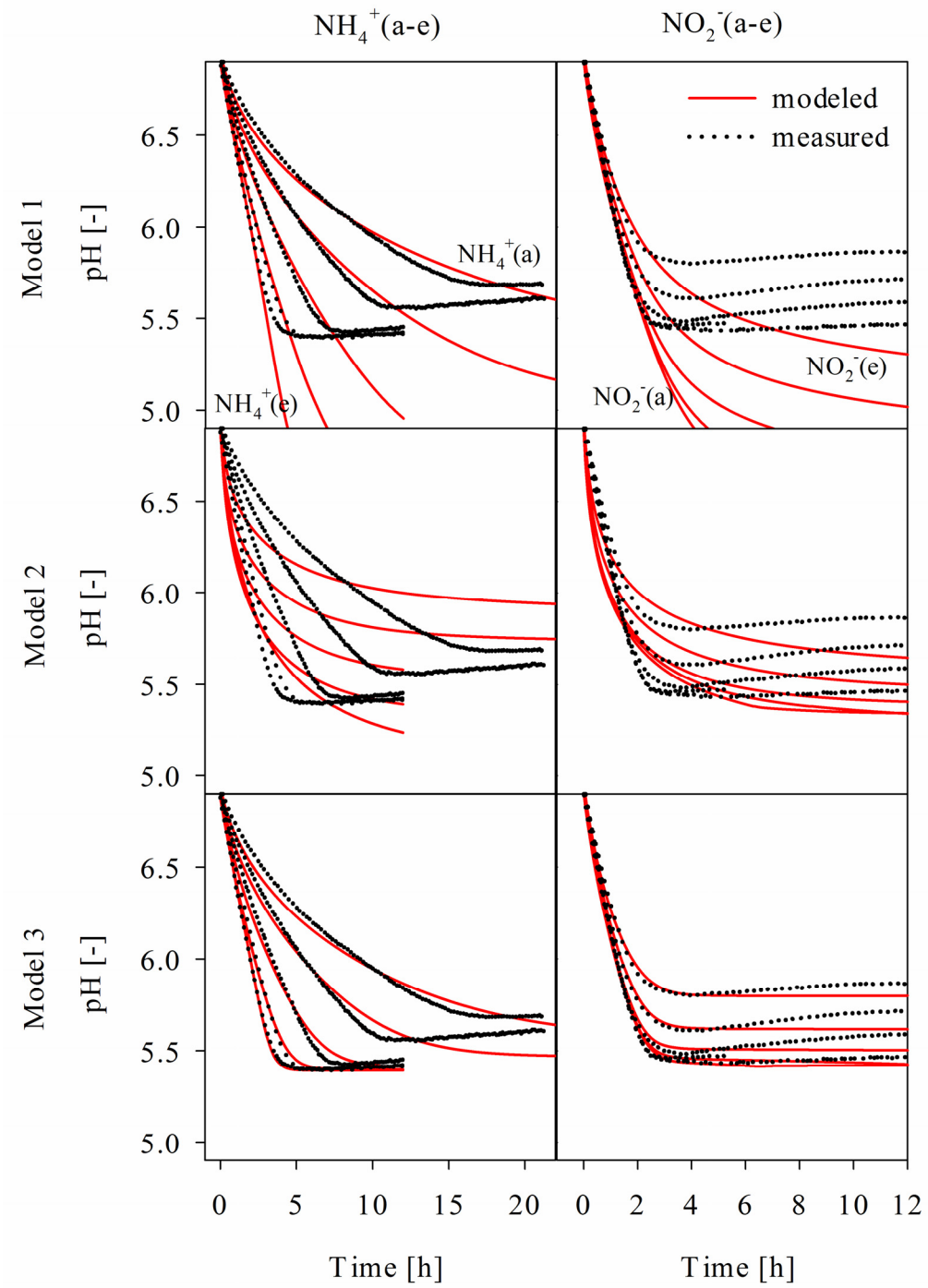

Figure 1: Measured and simulated pH values for ten different experiments with synthetic solutions, the five experiments NH_4^+(a-e) containing different total ammonia concentrations and the five experiments NO_2^-(a-e) containing different total nitrite concentrations. Measured pH values (dotted) for NH_4^+(a-e) are depicted in all Figures of the left column, whereas the ones for NO_2^-(a-e) are depicted in the right column. Three models with different kinetic expressions for the growth of AOB were tested and model simulations for Model 1 to 3 are shown in row 1 to 3.

The modeled decrease in pH in Model 2 (Monod-type kinetics and sigmoidal pH term) is overestimated in the beginning and then underestimated (Figure 1, second row). Between the

pH values of 7 and 6, the course of pH can be fitted well, if no sigmoidal pH term is used (Model 1). In the latter case, the activity decrease is only due to NH_3 limitation at lower pH values. Including the sigmoidal pH term results in an overestimation of the pH effect. Model 2 also fails to predict a complete process stop. Fitting of the parameter pK in Model 2 (Table 3) does not improve the fit of the data.

Model 3 (Monod-type kinetics and exponential pH term) fits the data considerably better than Model 1 and 2 (Figure 1, third row). Except from NH_4^+(a) and NH_4^+(b) Model 3 is also well suited to model the pH limit. In contrary to Model 2, the pH term in Model 3 affects the rate of AOB only at pH values below pH 6. In fact, this pH term decreases the rate of AOB sharply to zero as the pH limit is approaching. At pH values above pH 6 Model 3 is similar to Model 1. A value of 2.3 was fitted for K_{pH} in Model 3. The fitted initial biomass concentration for AOB were 0.09 ± 0.03 g COD·L^{-1} for Model 3 (Table S4, supplementary information), which is close to the AOB biomass concentration of 0.14 g COD·L^{-1} that can be calculated by assuming a biomass concentration of 1 g COD·L^{-1}, which was estimated for a similar reactor (Uhlmann 2014), and a relative AOB abundance of 14% (see below).

To model the pH limit of AOB in the experiments NO_2^-(a-e), we introduced a linear relationship for pH_{min} with the HNO_2 concentration (mol·L^{-1}):

$$pH_{min} = \frac{\{HNO_2\}+0.002}{0.00037} \tag{11}$$

This relationship was introduced, because the HNO_2 concentrations and the pH limit showed a linear correlation (Figure 2). This correlation was reproducible: a similar correlation was observed in four experiments in real nitrified urine with different amounts of nitrite added, and five experiments in synthetic nitrified urine (Figure 2, Table S3 supplementary information).

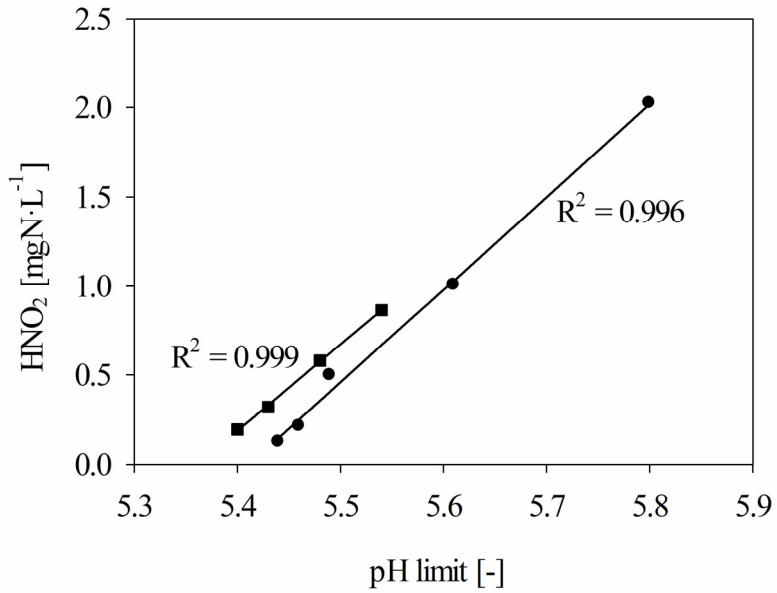

Figure 2: Calculated concentrations of HNO_2 at the observed pH limit for *Nitrosomonas eutropha*. Each of the dots represents the endpoint of one experiment (■: experiments in real nitrified urine solutions, ● experiments in synthetic urine solutions).

The model was set up as a suspended growth model, but was applied for a biofilm system. At high conversion rates, e.g. at the beginning of the experiment NH_4^+(d) and NH_4^+(e), oxygen may have been limiting in the biofilm. However, oxygen limitation did not have an influence on the pH end-point (Figure S4, supplementary information), when ammonia conversion rates became very low. To prove that the model is not restricted to biofilm systems, we fitted experimental data from an experiment with suspended sludge with Model 3 with the same parameter set (except from the initial biomass concentration X_{AOB}, Figure S5, supplementary information). Also in this case Model 3 was suited to represent the measured data within the pH range of 7 to the pH limit. The experiment with suspended sludge was performed in a real nitrified urine solution, proofing that the model approach for AOB can be directly applied to real urine solutions.

The pH limit was also investigated at higher TIC concentrations. In two experiments with increased CO_2 in the aeration air the pH limit was at 5.36 (10% CO_2) and 5.37 (5% CO_2), which is only slightly lower than the pH limit observed at 5.46 in an experiment without CO_2 in the aeration (Table S3, supplementary information). Assuming an equilibrium of CO_2 between water and air phase, the TIC concentration would correspond to 23 and 46 mg $C \cdot L^{-1}$ for the aeration with 5 and 10% CO_2, respectively. This is far more than during the experiment with synthetic aeration without CO_2, where TIC concentrations were far below the detection limit (4 mg $C \cdot L^{-1}$). Due to the very different TIC concentrations at the pH limit, this parameter cannot explain the pH limit.

Chemical speciation model as basis for predicting pH

Titration experiments were performed to validate the chemical speciation model. A high reliability of the pH modeling was required, because pH was used to calculate the AOB activity in the batch experiments (previous section). Figure 3 shows the calculated and measured buffer intensity from a titration experiment with the synthetic urine solution NH_4^+(a) (Table S1, supplementary information). The buffer intensity ($\beta = dC_b/dpH$, with C_b the concentration of strong base in $mol \cdot L^{-1}$) describes the tendency of a solution at any point of the titration curve to change the pH upon addition of an acid or base (Stumm and Morgan 1996). Modeled and observed buffer intensities correspond well, if acid-base equilibria, ionic strength and complex formation reactions are taken into account (Figure 3 and Figure S1 to S3, supplementary information). An in-depth discussion of the model development is given in the supplementary information.

Besides dissolved compounds also biomass may act as a buffer (Batstone et al. 2012, Westergreen et al. 2012). However, the overall effect of biomass was low, which resulted in very similar measured buffer intensities in experiments with and without biofilm carriers (Figure 3). To keep the complexity of the model low and to prevent the introduction of additional fitting parameters, we did not include biomass buffering into our model.

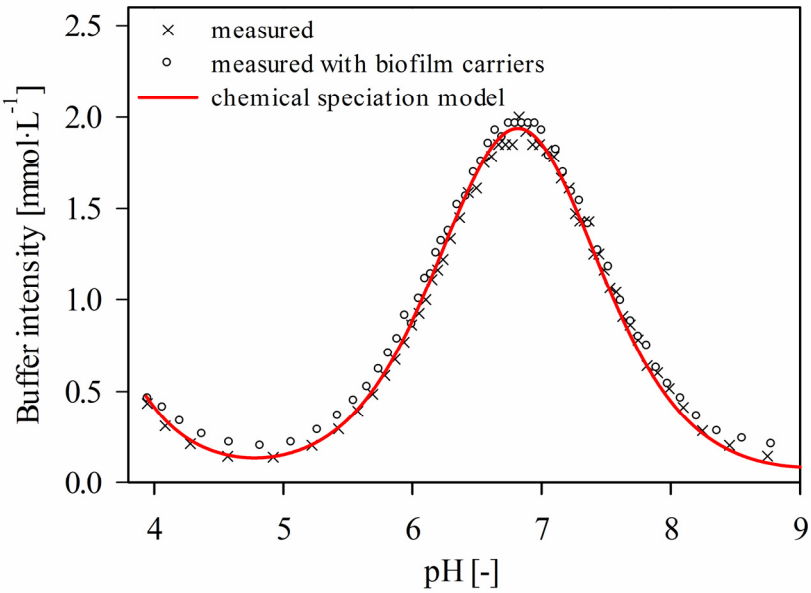

Figure 3: Measured buffer intensity of a synthetic urine solution with phosphate as buffer system (NH_4^+(a), Table S1, supplementary information) with and without biomass. The line represents the model prediction.

Characterization of the ammonium-oxidizing bacteria

According to the 16S rRNA gene-based amplicon pyrosequencing analysis conducted with the v1-v3 universal bacterial primers, the AOB populations present on the biomass carriers of the pilot-scale reactor predominantly affiliated with the *Nitrosomonas europaea/Nitrosococcus mobilis* lineage. A relative abundance of 77% of the reads of the AOB guild affiliated with the *Nitrosomonas eutropha* strain C71 (GenBank acno. AAJE01000012) and strain C91 (GenBank acno. NC008344) as the closest cultured relatives with a sequence identity of 98%. AOB accounted for 14% of the overall bacterial community (corresponding to 3930 reads).

The high abundance of *Nitrosomonas eutropha* in urine is not surprising as *Nitrosomonas eutropha* are often selected in high salt and high ammonia environments. The affinity constant for ammonia ranges between 0.42 and 0.85 $mgNH_3\text{-}N\cdot L^{-1}$(Koops and Pommerening-Röser 2001). The NH_3 affinity constant for NH_3 of 0.75 $mgNH_3\text{-}N\cdot L^{-1}$ that was used in the model simulations lies within this range (Van Hulle et al. 2007, Table 3).

Discussion

Bioenergetic considerations

The activity of AOB ceases, when the proton motive force is too small for ATP or NADH production (see section "Conceptual metabolic model"). NADH is required for many essential reductive biosynthesis pathways e.g., the capture of CO_2 (Ferguson et al. 2007), however, the production of NADH gets energetically more challenging at lower pH values (see below). The reduction of NAD^+ is coupled to the oxidation of ubiquinol (UQH_2) to ubiquinone (UQ), which can be written as:

$$NAD^+ + UQH_2 \rightleftharpoons NADH + UQ + H^+ \quad (12)$$

The ΔG° of this reaction is 113 kJ·mol^{-1} (25°C, Nicholls and Ferguson 1997). According to equation 12, the actual Gibbs free energy change ΔG depends on the concentration ratios of NAD^+/NADH and UQ/UQH_2, respectively. Furthermore it depends on the intracellular pH, as protons are released to the cytoplasm during NADH production:

$$\Delta G = \Delta G° + \ln(10) \cdot R \cdot T \cdot (\log\left(\frac{UQ \cdot NADH}{UQH_2 \cdot NAD^+}\right) - pH_{in}) \quad (13)$$

It was experimentally observed for *Nitrosomonas europaea* that the intracellular pH decreases with the extracellular pH (Kumar and Nicholas 1983). From the measured data in Kumar and Nicholas (1983), we derived a linear correlation for pH_{in} with pH_{out}:

$$pH_{in} = 0.6 \cdot pH_{out} + 2.7 \quad (14)$$

Hence, as pH_{in} correlates with pH_{out}, the ΔG for NADH production will be higher and therefore energetically less favorable at lower extracellular pH values.

Equations 13 and 14 can be substituted into equation 9 to calculate the thermodynamic potential factor (equation 15). This new equation depends on constants as well as on pH_{out}, which is similar to the pH term used in Model 3 (Presser et al. 1997):

$$F_T = 1 - 10^{\left(\frac{0.6}{\chi}\left(\frac{1}{0.6}\left(\frac{\Delta G° - m \cdot F \cdot \Delta p}{\ln(10) \cdot R \cdot T} + \log\left(\frac{UQ \cdot NADH}{UQH_2 \cdot NAD^+}\right) - 2.7\right) - pH_{out}\right)\right)} = 1 - 10^{(K_{pH}(pH_{min} - pH_{out}))} \quad (15)$$

from equation 15 K_{pH} and pH_{min} can be estimated as:

$$K_{pH} = \frac{0.6}{\chi} \quad (16)$$

and

$$pH_{min} = \frac{1}{0.6}\left(\frac{\Delta G° - m \cdot F \cdot \Delta p}{\ln(10) \cdot R \cdot T} + \log\left(\frac{UQ \cdot NADH}{UQH_2 \cdot NAD^+}\right) - 2.7\right. \quad (17)$$

To estimate K_{pH}, we assumed a stoichiometric coefficient χ of 0.248, as 0.248 moles of e^- are transferred from UQH_2 to NADH, when one mole of NH_3 is oxidized (Poughon et al. 2001). From equation 16, a K_{pH} of 2.4 can be estimated, which is almost identical to the fitted value of 2.3 in our experiments (Table 3).

To estimate pH_{min}, a proton motive force of 150 mV was assumed. This value was measured with little deviation for *Nitrosomonas europaea* over a wide pH range (Kumar and Nicholas 1983). It was assumed that m corresponds to 4, as four protons re-enter the cytoplasm through the reversed complex I of the electron transfer chain in AOB, when one mole of NADH is produced (Poughon et al. 2001), which agrees with the current evidence that the proton translocation stoichiometry for complex I is $4H^+/2e^-$ (Nicholls and Ferguson 1997). A pH_{min} of 5.4 can be estimated from equation 17, by assuming that NAD^+/NADH = 644 (Zhang et al. 2002) and UQ/UQH_2 = 0.1. The chosen NAD^+/NADH ratio of 644 is at the upper range of the reported NAD^+/NADH ratios (Lin and Guarente 2003), whereas the estimated UQ/UQH_2 ratio

of 0.1 is close to the reported minimal measured UQ/UQH_2 ratio of 0.25 in *Escherichia Coli* (Bekker et al. 2007). Even though the exact concentration ratios are not known, it is thermodynamically consistent that the NAD^+/NADH ratio approaches a minimal and the UQ/UQH_2 a maximal ratio in order to keep the NADH production feasible as long as possible.

We observed in our experiments that pH_{min} increased with higher HNO_2 concentrations (Figure 2). HNO_2, such as other small, uncharged molecules (e.g., lactic acid) penetrates the cell membrane, dissociates in the intracellular space and with that decreases the intracellular pH (Mortensen et al. 2008). A faster decrease in the internal pH decreases the thermodynamic feasibility of the NADH production (equation 13) and causes a faster depletion of energy. Vice versa, if AOB keep the internal pH at higher levels, the thermodynamic feasibility of the NADH production would be increased, allowing for lower pH_{min}. It is known that acid-tolerant bacteria have mechanisms to keep their cell internal pH closer to neutrality than the external pH value (pH homeostasis) (Slonczewski et al. 2009). pH homeostasis could therefore be an important feature of acid-tolerant AOB (Gieseke et al. 2006, Udert et al. 2005) growing at pH values below pH 5.4.

It is stunning how well the fitted pH term (equation 3) can be derived from bioenergetics principles, the general knowledge on energy metabolism in *Nitrosomonas europaea* and reported literature values. This is a strong indication that the pH limit observed for *Nitrosomonas eutropha*, which closely relates to *Nitrosomonas europaea*, is due to energy limitations connected to the proton transfer. For a complete proof of this concept, future studies should focus on the actual measurement of the parameter values that were taken from literature (e.g., proton motive force, intracellular pH, the concentration ratios of NAD^+/NADH and UQ/UQH_2).

Energy limitation

In previous studies it has been hypothesized that the pH limit of AOB is due to protein unfolding (Wiesmann et al. 2006), or membrane damage (Van Hulle et al. 2007). Low pH values can indeed compromise membrane stability and a prolonged decrease in the intracellular pH can lead to acid induced protein unfolding as well as DNA damages (Lund et al. 2014, Slonczewski et al. 2009). However, to prevent the detrimental effects of low intracellular pH values, most of the bacteria maintain a certain degree of pH homeostasis even in pH ranges, which do not allow for growth (Slonczewski et al. 2009). The pH range in which bacteria can survive without growth is therefore usually larger than the pH range where they can actually grow (Lund et al. 2014). Hence, it is unlikely that the pH limit of *Nitrosomonas eutropha* observed at a pH value close to 5.4 (Figure 1) is due to membrane, protein or DNA damages. We also observed that that the nitrification rate recovered quickly as soon as the pH was increased (results not shown), which is in line with the theory that AOB are de-energized at the pH limit, but can be reactivated at higher pH values.

However, AOB were not reactivated if the pH increased only very slightly after reaching the pH limit (Figure 1). We assume that the slight pH increase in the experiments is due to biomass decay. The pH increase was stronger for the experiments NO_2^-(a-e) than NH_4(a-e), which could be due to the increased HNO_2 concentrations: HNO_2 is known to increase the decay of activated sludge (Wang et al. 2013). Model 3 cannot represent this pH increase, because the rate of

ammonia oxidation increases with the pH increase and returns the pH immediately back to the pH limit. In reality, however, it seems that such a small pH increase is not sufficient to reactivate the cell.

Implications for nitrification models

Nitrification of low buffered wastewaters is a very dynamic process, because the growth rate of AOB depends strongly on pH, but the pH is likely to change due to the low buffer intensity in these wastewaters. In urine, already small pH changes can outcompete NOB, which ends in an irreversible process failure as shown for laboratory reactors (Udert and Wächter 2012) and pilot reactors (Etter et al. 2013). Nitrification models to describe such dynamic nitrification systems need therefore to accurately represent (1) the pH itself (chemical speciation), and (2) the pH dependent growth rates.

Only a few studies set up nitrification models that include explicit pH calculations based on acid-base equilibria (e.g., Hellinga et al. 1999). However, the results of the current study show that at least the effects of ionic strength must be included for a realistic pH calculation in urine (Figure S1-S3, supplementary information), as well as in digester supernatant due to the similar ionic strength (e.g., 0.16 $mol \cdot L^{-1}$, O'Neal and Boyer 2013 compared to 0.1 $mol \cdot L^{-1}$ in the urine solutions of this study). In general, titration experiments are a powerful tool to investigate the accuracy and the degree of complexity that is required for the chemical speciation model.

To model the pH dependency of AOB different kinetic expressions have been developed. Hellinga et al. (1999) set up a model based on NH_3 limitation and HNO_2 inhibition only and calibrated this model for a pH range of 6.5 to 8.5. Our model simulations were in agreement with the model proposed by Hellinga et al. (1999): between pH 6 and 7, this model was sufficient to describe the ammonia oxidation in urine (Figure 1). A direct pH term was only required at pH values below pH 6 in our simulations. This finding is in contrast with other studies for high strength nitrogen wastewaters, where sigmoidal or bell-shaped pH terms have been proposed (Antoniou et al. 1990, Claros et al. 2013, Jubany 2007, Van Hulle et al. 2007). The pH terms in the latter studies decrease the rate of ammonia oxidation strongly between pH 7 and 6.

To investigate the influence of pH within a range of 5 to 9 and 6 to 9 respectively, Van Hulle et al. (2007) and Claros et al. (2013) used solutions with total ammonia concentrations between 500 to 1100 $mgN \cdot L^{-1}$. It was assumed that this was sufficient to prevent any limitation of NH_3. However, considering an affinity constant of 0.75 $mgN \cdot L^{-1}$ (Van Hulle et al. 2007), limitation of NH_3 causes a decrease in AOB activity from 88% at pH 7 to 42% at pH 6 (25°C, 1000 $mgNH_4\text{-}N \cdot L^{-1}$), which is very close to the observed drop in activity in Van Hulle et al. (2007) and Claros et al. (2013). Hence, limitation of NH_3 and not a pH inhibition can explain the observed activity drop.

After being able to model pH adequately and after successful implementation of the pH dependency of AOB in the urine nitrification model, future studies should focus on the calibration and validation of the further kinetic parameters used to model AOB and NOB growth in urine, e.g. the maximal growth rates (Table 3).

Conclusion

- *Nitrosomonas eutropha*, which are abundant in high strength nitrogen wastewaters show a pH limit close to 5.4. This limit and rates close to the limit cannot be explained or modeled with kinetics based on NH_3 and TIC limitation, or HNO_2 inhibition. Nitrification models based on Monod-type kinetics are therefore not suitable to understand and improve the process stability of nitrification reactors that are operated between pH 6 and the pH limit (e.g., nitrification reactors with urine). For reactors operated close to the pH limit, the reaction rate of AOB has to be extended by a direct pH term. The pH term decreases the rate of ammonia oxidation to zero as the pH drops below pH 6.
- The applied pH term bases on bioenergetic principles: as soon as the critical reaction in the electron transfer chain (NADH production) is thermodynamically not feasible, the growth rate becomes zero. This term might not only be suitable to model the low pH limit of *Nitrosomonas eutropha*, but for many other bacteria growing close to their thermodynamic pH limits.
- For nitrification reactors operated between pH 7 and 6 no additional pH term is required in the growth rate of AOB. The introduction of an additional pH term (e.g., as sigmoidal pH function) leads to an underestimation of the rate of ammonia oxidation, which is detrimental for the design of nitrification systems.

Acknowledgement

This study was funded by the Bill and Melinda Gates Foundation and was conducted as part of the VUNA project (www.vuna.ch, Grant No. OPP1011603). The authors like to thank Chris Brouckaert (Pollution Research Group, University of KwaZulu-Natal) for the helpful discussion about modeling chemical speciation. We also thank David G. Weissbrodt and George F. Wells for their help with the biomass analysis, Bastian Etter for setting up a pilot-scale nitrification reactor, Karin Rottermann and Claudia Bänninger for the chemical analyses and Patrick Rambosson for the laboratory support.

Supporting Information for Chapter 2

Modeling the low pH limit of *Nitrosomonas eutropha* in high-strength nitrogen wastewaters

Alexandra Fumasoli, Eberhard Morgenroth, Kai M. Udert

Water Research, 2015, 83, 161-170

S1 Urine solutions

For the batch experiments we used synthetic as well as real nitrified urine solutions. The compositions of the solutions are given in Table S1. Compared to the synthetic urine solutions, the real nitrified urine solutions contained high concentrations of nitrate and a low amount of organic substances. The concentrations of total organic substances remained constant during the experiments with the real nitrified urine solutions indicating that the organic substances were hardly biodegradable. The recipes for all batch experiments with synthetic solutions are given in Table S2.

Table S1: Concentrations in synthetic and real nitrified urine solutions used in the titration and in the batch experiments. The standard deviation for all measurements was below 4%.

		Concentrations [mg·L^{-1}]											
Experim.	Solution	NH_4^+-N	NO_2^--N	NO_3^--N	SO_4^{2-}	PO_4^{3-}-P	Na^+	K^+	Cl^-	Ca^{2+}	Mg^{2+}	TIC	TOC
Titration:													
NH_4^+(a)	synthetic with biomass	0.8	<0.1	<1	429	106	1230	918	2460	<4	<4	<4	n. m.
NH_4^+(a)	synthetic	0.16	<0.1	<1	418	107	1160	890	2420	<4	<4	<4	n. m.
NH_4^+(e)	synthetic	968	<0.1	<1	426	109	85	353	2510	<4	<4	<4	n. m.
NO_2^-(e)	synthetic	318	905	<1	1120	111	1280	932	237	<4	<4	<4	n. m.
Batch experiments:													
NH_4^+(a)	synthetic	35	0.7	34.7	466	117	1390	958	2450	<4	<4	<4	n. m.
NH_4^+(b)	synthetic	69	1.0	29.7	430	113	1310	981	2420	<4	<4	<4	n. m.
NH_4^+(c)	synthetic	145	0.8	34.5	433	113	1190	960	2430	<4	<4	<4	n. m.
NH_4^+(d)	synthetic	333	2.1	34.8	449	114	865	918	2430	<4	<4	<4	n. m.
NH_4^+(e)	synthetic	1010	1.7	34.4	419	113	200	409	2450	<4	<4	<4	n. m.
NO_2^-(a)	synthetic	333	28.1	34.2	1070	101	1340	965	2660	<4	<4	<4	n. m.
NO_2^-(b)	synthetic	326	41.6	34.6	1050	105	1320	970	2250	<4	<4	<4	n. m.
NO_2^-(c)	synthetic	326	105	30.5	1050	98	1310	960	2370	<4	<4	<4	n. m.
NO_2^-(d)	synthetic	326	310	25.5	1080	103	1250	923	1820	<4	<4	<4	n. m.
NO_2^-(e)	synthetic	319	898	28.7	1080	107	1230	881	283	<4	<4	<4	n. m.
Real(a)	real	850	49.7	800	403	96	940	885	n. m.	<4	<4	<4.	n. m.
Real(b)	real	857	64	650	446	115	1550	1160	2360	32	<4	15	80
Real(c)	real	873	105	610	490	120	1560	1100	3210	22	<4	18	79
Real(d)	real	882	208	652	347	81	1470	946	1860	<4	<4	18	75
CO_2(a)	synthetic	996	2.0	1010	440	110	1360	1130	2520	<4	<4	<4	n. m.
CO_2(b)	real	814	16.5	665	424	105	1030	792	2220	36	<4	20	66
CO_2(c)	real	801	17.6	678	440	108	974	790	2290	32	<4	<4	68
Suspended	real	855	2.0	992	495	105	1140	932	1990	23	<4	<4	n. m.

n. m.: not measured

Table S2: Recipes for the synthetic urine solutions. The amount of salts is given per liter of solution.

Experiment ID	Na_2SO_4 [g]	$NaH_2PO_4 \cdot 2H_2O$ [g]	NaCl [g]	KCl [g]	NH_4Cl [g]	$(NH_4)_2SO_4$ [g]	$NaNO_2$ [g]	KNO_3 [g]	$NaNO_3$ [g]
NH_4^+(a)	0.65	0.55	2.7	1.9	0	0	0	0	0
NH_4^+(b)	0.65	0.55	2.5	1.9	0.14	0	0	0	0
NH_4^+(c)	0.65	0.55	2.2	1.9	0.42	0	0	0	0
NH_4^+(d)	0.65	0.55	1.3	1.9	1.3	0	0	0	0
NH_4^+(e)	0	0.55	0	0.7	3.3	0.59	0	0	0
NO_2^-(a)	0	0.55	3	1.9	0	1.55	0.06	0	0
NO_2^-(b)	0	0.55	2.9	1.9	0	1.55	0.18	0	0
NO_2^-(c)	0	0.55	2.6	1.9	0	1.55	0.55	0	0
NO_2^-(d)	0	0.55	1.6	1.9	0	1.55	1.65	0	0
NO_2^-(e)	0	0.55	0.4	0	0	1.55	3.15	0	0
CO_2(a)	0.65	0.55	0	0	3.8	0	0	2.9	3.7

S2 Mathematical model

Estimation of K_{LaCO2}

The K_La_{CO2} was not determined experimentally, but was calculated from the K_La_{O2}.

Diffusions coefficients in water (25°C):

$D_{CO2} = 1.91 \cdot 10^{-5}\ cm^2 \cdot s^{-1}$ (Lide 2009)

$D_{O2} = 2.42 \cdot 10^{-5}\ cm^2 \cdot s^{-1}$ (Lide 2009)

$D_{CO2} = 0.79 \cdot D_{O2}$

According to the penetration theory (Higbie 1935), the gas exchange coefficient K_La is a function of the square root of the diffusion coefficient:

$K_La_{O2} = f(D_{O2}^{0.5})$

$K_La_{CO2} = f(D_{CO2}^{0.5}) = f((0.79 \cdot D_{O2})^{0.5}) = f(0.89 \cdot D_{O2}^{0.5})$

$K_La_{CO2} = 0.89 \cdot K_La_{O2}$

K_{LaO2} was experimentally determined in deionized water with the same reactor configuration as in the batch experiments. The determined value was 650 d^{-1}. Hence, K_La_{CO2} was estimated as 579 d^{-1}.

Estimation of $CO_{2,sat}$

The saturation concentration of CO_2 was calculated as follows:

$$CO_{2,Sat} = \frac{p_{CO_2}}{R \cdot T \cdot H_{CO_2}}$$

With $CO_{2,sat}$ the saturation concentration of CO_2 (mol·L^{-1}), p_{CO2} the CO_2 partial pressure (0.00039 bar), R the gas constant ($8.314 \cdot 10^{-2}$ L·bar·K^{-1}·mol^{-1}), T the temperature (K), and H_{CO2} the Henry constant for CO_2 (1.2 mol(g)·mol(aq)$^{-1}$, Stumm and Morgan 1996).

S3 Concentrations at the pH limit

Table S3: End-pH values as well as calculated NH_3, HNO_2 and TIC concentrations in the solutions for all conducted batch experiments.

Experiment ID	NH_3-N [mg N·L^{-1}]	HNO_2-N [mg N·L^{-1}]	TIC* [mg C·L^{-1}]	End-pH [-]
NH_4^+(a)	0.0048	bld	0.2	5.69
NH_4^+(b)	0.0088	bld	0.2	5.55
NH_4^+(c)	0.014	bld	0.2	5.42
NH_4^+(d)	0.036	bld	0.2	5.39
NH_4^+(e)	0.11	bld	0.2	5.39
NO_2^-(a)	0.038	0.12	0.2	5.44
NO_2^-(b)	0.039	0.21	0.2	5.46
NO_2^-(c)	0.042	0.49	0.2	5.49
NO_2^-(d)	0.054	1.00	0.2	5.61
NO_2^-(e)	0.084	2.02	0.2	5.80
CO_2(a)	0.13	bld	0	5.46
CO_2(b)	0.077	bld	23	5.36
CO_2(c)	0.077	bld	46	5.37
Real(a)	0.095	0.19	0.2	5.40
Real(b)	0.093	0.32	0.2	5.43
Real(c)	0.108	0.58	0.2	5.48
Real (d)	0.125	0.87	0.2	5.54

* calculated concentration assuming equilibrium conditions between air and water phase
bld: below limit of detection (<0.001 mg HNO_2·L^{-1})

S4 Testing of the chemical speciation model: influence of acid-base equilibria, ionic strength and complex formation

The chemical speciation model was tested with different degrees of complexity in order to see which model complexity was required for sufficient accuracy:

- Model 1 included acid-base equilibria only (according to Table 4 of the main paper).
- Model 2 included acid-base equilibria and the effects of ionic strength.
- Model 3 included acid-base equilibria, effects of ionic strength and in addition complex formation (Table 4 of the main paper).

Figure S1 to S3 show the calculated and measured buffer intensities in titration experiments with the synthetic urine solutions NH_4^+(a), NH_4^+(e) and NO_2^-(e) (Table S1).

The main buffer system in Figure S1 is phosphate ($H_2PO_4^-/HPO_4^{2-}$). The maximal buffer intensity usually occurs at the pH value, which equals the pK_a value of the main buffer system (van Vooren 2000). Model 1 (acid-base equilibria only) predicts the maximal buffer intensity at 7.2 (Figure S1), which corresponds to the pK_a value at zero ionic strength (Table 4 of the main paper). However, the maximum buffer intensity was measured for a pH of 6.8. The accuracy of the modeled buffer intensity peak increased strongly when the effect of ionic strength was considered (Model 2). The prediction of the buffer intensity peak was further improved by including complex formation (Model 3), presumably because $KHPO_4^-$ and $NaHPO_4^-$ complexes were included. The effect of complexation on phosphate concentrations was significant: our model predicted that $KHPO_4^-$ and $NaHPO_4^-$ complexes bound up to 5 and 19% of the total phosphate in the solution NH_4^+(a). The effect of complexation was even more pronounced in solutions that contained ammonia in addition to phosphate (Figure S2 and S3). In these cases up to 29% of the phosphate was bound as $NH_4PO_4^-$, which indicates the importance of considering complex formation along with acid-base equilibria and ionic strength. However, the improvement of the model by including complexation depends on the quality of the data of the chemical constants. The complexation constants of some compounds vary widely in literature, e. g. the one for $KHPO_4^-$ ranges from 6.12 (Vieillard and Tardy 1984) to 6.91 (wateq4f.dat, standard database of PHREEQC, Parkhurst and Appelo 1999). The best data fit was obtained with the complexation constants given in Visual MINTEQ (Gustafsson 2012).

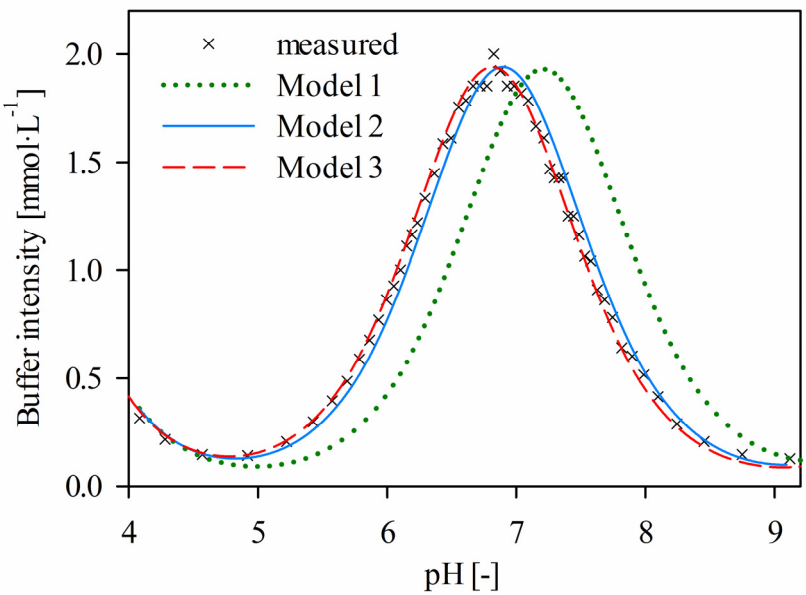

Figure S1: Measured and modeled buffer intensities for solution NH_4^+(a), which contained phosphate as buffer compound.

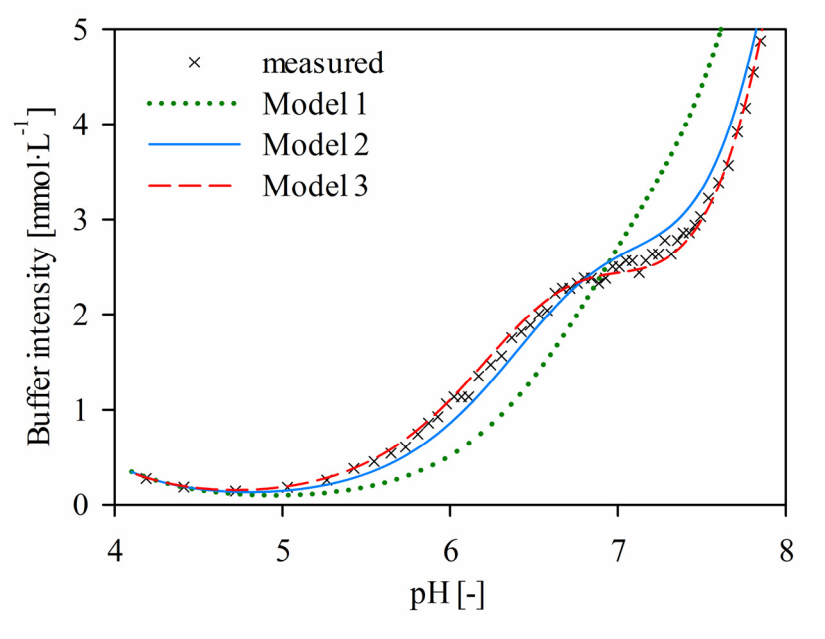

Figure S2: Measured and modeled buffer intensities for solution NH_4^+(e), which contained ammonia and phosphate as buffer compounds.

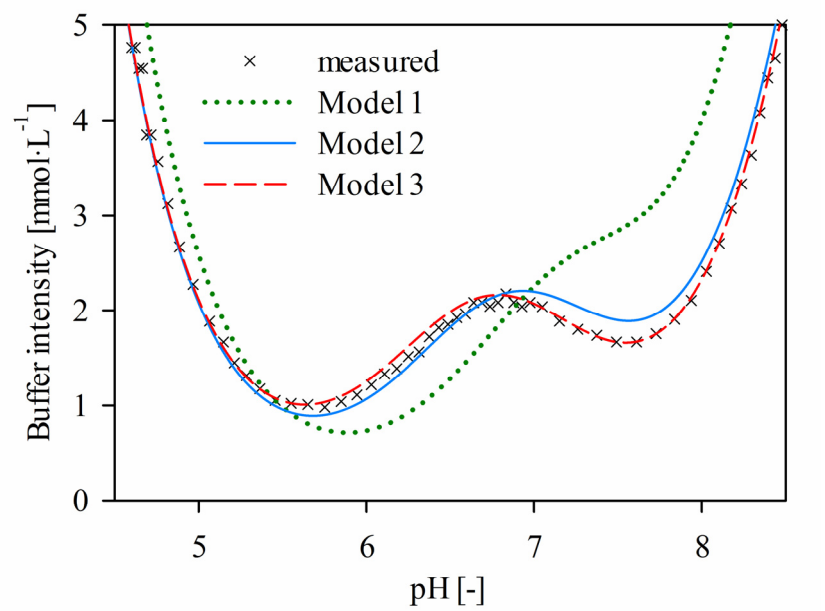

Figure S3: Measured and modeled buffer intensities for solution NO_2^-(e), which contained ammonia, phosphate, and nitrite as buffer compounds.

S5 Initial biomass concentrations and standard errors for estimated parameters

The estimated values and standard errors of all estimated parameters are given in Table S4. Estimates for the standard errors were calculated by the secant method in AQUASIM (Reichert 1994).

For parameter estimation of X_{AOB} for Model 1 pH values between 7 and 5.8 for experiments NH_4^+(a-e) and between 7 and 6 for experiments NO_2^-(a-e) were considered, because we assumed that these pH values were sufficiently far away from the pH limit, where other effects might have been effective. Including all pH measurement for the estimation of X_{AOB}, did not improve the poor ability of Model 1 to represent AOB activity below pH 6.

All pH measurements were used to fit the initial X_{AOB} in Model 2 and 3.

Table S4: Estimated values and standard errors for K_{pH} and the initial AOB concentrations.

	Estimated Values	Estimated standard errors	
K_{pH}	2.26	4.1E-03	-
Initial X_{AOB}:			
Model 1			
NH_4^+(a)	0.120	3.8E-04	g COD·L^{-1}
NH_4^+(b)	0.084	2.0E-04	g COD·L^{-1}
NH_4^+(c)	0.065	1.2E-04	g COD·L^{-1}
NH_4^+(d)	0.050	1.7E-04	g COD·L^{-1}
NH_4^+(e)	0.036	2.1E-05	g COD·L^{-1}
NO_2^-(a)	0.095	4.0E-04	g COD·L^{-1}
NO_2^-(b)	0.100	2.1E-05	g COD·L^{-1}
NO_2^-(c)	0.096	3.1E-04	g COD·L^{-1}
NO_2^-(d)	0.094	7.3E-04	g COD·L^{-1}
NO_2^-(e)	0.094	7.3E-04	g COD·L^{-1}
Suspended sludge	0.036	1.0E-04	g COD·L^{-1}
Model 2			
NH_4^+(a)	0.63	1.3E-02	g COD·L^{-1}
NH_4^+(b)	0.55	1.4E-02	g COD·L^{-1}
NH_4^+(c)	0.41	8.6E-03	g COD·L^{-1}
NH_4^+(d)	0.29	5.8E-03	g COD·L^{-1}
NH_4^+(e)	0.15	9.4E-04	g COD·L^{-1}
NO_2^-(a)	0.50	8.5E-03	g COD·L^{-1}
NO_2^-(b)	0.51	1.1E-02	g COD·L^{-1}
NO_2^-(c)	0.48	3.3E-04	g COD·L^{-1}
NO_2^-(d)	0.41	4.8E-03	g COD·L^{-1}
NO_2^-(e)	0.36	5.4E-03	g COD·L^{-1}
Suspended sludge	0.20	1.2E-03	g COD·L^{-1}

Model 3			
NH_4^+(a)	0.13	3.1E-04	g COD·L^{-1}
NH_4^+(b)	0.088	2.7E-04	g COD·L^{-1}
NH_4^+(c)	0.071	6.4E-05	g COD·L^{-1}
NH_4^+(d)	0.054	1.2E-04	g COD·L^{-1}
NH_4^+(e)	0.036	3.7E-05	g COD·L^{-1}
NO_2^-(a)	0.099	3.2E-05	g COD·L^{-1}
NO_2^-(b)	0.11	2.6E-04	g COD·L^{-1}
NO_2^-(c)	0.10	3.3E-04	g COD·L^{-1}
NO_2^-(d)	0.10	3.2E-04	g COD·L^{-1}
NO_2^-(e)	0.10	4.9E-04	g COD·L^{-1}
Suspended Sludge	0.036	2.9E-05	g COD·L^{-1}

S6 Experiments with different aeration rates

The computer model was designed for a suspended growth system, whereas we used a biofilm system for our experiments. Mass transfer in the biofilm could limit conversion rates, especially if high rates are expected. Based on stoichiometry we would expect O_2 to be the limiting compound, if the biofilm is limited by mass transfer processes. Hence, we performed four experiments with different aeration rates, but in the same solution NH_4^+(d).

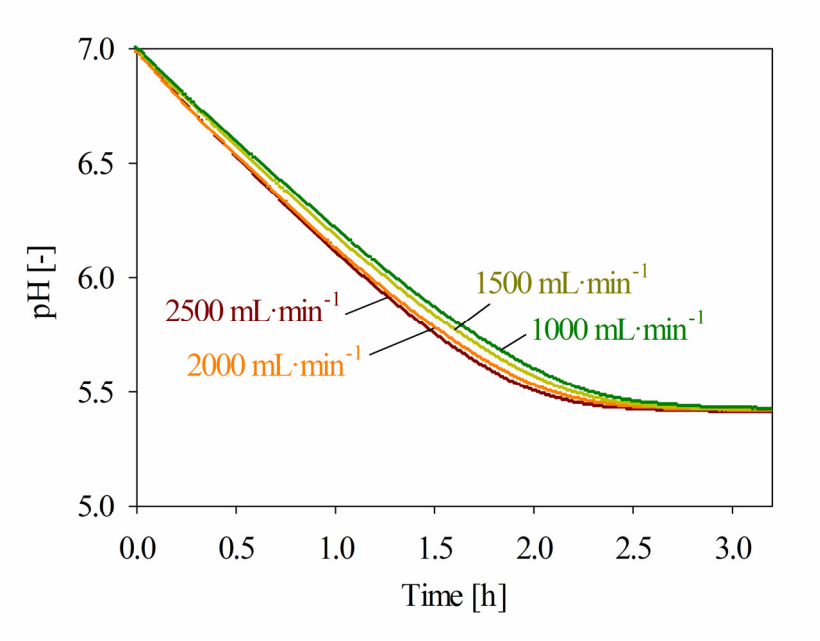

Figure S4: Observed pH values for four experiments with different aeration rates, but in the same synthetic solution.

Figure S4 shows that increased aeration reduced the experimental duration. This was especially true in the beginning of the experiment, where high NH_3 concentrations and high rates of microbial ammonia oxidation were observed. However, processes close to the pH limit were not affected, because microbial ammonia oxidation was so slow, that the biofilm was not affected by O_2 limitation.

S7 Modeling the pH limit in an experiment with suspended sludge

Figure S5 shows a model comparison of Model 1, 2, and 3 described in the manuscript for an experiment with suspended sludge. Initial biomass concentrations were fitted (Table S4), but the same parameters were used as specified in Table 3 of the main paper. Similarly to the experiments with the biofilm carriers, Model 3 is well suited to model the rate of ammonia oxidation.

The experiment was performed in a real nitrified urine solution, indicating that the model approach for AOB is not only applicable for synthetic, but also for real urine solutions.

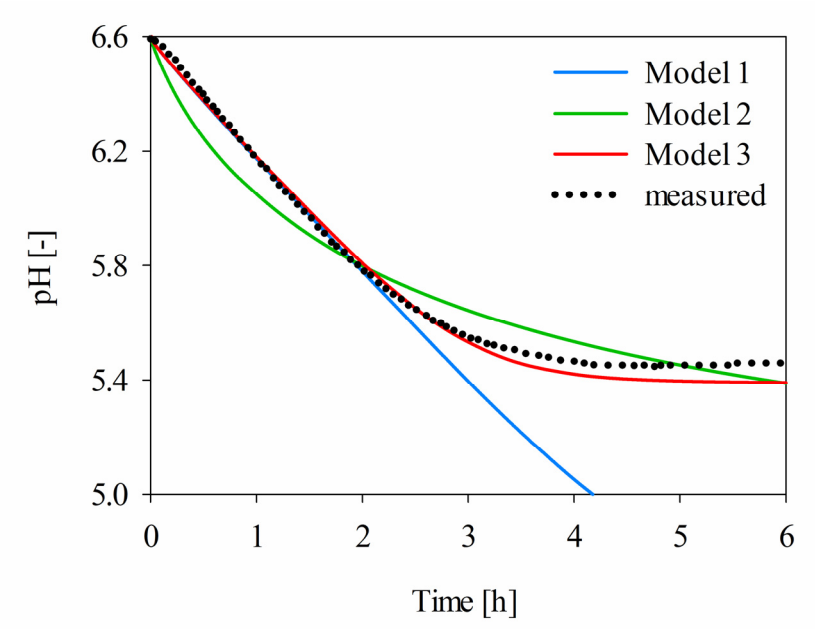

Figure S5: Modeled and observed pH values in an experiment with suspended sludge in real nitrified urine.

Chapter 3

The growth of *Nitrosococcus*-related ammonia oxidizing bacteria causes strong acidification in high strength nitrogen wastewater

Alexandra Fumasoli, Helmut Bürgmann, David G. Weissbrodt, George F. Wells, Karin Beck, Joachim Mohn, Eberhard Morgenroth, Kai M. Udert

In preparation

Graphical abstract

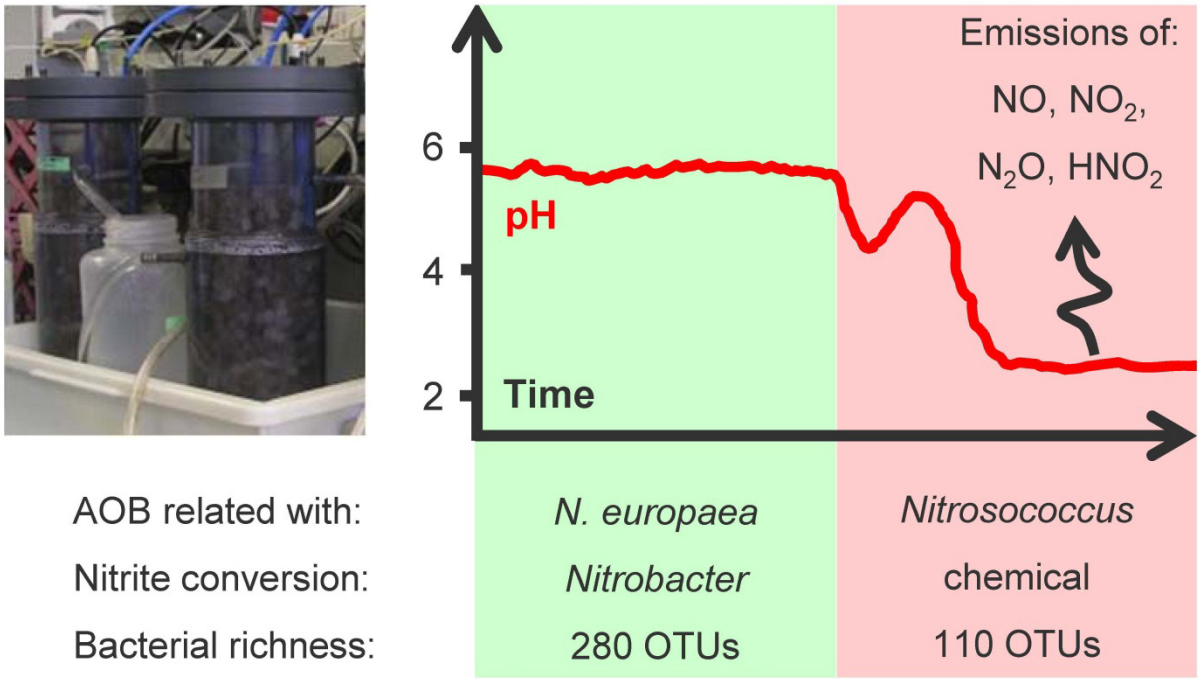

Abstract

Ammonia oxidation decreases the pH in wastewaters where the alkalinity is limited relative to the total ammonia. The activity of ammonia oxidizing bacteria (AOB), however, typically decreases with pH and often ceases completely in slightly acidic wastewaters. Nevertheless, low pH nitrification has been reported in reactors treating human urine, but it is not clear which organisms are involved. In this study, we followed the population dynamics of ammonia oxidizing organisms and reactor performance in synthetic, fully hydrolysed urine as the pH decreased over time in response to a decrease in the loading rate. Populations of the β-proteobacterial *Nitrosomonas europaea* lineage were abundant at the initial pH close to 6, but the growth of a possibly novel *Nitrosococcus*–related AOB genus decreased the pH to the new level of 2.2, challenging the perception that nitrification is inhibited entirely at low pH values, or governed exclusively by β-proteobacterial AOB or archaea. With the pH shift nitrite oxidizing bacteria were not further detected, but nitrous acid (HNO_2) was still removed through chemical decomposition to nitric oxide (NO) and nitrate. To prevent strong emissions of volatile nitrogen compounds such as NO, the pH has to be controlled at sufficiently high values.

Introduction

Ammonia oxidation to nitrite, the first step of nitrification, is a biological process that releases protons. Ammonia oxidation can therefore substantially decrease the pH in terrestrial and aquatic systems that do not contain sufficient alkalinity to buffer the proton release, e.g., in acidic soils or wastewaters with a low alkalinity to total ammonia ratio.

AOB in wastewater treatment, however, are typically found to be acid-sensitive: the activity of AOB was found to decrease with pH and to completely cease at pH values slightly below pH 6 (Painter 1986). Occasional reports indicate that ammonia oxidation can still occur at lower pH: it was observed that ammonia oxidation proceeds at pH values of around 4 in engineered reactors containing synthetic wastewaters (Gieseke et al. 2006, Tarre et al. 2004, Tarre and Green 2004, Tarre et al. 2007) and pH values dropped to values as low as 2.5 in nitrified urine (Udert et al. 2005). The minimal pH value of 2.5 is stunning, as a lower pH limit of 2.9 was demonstrated for ammonia oxidation in acidic tea soils (Hayatsu 1993) and as nitrification is not expected at pH values below 3 in acidic lakes (Jeschke et al. 2013). It has been shown that the ammonia oxidation in urine was due to biological activity (Udert et al. 2005). However, it is not clear which organisms were involved.

Low pH values can be reached during the nitrification of urine, as stored human urine contains an alkalinity to total ammonia ratio of 1 $mol \cdot mol^{-1}$ (Udert et al. 2006), while a minimal molar ratio of 2 $mol \cdot mol^{-1}$ would be required for complete ammonia oxidation. Consequently, only 50% of the total ammonia in urine is oxidized until most of the alkalinity has been consumed and the pH has dropped substantially. The drop of pH to very low values is a concern for engineered reactors: at pH values below 4.5, nitrous acid (HNO_2) decomposes chemically (Udert et al. 2005). It has been observed that at low pH values around 16% of the transformed nitrogen was lost by chemical HNO_2 decomposition and volatilization, partially in the form of harmful gases (HNO_2, nitric oxide and nitrous oxide) (Udert et al. 2005), while the overall nitrogen loss was negligible in a urine nitrification reactor at neutral pH values (Udert et al. 2003a). To keep off-gas emissions low, nitrification at low pH must be prevented rather than promoted in practical applications.

The main population of AOB in urine nitrification reactors at neutral pH values was found to be affiliated with the *Nitrosomonas europaea* lineage (Fumasoli et al. 2015). Their activity was shown to cease at pH values close to 5.4 (Fumasoli et al. 2015). Hence, it has to be expected that a population shift from this acid-sensitive to other, acid-tolerant, AOB is responsible for low-pH nitrification in urine. A complete population shift from *Nitrosomonas europaea* to *Nitrosomonas oligotropha* has been observed in a reactor operated with synthetic low strength nitrogen wastewater as the pH dropped from above 6 to 4.5 (Tarre et al. 2007). However, the wastewater used in these experiments contained far lower salt and total ammonia concentrations than the concentrations expected in urine (Udert et al. 2006). *Nitrosomonas oligotropha* have a high ammonia affinity, but also a high salt sensitivity (Koops et al. 2006). Hence, it remains unclear whether these AOB are also selected in high strength nitrogen wastewaters, such as urine.

Several AOB are better adapted to high salt concentrations, e.g., the γ-proteobacterial AOB (e.g. genus *Nitrosococcus*) (Koops et al. 1990). It has been hypothesized based on

morphological observations that the AOB active at a pH value as low as 2.9 in acidic tea soils belongs to the genus of *Nitrosococcus* (Hayatsu 1993). However, γ-proteobacterial AOB are predominantly found in marine environments (Ward and O'Mullan 2002) and are very rarely detected in wastewater treatment reactors (Nielsen et al. 2009). Recent studies showed that ammonia oxidizing archaea (AOA) outnumber AOB at low soil pH values (Nicol et al. 2008) and play a more important role than AOB in strongly acidic soils (Zhang et al. 2012). While the relative abundance of AOA is low compared to the relative abundance of AOB in municipal wastewater treatment (Wells et al. 2009), the occurrence of AOA in wastewater reactors at low pH values has, to our knowledge, so far not been investigated.

The growth of bacteria in acidic environments requires specific adaptation mechanisms: bacteria need to keep their cell internal pH values close to neutrality against the extracellular pH, a phenomenon known as pH homeostasis (Slonczewski et al. 2009). One known mechanism of pH homeostasis is the uptake of potassium ions, which allows for the inversion of the membrane potential and decreases the proton pressure on the cytoplasmic membrane (Baker-Austin and Dopson 2007).

The aim of this study was to select for the ammonia oxidizing organisms that drive the pH in high strength nitrogen wastewaters to very low values and to investigate how the selection of these organisms affect the reactor performance and the overall bacterial community structure. The bacterial population dynamics and reactor performance in high strength nitrogen wastewaters are compared with parallel reactors operated using low strength nitrogen wastewaters. The availability of potassium ions was altered to test its importance for bacterial survival at low pH.

Materials & Methods

Reactor operation under continuous-flow regime

Reactor configurations. Four moving bed biofilm reactors (MBBR) with a volume of 2 L each were operated under continuous-flow conditions over more than 160 days. Each reactor was filled with 40% (volumetric ratio) K1 Kaldnes® biofilm carriers with a specific surface area of 500 $m^2 \cdot m^{-3}$ (Rusten et al. 2006). The reactor temperature was adjusted to 25.4 ± 0.1°C with a thermostat (F32, Julabo Labortechnik GmbH, Seelbach, Germany). To maintain constant nitrogen loading rates, as detailed below, reactors were supplied with influent at specific volumetric flow rates (REGLO Digital, ISMATEC, Wertheim, Germany). Sufficient mixing of biofilm carriers was ensured by aeration with pressurized, pre-moisturized ambient air at 35 $NL \cdot h^{-1}$ (22R1411/01807, Wisag, Fällanden, Switzerland). In combination with low nitrification rates, the high air flow maintained the dissolved oxygen close to saturation. Online pH monitoring, the set-up for batch experiments and the characteristics of the inoculum are described in the supplementary information.

Influent compositions. The experimental design consisted of four reactors fed with different synthetic influent solutions to investigate the effects of urine and wastewater matrices, and of potassium and sodium cations (Table 1). Two so-called urine reactors (UR) were supplied with influent that contained total ammonia and total salt concentrations similar to women's urine (Fumasoli et al. 2016), but varied in their potassium and sodium concentrations. Ammonia

rather than urea was added, as we assumed urine to be completely hydrolyzed. Two wastewater reactors (WWR) were fed with a synthetic substrate containing lower total ammonia and total salt concentrations, and high potassium (WWR-K) or sodium (WWR-Na) concentrations. Influents with high potassium (UR-K, WWR-K) or sodium concentrations (UR-Na, WWR-Na) should provide information on the necessity of potassium for AOB growth at low pH values. The recipes of all synthetic influent solutions are given in Table S1. Micro- and macronutrients were added as specified in the Table S2. The influent solutions did not contain organic substances. The liquid phase sampling and chemical analyses are described in the supplementary information. The standard deviation for liquid phase analysis was below 4% for all compounds.

Table 1: Average measured concentrations of ammonium and accompanying salts in the reactor influent solutions. The urine reactors (UR-K and UR-Na) contained high salts and total ammonia concentrations, the wastewater reactors (WWR-K and WWR-Na) low salts and total ammonia concentrations. Influent solutions to the urine reactors as well as the influent solutions to the wastewater reactors varied also in their sodium and potassium content. All influent solutions had alkalinity to ammonia ratios of less than 2 $mol \cdot mol^{-1}$.

		UR-K	UR-Na	WWR-K	WWR-Na
pH	-	9.18 ± 0.06	9.32 ± 0.07	8.09 ± 0.34	8.16 ± 0.33
NH_4-N	$mg \cdot L^{-1}$	1710 ± 140	1630 ± 90	149 ± 8	145 ± 16
TIC	$mgC \cdot L^{-1}$	753 ± 60	695 ± 123	219 ± 10	211 ± 24
PO_4-P	$mg \cdot L^{-1}$	146 ± 6	138 ± 13	11.0 ± 1.5	11.4 ± 1.6
Cl	$mg \cdot L^{-1}$	1740 ± 100	1550 ± 130	387 ± 22	381 ± 33
Na	$mg \cdot L^{-1}$	5.59 ± 0.40	1160 ± 130	6.20 ± 0.62	424 ± 130
K	$mg \cdot L^{-1}$	2100 ± 260	<1	799 ± 35	<1
Alkalinity*	$meq \cdot L^{-1}$	123	130	19	19

* calculated

Operational conditions. During a start-up phase of 9 days, the urine and wastewater reactors were fed with a nitrogen loading rate of 355 ± 15 and 95± 5 mg NH_4-$N \cdot L^{-1} \cdot d^{-1}$, respectively. The experiment was initiated (time point zero) by a decrease in the influent rates to 22.8 $mL \cdot d^{-1}$ (UR) and 101 $mL \cdot d^{-1}$ (WWR), resulting in nitrogen loading rates of 19 ± 2 (UR) and 8 ± 2 mg NH_4-$N \cdot L^{-1} \cdot d^{-1}$ (WWR). Thereafter, influent flow rates were kept constant for the rest of the experiment. Hydraulic retention times were 88 (UR) and 20 d (WWR).

Analysis of nitric oxide (NO), nitrous oxide (N_2O) and nitrogen dioxide (NO_2) off-gas concentrations

At day 246, the NO, N_2O and NO_2 concentrations in the off-gas of all four reactors were analyzed by FTIR spectroscopy (GASMET CX-4000, Temet Instruments, Helsinki), equipped with a heated (40°C) flow-through gas cell with a 9.8 m path length. The quantification limits

for NO, N_2O and NO_2 were 2, 0.2 and 1 ppm respectively, and the expanded standard uncertainty is around 15% for NO and N_2O and 25% for NO_2 (95% confidence level) (Mohn et al. 2008).

Molecular biology and numerical methods

16S rRNA gene-based amplicon sequencing and polymerase chain reaction (PCR). Biomass sampling and extraction of genomic DNA is described in the supplementary information. DNA extracts were sent to Research and Testing Laboratory (Lubbock, TX, USA) for 16S rRNA gene-based amplicon sequencing according to facility's protocol (Sun et al. 2011) adapted to the MiSeq Illumina desktop technology. The primer pair 341F (5'-CCTACGGGNGGCWGCAG-3') / 785R (5'-GACTACHVGGGTATCTAATCC-3') was used to target the v3-v4 hypervariable region of the bacterial 16S rRNA gene pool (Herlemann et al. 2011). I*n silico* testing, analysis of samples with primers targeting archaea, analysis with quantitative polymerase chain reaction (qPCR) for the relative abundance of archaea and *Nitrosococcus*, as well as with qualitative PCR for AOA are described in the supplementary information.

Bioinformatic processing of amplicon sequencing datasets. The amplicon sequencing datasets were processed using the bioinformatics workflow implemented in the MIDAS field guide including taxonomic assignment using the RDP classifier (Lan et al. 2012, Wang et al. 2007) against the MIDAS database of reference sequences curated from SILVA for wastewater environments. Relative abundance of operational taxonomic units (OTU) or phylotypes were estimated from the number of assigned sequence reads to total reads per sample.

Phylogenetic and numerical analyses. The sequencing data has been submitted to NCBI with the BioProject ID 293261. Data files were imported into R package `Phyloseq` (McMurdie and Holmes 2013) for further processing. Samples with a sequencing depth of less than 10'000 reads were removed from the sequencing data set. Sequencing depths were between 15'722 and 48'338 reads and a median sequencing depth of 42'488 reads was obtained per sample. Non-bacterial and chloroplast sequences were removed from the dataset prior to analysis. `Phyloseq` was used for analysis and plotting of alpha diversity measures. For further analysis OTUs that did not have more than two reads in three or more samples were removed from the dataset. Package `vegan` (Oksanen et al. 2015) was used to perform Nonmetric Multidimensional Scaling with function metaMDS `()`. Function `bioenv()` was used to determine most relevant parameters to explain community variation (Clarke and Ainsworth 1993). Function `envfit()` was used to fit the determined environmental variables to the ordination.

A Neighbor Joining phylogenetic tree was constructed in MEGA (version 6.06) (Tamura et al. 2013) using the Maximum Composite Likelihood model on a ClustalW alignment of OTU reference sequences best BLAST matches from NCBI and reference organism sequences obtained from RDP. 500 bootstrap resamplings were carried out to test the tree topology.

Analyses of variance (ANOVA) were conducted to assess the extent and significance of the effects of the two main factors of feed composition (urine vs. wastewater) and monovalent

cationic specie (K^+ vs. Na^+) on microbial population dynamics, by analogy to Weissbrodt et al. (2013). Heatmaps of Spearman's rank-order correlation coefficients were computed according to Weissbrodt et al. (2014) in order to delineate clusters of predominant OTUs (>5%) sharing similar dynamics in relationship with operational conditions and process responses.

Results

Nitrification performance of MBBRs with synthetic urine and synthetic wastewater

Urine reactors. After the decrease in the influent loading (time point zero) the pH started to drop to a level of 4.3 after 30 (UR-K) and 25 days (UR-Na, Figure 1), indicating an increase in ammonia oxidation. In parallel with the pH drop, the total nitrite (NO_2^- and HNO_2) concentrations increased. Subsequently, the pH increased again indicating an inhibition of ammonia oxidation. A second decrease of pH was observed despite high HNO_2 concentrations (Figure S1) after 52 (UR-K) and 46 days (UR-Na) to average pH values of 2.2 ± 0.1 (UR-K) and 2.3 ± 0.3 (UR-Na). During this phase, the total nitrite concentrations decreased from around 100 $mgN \cdot L^{-1}$ to 3.7 ± 0.8 (UR-K) and 5.9 ± 1.4 $mgN \cdot L^{-1}$ (UR-Na) and remained stable for the rest of this study. The pH increased only slightly after an aeration failure at day 68 and 98. Despite the low pH values, average ammonia oxidation rates of 13.8 ± 0.3 (UR-K) and 14.5 ± 0.8 $mgN \cdot L^{-1} \cdot d^{-1}$ (UR-Na) were maintained until day 160. These rates were slightly higher than the nitrification rates of 12.0 ± 0.8 (UR-K) and 11.8 ± 1.0 $mgN \cdot L^{-1} \cdot d^{-1}$ (UR-Na) observed before the second pH drop.

After the second pH drop, the total nitrogen concentration (sum of total ammonia, total nitrite and nitrate) in the reactor decreased. Nitrogen losses accounted to 9.2 (UR-K) and 9.4 $mgN \cdot L^{-1} \cdot d^{-1}$ (UR-Na) corresponding to 53 and 50%, respectively (Figure 1). Off-gas measurement for NO, NO_2 and N_2O revealed that the losses were mainly due to the volatilization of NO: 8.7 (UR-K) or 7.1 $mgN \cdot L^{-1} \cdot d^{-1}$ (UR-Na) were detected. NO_2 and N_2O were also detectable: NO_2 was 1.3 or 1.6 $mgN \cdot L^{-1} \cdot d^{-1}$ in UR-K and UR-Na, whereas N_2O accounted for 0.4 or 0.2 $mgN \cdot L^{-1} \cdot d^{-1}$, respectively. Total emissions of analyzed nitrogen compounds in the off-gas were 10.7 $mgN \cdot L^{-1} \cdot d^{-1}$ and 8.9 $mgN \cdot L^{-1} \cdot d^{-1}$, which corresponds well to the nitrogen losses in the liquid phase (Table S3). HNO_2 emissions were not analyzed, but are expected to be small estimated from Henry's Law. NO was thus the major compound produced at low pH in the urine reactors, followed by NO_3^- (Table S3).

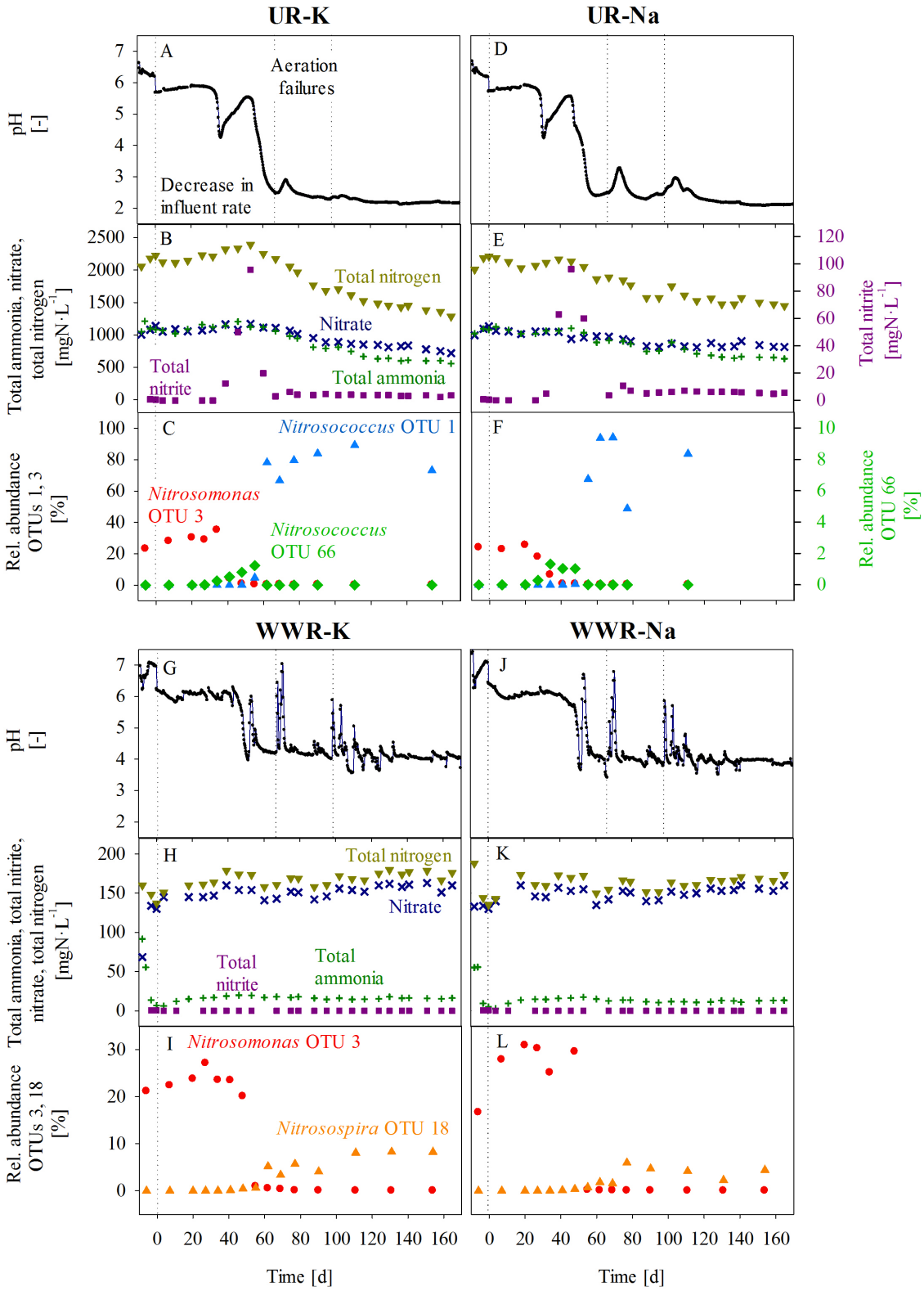

Figure 1: For each experimental condition pH, and nitrogen species in the reactor (total ammonia, total nitrite, nitrate, and total nitrogen) are shown together with the relative abundance of AOB. Results for the synthetic urine reactors (UR-K and UR-Na), and the synthetic wastewater reactors (WWR-K and WWR,Na) are presented in panels A-C, D-F, G-I, and J-L, respectively. Experimental conditions are described in more detail in the text and in Table 1. Sequencing samples from the days 131 (both urine reactors), as well as 90 and 154 (UR-Na) were excluded due to the low sequencing depth.

Wastewater reactors. In the wastewater reactors the pH decreased after around 40 days (Figure 1). Total nitrite concentrations in the reactor remained below the detection limit of 0.015 $mgN \cdot L^{-1}$ in almost all samples and were thus clearly lower than in the urine reactors. In contrast to urine reactors, nitrogen losses from the liquid phase were negligible (Table S3). A new pH level of 4.2 ± 0.4 (WWR-K) and 4.0 ± 0.4 (WWR-Na) was reached. Nitrification rates of 8.2 ± 0.6 (WWR-K) and 8.0 ± 0.5 $mgN \cdot L^{-1} \cdot d^{-1}$ (WWR-Na) were retained, which is similar to the nitrification rate before the pH drop (7.9 ± 1.1 and 8.7 ± 0.8 $mgN \cdot L^{-1} \cdot d^{-1}$).

Thermodynamic calculations showed that based on the synthetic wastewater composition a minimal pH value of 2.6 would be reached, if all ammonia was converted to nitrate, while synthetic urine allows the pH theoretically to decrease to a minimal values of 0.9 (supplementary information). The buffer capacity of the influent is therefore at least one of the factors influencing the pH levels in the reactors.

Low impact of monovalent cations. The two urine reactors showed very similar reactor behavior, as did the two wastewater reactors: the difference in K^+ and Na^+ content had little effect (Figure 1). Potassium concentrations in the Na reactors were higher than expected from the influent composition (Table 1): 25.8 ± 21.3 $mg \cdot L^{-1}$ and 13.2 ± 4.4 $mg \cdot L^{-1}$ in UR-Na and WWR-Na, respectively (Table S4), likely due to the leakage of potassium ions from the pH electrodes. The potassium levels were, however, still more than 80 and 60 times lower compared to the potassium reactors UR-K and WWR-K, respectively.

Shifts in nitrifying populations

Urine reactors. *Nitrosomonas* OTU 3 was the most abundant AOB in the beginning of the experiment (>15% relative abundance according to 16S rRNA gene sequencing results) and the relative abundance of all other AOB was below 0.2%. According to BLAST, *Nitrosomonas* OTU 3 affiliates with the *Nitrosomonas europaea* lineage. As soon as the pH in the urine reactors decreased, the relative abundance of *Nitrosomonas* OTU 3 declined to values below 0.5% (Figure 1). Concomitantly with this first pH decrease, the relative abundance of OTU 66 sequence, which according to BLAST showed greatest similarity to *Nitrosococcus oceani* (95% identity) increased to above 1%. However, the relative abundance of OTU 66 decreased again with the second pH drop, whereas the closely related OTUs 1 and 187, with 93% BLAST similarity to *Nitrosococcus halophilus* strain Nc4, increased strongly. OTU 1 reached maximal relative abundances of 94% and remained the only AOB with relative abundance of more than 0.5% until the end of the experiment. The dynamics of the *Nitrosococcus*-related OTU 1 was also confirmed by a TaqMan qPCR assay designed to specifically quantify this OTU (Figure S2). A *de novo* phylogenetic tree indicated that *Nitrosococcus* OTU 1 clustered separately from known *Nitrosococcus* sequences, while the rare OTU 187 was 99% similar to an environmental sequence retrieved from leaf cutter ant nests (Figure 2). Although these results would have to be confirmed e.g. by full-length 16S rRNA gene sequences and other indicators, this suggests that the sequences of OTU 1 belong to an undescribed species, possibly even a new genus.

Bradyrhizobiaceae OTU 2, an abundant sequence that was assigned by our pipeline to the family of *Bradyrhizobiaceae,* showed 100% identity to *Nitrobacter* (*Nitrobacter* sp. 219, AM286375.1). OTU 2 was abundant at the beginning of the experiment, but disappeared in the urine reactors after the second pH drop (Figure 3, and S3). The absence of nitrite oxidizing

bacteria (NOB) in the urine reactors was confirmed with batch experiments demonstrating no nitrite oxidation (Figure S4).

DNA yield per carrier was determined as an estimator for total biomass. The overall DNA yield from urine reactor carriers decreased very strongly after the second pH drop (Figure S3). The high relative abundance of *Nitrosococcus* OTU 1 was thus at least partly due to a strong biomass decay. However, when using the DNA yield and the relative abundance of OTU 1 to estimate the total abundance of this group, then this value increased from below 0.01 to average values of 0.8 µg DNA·carrier^{-1} after the second pH drop, indicating that OTU 1 was actually growing. This was further confirmed by qPCR analysis of OTU 1 abundance (Figure S2).

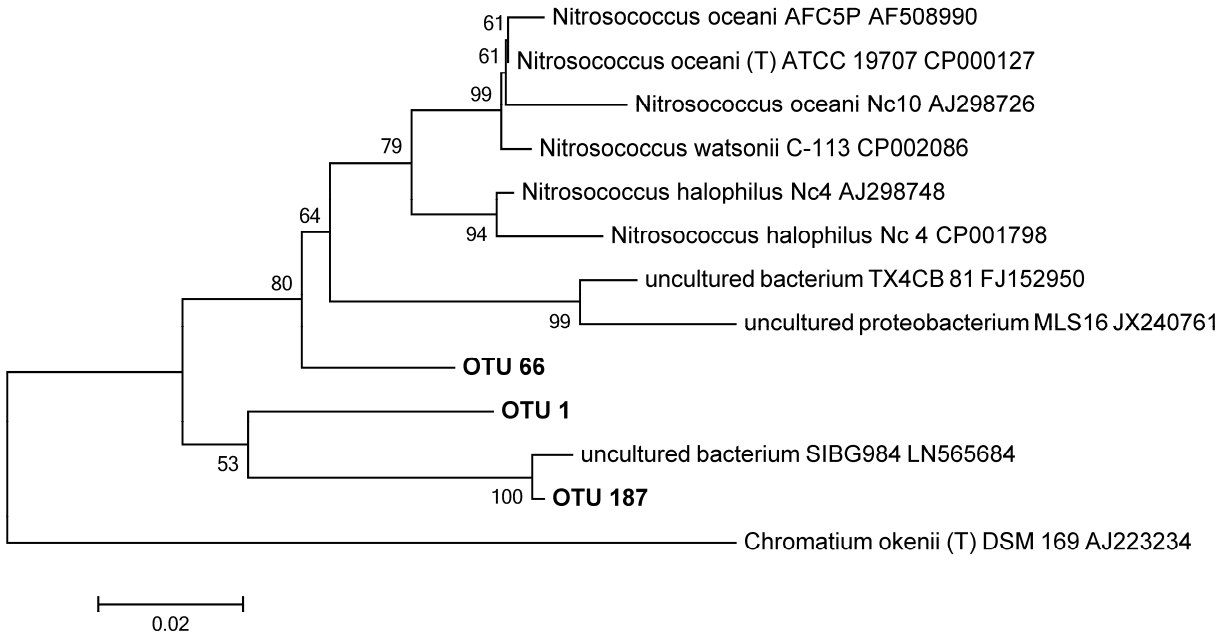

Figure 2: Neighbor Joining tree of *Nitrosococcus*-like sequences based on 16S rRNA gene-based amplicon sequencing and reference sequences, based on 421 nucleotide positions. Numbers indicate % of 500 bootstrapped tree topologies supporting the displayed phylogeny. Scale indicates substitutions per position. *Chromatium okenii* was included as an outgroup within the class of γ-*Proteobacteria*.

Wastewater reactors. Similar to the urine reactors, the relative abundance of *Nitrosomonas* OTU 3 decreased below 0.5% as the pH in the wastewater reactors started to drop (Figure 1). Instead, the relative abundance of *Nitrosospira* sp. (OTU 18) increased to maximal values of 8%. *Nitrobacter*-like sequences from the family of *Bradyrhizobiaceae* remained constant over the whole experimental duration (Figure 3, and S3), indicating that NOB remained viable under the low pH conditions in the wastewater reactors, which was also confirmed in batch experiments (Figure S4). DNA yield per carrier remained relatively constant in the wastewater reactors (Figure S3).

Low abundance of archaea. AOA were not detected in any of the low pH reactors by any of the primer pairs used for the 16S rRNA gene-based amplicon sequencing. AOA were also not detected with the AOA-specific PCR assay (Francis et al. 2005) (Figure S5). qPCR for overall abundance of archaea compared to bacteria also failed to detect archaea in the low pH urine

reactors, and showed that archaea never exceeded a relative abundance of more than 0.7% at any time in any of the reactors (Figure S6).

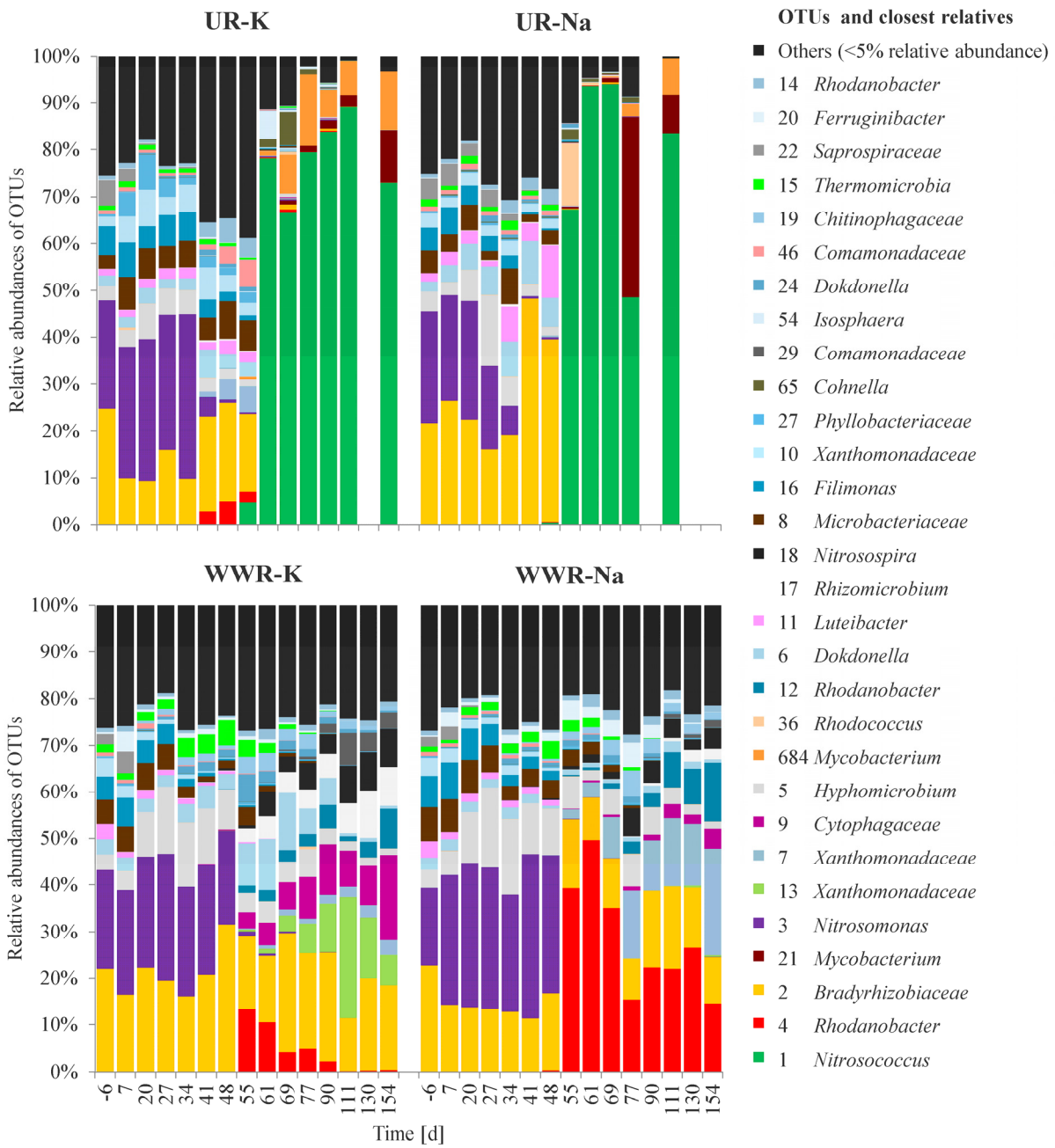

Figure 3: Dynamics of OTUs that displayed relative abundances above 5% of the bacterial community over the experimental period in the four reactors operated with synthetic urine (UR-K and UR-Na) and synthetic wastewater (WWR-K and WWR-Na). Their relative abundances and closest neighbors were retrieved from the high-resolution MiSeq datasets of 16S rRNA gene-based amplicon sequencing and after mapping against MIDAS. These phylotypes were identified at family (-*aceae* suffix) and genus levels.

Shifts in overall bacterial community compositions

The estimated Chao1 richness of the sequencing datasets was correlated to the pH ranges in the reactors (Figure 4). Whereas the richness remained at around 280 OTUs during the first pH

drop to 4.3 in the urine reactors, it decreased dramatically to 110 OTUs as the pH dropped to average values of 2.2. The richness in the wastewater reactors decreased only slightly from around 340 to 280 OTUs as the pH regime shifted from above pH 5.5 to average values of 4.1, which corresponds well with the richness in the urine reactors in the same pH range (pH 5.5-3.5).

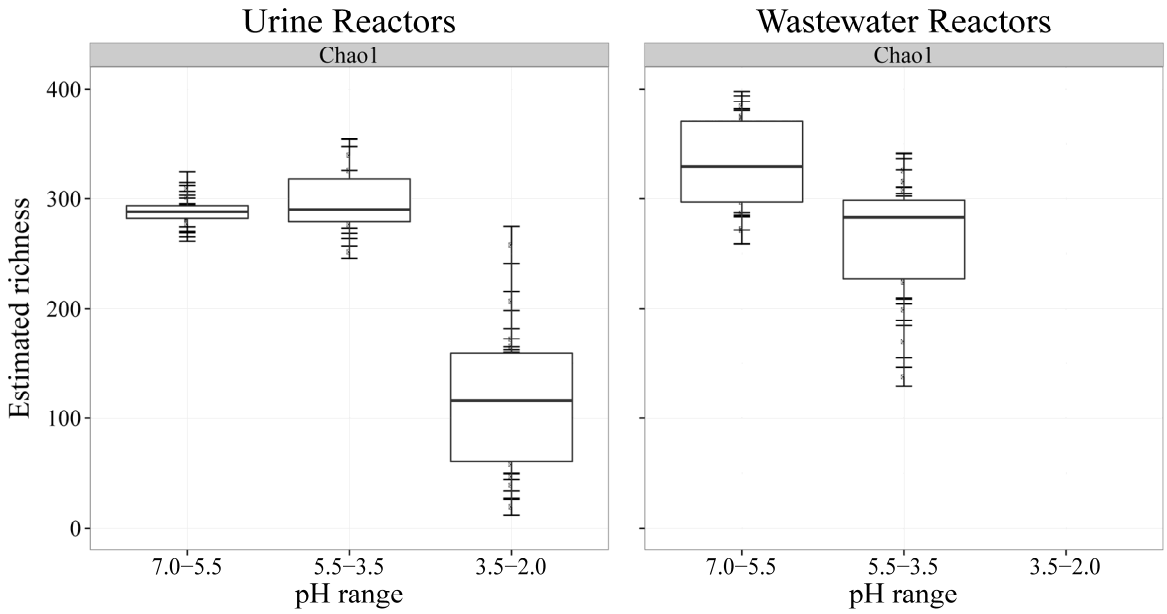

Figure 4: Chao 1 estimated richness for the urine and wastewater reactors as a function of the reactor pH. Samples were divided into three pH ranges: 7.0 to 5.5, 5.5 to 3.5, and 3.5 to 2.0. The wastewater reactors did not reach pH levels below 3.5. Number of samples per pH range for urine reactors: 9 (pH 7.0 to 5.5), 6 (5.5 to 3.5), 11 (3.5 to 2.0); wastewater reactors: 14 (7.0 to 5.5), 16 (5.5 to 3.5), 0 (3.5 to 2.0).

Urine and wastewater reactors originally contained very similar microbial communities that differentiated increasingly over the course of the experiment, as represented in the non-metric multidimensional scaling analysis (Figure 5). pH and HNO_2 showed the best correlation of the tested environmental variables (pH, HNO_2, NO_2^-, NH_3, NH_4^+, and total salts) with community structure (spearman correlation coefficients: 0.74 for pH, 0.59 for HNO_2).

The heatmap of Spearman's rank-order correlations delineated three major clusters of co-evolving predominant OTUs (>5%). *Nitrosococcus* OTU 1, *Nitrosomonas* OTU 3, *Nitrosospira* OTU 18 belonged to one cluster each. Hardly any OTUs clustered together with *Nitrosococcus* OTU 1, except of the two OTUs 21 and 684 affiliated with the genus of *Mycobacterium* (Figure S7). These two OTUs reached maximal abundances of 38.3% (OTU 21) and 15.1% (OTU 684) in the urine reactors after the second pH drop (Figure 3).

Analyses of variance (ANOVA) conducted on the population profiles further confirmed that the liquid matrix (i.e. urine or wastewater) was the main factor for the selection of *Nitrosococcus*, *Nitrosospira*, and *Bradyrhizobiaceae* affiliates (maximal F-values of 940, 1930, and 136, respectively; P-values of 0.02, 0.01, and 0.05, respectively), rather than the type of monovalent cation (i.e. K^+ or Na^+; maximal F-values of 1, 1, and 11, respectively; P-values of 0.5, 0.5, 0.2, respectively).

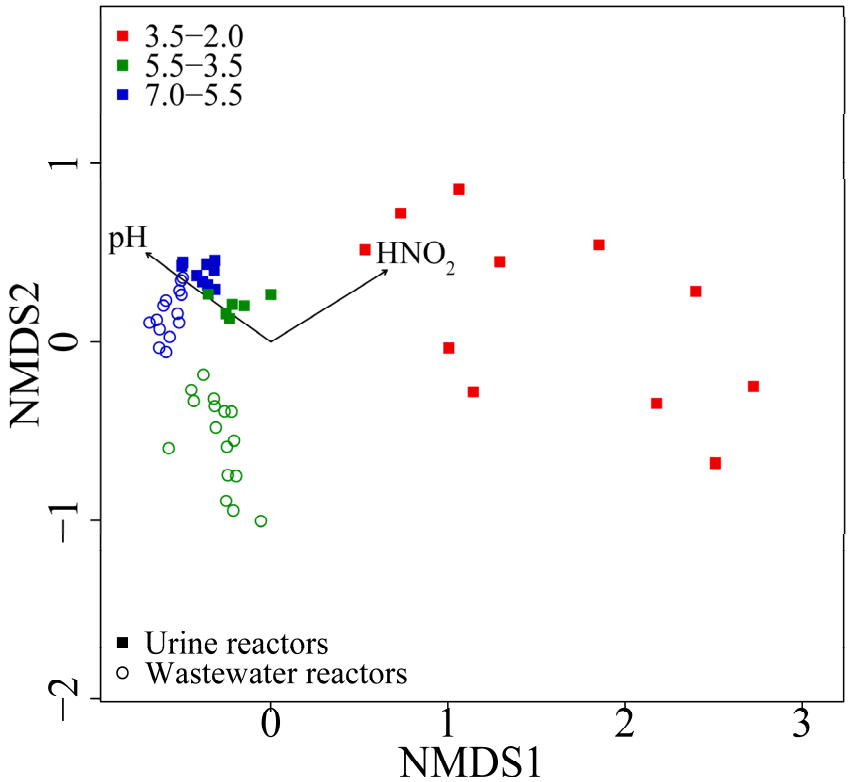

Figure 5: Non-metric multidimensional scaling analysis (NMDS) of the community structure for all biomass samples and the fitted environmental variables pH and HNO_2. Proximity in the NMDS plot indicates similarity in the composition of microbial communities of the samples. Microbial communities in the two reactor types were very similar after inoculation, but differentiated over time as the pH dropped. The drop to highly acidic conditions in urine reactors went along with a shift to a very distinct community that was correlated also with the increase in HNO_2 (spearman correlation coefficients: 0.74 for pH, 0.59 for HNO_2).

Discussion

Selection of AOB populations

It has been hypothesized that *Nitrosomonas europaea* are outcompeted at low pH values, because they have a low affinity for NH_3 and the availability of NH_3 decreases with decreasing pH (Tarre et al. 2007). However, rather than NH_3 limitation, a direct effect of the high proton concentration on the energy conservation is the likely reason for the low pH limit of 5.4 of AOB from the *Nitrosomonas europaea* lineage (Fumasoli et al. 2015). Correspondingly, *Nitrosomonas* OTU 3 disappeared in this study as soon as the pH dropped, independently of the NH_3 concentrations, which varied significantly between the urine and wastewater reactors (Figure 1).

The low pH selected for γ-proteobacterial AOB or *Nitrosospira* sp. in the urine and wastewater reactors, respectively (Figure 1). Cultured *Nitrosococcus* species grow optimally at salt concentrations of 300-700 $mmol \cdot L^{-1}$ NaCl depending on the species (Koops et al. 1990), while at least the *Nitrosospira* sp. of *Nitrosospira briensis* are characterized by a maximum salt tolerance of 250 $mmol \cdot L^{-1}$ only (Koops et al. 2006). The *Nitrosococcus*-related organisms in

the urine reactors appears to share this trait of a high salt tolerance as they were apparently better adapted to the salinity of 300 mmol·L^{-1} in the urine reactors, whereas *Nitrosospira* sp. were better adapted to the 45 mmol·L^{-1} in the wastewater reactors and could not thrive in the urine reactors. The different NH_3 concentrations may have been an additional selection criterion. However, the similar NH_3 affinity constants of 6-11 µmol·L^{-1} for *Nitrosospira* (Jiang and Bakken 1999) and 8.1 µmol·L^{-1} for *Nitrosococcus oceani* (Ward 1987), stress salt tolerance as major selection criterion.

The shift from *Nitrosococcus* OTU 66 to OTU 1 corresponds with an increase in the HNO_2 concentrations (Figure S1) and is thus likely due to a higher HNO_2 tolerance of OTU 1. These traits, in particular acid and HNO_2 tolerance, ultimately allowed *Nitrosococcus* OTU 1 to drive the system to a new stable state in which it dominated the bacterial community. *Nitrosospira* OTU 18 may be less resistant to extreme environments and did therefore not cause such strong acidification.

Nitrosococcus OTU 1 causes - and grows in – environments with low pH values and high HNO_2 concentrations

The decrease in pH and increase in HNO_2 levels caused by the growth of *Nitrosococcus* OTU 1 corresponded with the decrease in microbial richness and overall DNA yields per carrier (Figure 4, and S3). A strong influence of pH on microbial diversity has been reported for soils: soil pH was the major factor determining the richness of soil bacterial communities (Fierer and Jackson 2006). Low environmental pH values decrease the intracellular pH value in bacteria, which in turn compromises enzyme activity, as well as protein and DNA stability (Lund et al. 2014). Low intracellular pH values also hamper the energy generation in certain bacteria, e.g. AOB affiliating with the *Nitrosomonas europaea* lineage (Fumasoli et al. 2015). pH homeostasis is therefore an essential requirement for the survival of bacteria at low pH values (Slonczewski et al. 2009). HNO_2 impedes pH homeostasis under acidic conditions as it diffuses passively across the cytoplasmic membrane and decreases the intracellular pH value (Mortensen et al. 2008). HNO_2 also inhibits enzymes (Zhou et al. 2011) and it decomposes to NO (see next section), which is another toxic compound for bacteria (Zumft 1993). It is therefore not surprising that most of the bacteria did not survive these toxic conditions.

Nitrosococcus OTU 1 and *Mycobacterium* OTUs 21 and 684, however, still managed to grow (Figure 3, and S3). The uptake of potassium ions to inverse the membrane potential is a known pH homeostasis mechanism (Baker-Austin and Dopson 2007). The potassium concentration, however, did not have a significant impact on the reactor performance or the microbial community in our experiments (Figure 1, and 3), indicating that either still sufficient potassium was available in the Na reactors or that sodium ions were used instead. Sodium ions were found to increase the activity of *Thiobacillus thiooxidans* at low pH values, but the positive influence of sodium was less pronounced than the one for potassium (Suzuki et al. 1999). The gram-positive bacteria of the genus *Mycobacterium* are also known to have lipid-rich cell walls, which play an important role in their resistance to acids (Vandal et al. 2009). Highly impermeable cell membranes are another prerequisite for bacterial growth at low pH values as they reduce the leakage of protons (Slonczewski et al. 2009). Thus, acid tolerance can be due to a large variety of factors and the presence of potassium or possibly sodium alone does not determine, whether the acid-tolerant bacteria grew in.

Biological versus chemical nitrite oxidation

NOB are in general able to grow in acidic environments: NOB of the genus *Nitrospira* have been detected in engineered reactors (Gieseke et al. 2006, Tarre et al. 2004, Tarre and Green 2004, Tarre et al. 2007), and NOB of the genus *Nitrobacter* have been widely detected in acidic soils (De Boer and Kowalchuk 2001) and were also observed at average pH values of 4.1 in the synthetic wastewater in this study (Figure 1). It is therefore likely that accumulated HNO_2 rather than pH alone inhibited *Nitrobacter* sp. in the urine reactors with the first pH drop to 4.3 and caused the accumulation of total nitrite.

Despite the absence of NOB, total nitrite remained low once the pH dropped to pH levels below 2.5 (Figure 1), indicating conversion. At low pH values, HNO_2 is chemically converted to NO_3^-, involving several volatile intermediates, such as NO, NO_2, and N_2O_3 (Udert et al. 2005). Van Cleemput and Baert (1984) observed experimentally that NO is the major gaseous decomposition product, while NO_3^- production was favored under conditions where NO was not stripped, which corresponds very well with the results in this study: strong emissions of NO were observed due to the strong aeration in the MBBR, while also some NO_3^- was formed. NO can also be produced by AOB via the nitrifier denitrification pathway (Wrage et al. 2001), however, McKenney et al. (1990) found that emissions due to the chemical process are dominant at pH values below 4.5. NO is an unwanted nitrification by-product as it impacts human health and is considered to be the main precursor of ground-level tropospheric ozone in rural areas (Medinets et al. 2015).

Implications for wastewater treatment

With our results we show that γ-proteobacterial AOB and *Nitrosospira* sp. are important players in high and low strength nitrogen wastewaters, respectively, and can cause strong pH decreases. This finding challenges the perception that low pH nitrification is either not possible or dominated by AOA. The growth of γ-proteobacterial AOB is more critical than the growth of *Nitrosospira* sp., as γ-proteobacterial AOB acidify the wastewater more strongly allowing for the chemical decomposition of HNO_2 (Figure 1). The selection of γ-proteobacterial AOB may not only be a risk in urine nitrification reactors, but also during the treatment of other high strength nitrogen wastewaters with limited alkalinity, e.g., digester supernatant, animal wastewaters, or landfill leachate. Besides several reports on low pH nitrification with human urine (Schielke 2015, Udert et al. 2005), nitrification at pH values below 5 has also been observed in poultry manure (Prakasam and Loehr 1972). In order to avoid emissions of chemically produced NO, N_2O, NO_2, and HNO_2 gases, the growth of γ-proteobacterial AOB should be prevented in these wastewaters by maintaining the pH at sufficiently high values (>pH 6).

Acknowledgements

This study was funded by the Bill and Melinda Gates Foundation and was conducted as part of the VUNA project (www.vuna.ch, Grant No. OPP1011603). The authors like to thank Karin Rottermann and Claudia Bänninger for the chemical analyses, Bettina Sterkele and Hanspeter Zöllig for the laboratory support, and Mads Albertsen for bioinformatics guidance.

Supporting Information for Chapter 3

The growth of *Nitrosococcus*-related ammonia oxidizing bacteria causes strong acidification in high strength nitrogen wastewater

Alexandra Fumasoli, Helmut Bürgmann, David G. Weissbrodt, George F. Wells, Karin Beck, Joachim Mohn, Eberhard Morgenroth, Kai M. Udert

In preparation

Supplementary Materials & Methods

pH measurement

The pH was monitored on-line with pH sensors (Sentix 41, WTW, Weilheim, Germany and 405-DXX-S8/225, Mettler-Toledo, Greifensee, Switzerland) connected to amplifiers (pH-meter 605, Metrohm, Herisau, Switzerland and pH 340, WTW, Weilheim, Germany). The pH sensors were calibrated with pH standard solutions 7 and 4 on a bi-weekly basis. The on-line pH measurements were recorded with one minute intervals using a data logger (Memograph S, RSG40, Endress + Hauser, Reinach, Switzerland).

Characteristics of the inoculum

AOB from the inoculum were adapted to total ammonia concentrations of around 900 $mgNH_4$-$N \cdot L^{-1}$, a pH of around 6 and total salt concentrations of around 250 $mmol \cdot L^{-1}$. Additionally, 20 mL of activated sludge from the Eawag pilot-scale wastewater treatment plant operated with municipal wastewater were added to each reactor in order to diversify the initial AOB populations in the reactors.

Trace elements

A volume of 2 mL of the trace element solution (Table S2) was added to each liter of influent solution for the urine reactors, and 1 mL per liter of influent solution for the wastewater reactors. To compensate for water losses due to evaporation, 180 and 30 mL of deionized water were added to each liter of urine and wastewater influent.

Liquid phase sampling and analysis

Concentrations of total inorganic carbon (TIC) and total ammonia were measured biweekly in the influent. Total ammonia, total nitrite, and nitrate in the reactor were measured weekly, total and soluble chemical oxygen demand (COD) biweekly. The concentrations of phosphate (PO_4-P), chloride (Cl), sodium (Na) and potassium (K) in the influent and the reactor were measured in at least 8 samples during the first 90 days of reactor operation. Liquid phase samples were filtered (0.45 µm, MN GF-5, Macherey–Nagel, Düren, Germany) prior to analysis. Samples for total COD were homogenized (DIAX 600, Heidolph Instruments, Schwabach, Germany) prior to analysis.

The cations sodium and potassium and the anions nitrate, chloride, and phosphate were analyzed with ion chromatography (IC 881 Compact IC pro, Metrohm, Herisau, Switzerland). Total ammonia (NH_4^+ and NH_3) and total nitrite (NO_2^- and HNO_2) were either measured with IC or photometrically with cuvette tests (LCK 303, LCK 341, LCK 342, Hach-Lange, Berlin, Germany). Soluble and total COD were quantified photometrically with cuvette tests (LCK 614). TIC was measured using a total inorganic/total organic carbon analyzer (TOC-L, Shimadzu, Kyoto, Japan) according to manufacturers' protocol (Shimadzu Corporation 2010). Nitrification rates were calculated based on the input and output load of total ammonia. The output flow rate was corrected for a constant humidity loss through evaporation of 7.5 $mL \cdot d^{-1}$ caused by aeration of the reactors.

Batch experiments for NOB activity

The activity of NOB in urine reactor UR-Na and in wastewater reactor WWR-Na was checked on days 171 and 172, respectively, which was clearly after the pH shift in all reactors. For this purpose, 100 mL of Kaldnes® biofilm carriers were removed from UR-Na and WWR-Na, respectively, and were placed in a batch reactor with a volume of 250 mL. The temperature in the reactor was controlled with a water jacket (Colora Messtechnik GmbH, Lorch, Germany) at 24.3 ± 0.4°C and pH was monitored. The solution was stirred at 350 rpm using magnetic stirrers (RCT classic, IKA®-Werke GmbH & Co. KG, Staufen, Germany). The solution in the batch reactor contained KH_2PO_4 at 0.8 $g \cdot L^{-1}$ and $NaNO_2$ at 0.05 $g \cdot L^{-1}$. To prevent chemical degradation of HNO_2 at low pH values (Udert et al. 2005), the pH of the solution was adjusted to 6 by adding NaOH once in the beginning of the experiment. The pH was not controlled actively, but remained stable during the experiment (pH 6.0 ± 0.03 with UR-Na, pH 6.1 ± 0.03 with WWR-Na). The temporal trends in total nitrite and nitrate concentrations were analyzed by taking aliquots in an hourly interval. The experiments lasted 10 hours (WWR-Na) and 24 hours (UR-Na).

Biomass sampling and conditioning

The biomass of all four reactors was sampled every week. For each sampling point, four biofilm carriers were removed and replaced by new, unused carriers. The total number of removed biofilm carriers of around 90 was small compared to the estimated 900 carriers in the reactor. The carriers were cut in pieces using a sterile scalpel in preparation for direct use in DNA extraction kits and then stored at -20°C prior to molecular analysis.

Extraction of genomic DNA

Genomic DNA was extracted from two biofilm carriers from days -6, 7, 20, 27, 34, 41, 48, 55, 61, 69, 77, 90, 111, 131, and 154 using the FastDNA SPIN Kit for Soil (MP Biomedicals, Santa Ana, CA, USA), with adaptations to manufacturer's protocol. In short, the bead-beating step was performed under conditions close to the MIDAS field guide (McIlroy et al. 2015) in series of 4×20 s at 6 m s^{-1} separated by 2 min on ice. The purified DNA extracts were eluted in a final volume of 60 µL of nuclease-free water provided with the kit. The quality and rough concentration of the DNA extracts were assessed using a NanoDrop-1000™ UV/VIS spectrophotometer (Thermo Fischer Scientific Inc., Wilmington, DE, USA). DNA extracts were characterized by a median concentration of 18 $ng \cdot uL^{-1}$ and an absorbance ratio (260 to 280 nm) of 1.8.

In silico analysis and sequencing with primers targeting archaea

In silico testing of the primers set 341F (5'-CCTACGGGNGGCWGCAG-3') / 785R (5'-GACTACHVGGGTATCTAATCC-3') was conducted against the SILVA database of 16S rRNA gene reference sequences (Quast et al. 2013) by following Klindworth et al. (2013) with one mismatch allowed, and indicated that this primer pair can provide a theoretical coverage of 94% of the more than 400'000 reference sequences related to the kingdom of bacteria as well as of 95 to 100% of the reference sequences related to known AOB and NOB (Weissbrodt et al. 2015).

The samples from day -6 and 61 were analyzed with the primer pair 340wF (5'-CCCTAYGGGGYGCASCAG-3') / 958R (5'-YCCGGCGTTGAMTCCAATT-3') (v3-v6) for archaea diversity, as well as 926F (5'-AAACTYAAAKGAATTGRCGG-3') / 1392R (5'-ACGGGCGGTGTGTRC-3') (v6-v8) for bacterial and archaea diversity.

PCR for AOA

PCR for the detection of the *amoA* gene of ammonium oxidizing archaea was carried out using the primer-set (Arch-amoAF: STAATGGTCTGGCTTAGACG and Arch-amoAR: GCGGCCATCCATCTGTATGT) and PCR method of Francis et al. (2005): PCR cycling conditions were as reported previously, except using 40 cycles and the Promega GoTaq G2 Flexi DNA Polymerase and buffer with 2 mM $MgCl_2$ (Promega, Madison, WI, USA). Reaction products were visualized by gel electrophoresis on 1.4% agarose gels stained with EtBr. Positive controls consisting of a plasmid containing a cloned *amoA* PCR amplicon derived from activated sludge and previously sequenced to verify identity (Wells et al. 2009) were run alongside samples, and samples from reactor 1 in 10 to 1000-fold dilutions were spiked with positive control DNA to test for inhibition problems.

qPCR for archaea and *Nitrosococcus* OTU 1

All qPCR reactions were performed on a LightCycler 480-II (Roche, Rotkreuz, Switzerland) and analyzed using the LightCycler 480 ver. 1.5.1 software (Roche, Rotkreuz, Switzerland). Total reaction volumes were 10 µl with a sample volume of 2 µl. DNA extracts with DNA concentrations ranging from 9 to 166 ng μl^{-1} were diluted 1000 times (bacteria) or 100 times (archaea, *Nitrosococcus* OTU assay) and repeated at 100- or 10-fold dilutions if results were below or close to the limit of detection. 10- to 1000-fold dilutions of selected samples were also run in parallel to test for inhibitory effects.

Real-time PCR protocols for the quantification of bacterial 16S rRNA genes were carried out using the primer and probe set (Bact349F/Bact806R, Probe Bac516F) of Takai and Horikoshi (2000). Reaction conditions were adapted as follows: For bacterial 16S: 95°C 10 min initial denaturation and 45 cycles of: 95°C for 40 sec, 53°C for 40 sec, and 72°C for 1 min, using LightCycler 480 Probes Master hot start reaction mix (Roche, Rotkreuz, Switzerland) and each primer at a concentration of 0.9 $\mu mol \cdot L^{-1}$ and the probe at 0.3 $\mu mol \cdot L^{-1}$. Archaeal 16S rRNA genes were quantified using the primer and probe set (Arch349fF and Arch806R, Probe Arch516F) of Takai and Horikoshi (2000). Reactions were set up using the LightCycler 480 Probes Master hot start reaction mix (Roche, Rotkreuz, Switzerland) with each primer at a concentration of 1 $\mu mol \cdot L^{-1}$ and the probe at 0.15 $\mu mol \cdot L^{-1}$ and the following cycling conditions: 95°C for 10 min initial denaturation and 45 cycles of 95°C for 20sec, 60°C for 2400 sec. Results were evaluated using the point-fit method for absolute quantification.

To confirm the dynamics of a *Nitrosococcus*-related OTU 1 obtained from sequencing, a TaqMan qPCR assay was developed. Target and reference sequences were assembled from the reference sequence obtained by our own Illumina sequencing and closely related reference sequences obtained from public databases and aligned. A primer and TaqMan probe set specific for the target OTU sequence and discriminating against all other sequences was designed using AlleleID (ver. 7.82; PREMIER Biosoft, Palo Alto, CA): Forward primer: Nc. acid. F-1:

CGCTACCTACAGAAGAAG; reverse primer: Nc. acid. R-1: GGGATTTCACACCTAACTTA; Probe: Nc. acid. FAM-AAACCGCCTACATGCCCTTT-TAMRA. Reaction chemistry was the same as described for the bacterial 16S assay and cycling conditions were: initial denaturation of 95°C for 5 min and 45 cycles of 95°C for 10 sec, 60°C for 20 sec.

Thermodynamic calculations with PHREEQC

The computer program PHREEQC Interactive (Version 2.15.0, Parkhurst and Appelo 1999) was used to calculate the minimal pH values that can be reached, if the total ammonia in synthetic urine or synthetic wastewater is completely converted to nitrate. We used the database "wateq4f.dat" included in the PHREEQC package. For the initial solution, we used the measured concentrations in the reactors and the observed reactor pH values (Table S4). The chloride ion was used for charge balance. The proton release from the oxidation of ammonium to nitrate was simulated by the addition of chloride ions and a charge balance of pH. We assumed that two moles of protons are released per mole of ammonium that is oxidized to nitrate.

Supplementary Results

Nitrogen mass balance

Table S3 shows the mass balance of the nitrogen compounds in both urine and wastewater reactors. High nitrogen emissions of 53 and 50% were observed in UR-K and UR-Na, respectively, while nitrogen emissions from the wastewater reactors were low. The nitrogen loss from the liquid phase is balanced by emissions of NO, NO_2, and N_2O in the off-gas. In addition, at low pH values, HNO_2 might be stripped from the reactors. HNO_2 was not analyzed in the off-gas, but maximal emissions were estimated to be 1.2 and 1.8 $mgN \cdot L^{-1} \cdot d^{-1}$ for UR-K and UR-Na assuming equilibrium between liquid and air, a Henry coefficient for HNO_2 of 0.00083 $mol(g) \cdot mol^{-1}(aq)$ (Schwartz and White 1981) and average HNO_2 concentration in the liquid of 3.4 and 5.3 $mgN \cdot L^{-1}$. HNO_2 emissions are therefore far lower than the observed NO emissions.

Sequencing with primers targeting archaea

Very few sequences of AOA from affiliates of the family of *Nitrososphaeraceae* were found in UR-K at day -6, but none of the sequencing results revealed AOA at the later data point after 61 days.

Batch experiment for NOB

Figure S4 displays the total nitrite and nitrate concentrations in two batch experiments with biofilm carriers from urine reactor UR-Na and wastewater reactor WWR-Na, respectively. In the batch experiment with sludge from UR-Na the total nitrite as well as the nitrate concentrations remained constant, whereas with sludge from WWR-Na the total nitrite was converted to nitrate. Hence, NOB were active in the wastewater but not in the urine reactors.

This results support the molecular analysis where NOB remained below the detection limit in the urine reactors, but were still present in the wastewater reactors.

Supplementary Tables

Table S1: Recipes for the synthetic influent solutions to the urine and wastewater reactors. Urine and wastewater reactors contained different total ammonia and total salts concentrations. The urine reactors (UR-K and UR-Na) as well as the wastewater reactors (WWR-K and WWR-Na) differed in their potassium and sodium concentrations.

		UR-K	UR-Na	WWR-K	WWR-Na
KCl	$g \cdot L^{-1}$	4.4	0	0	0
NaCl	$g \cdot L^{-1}$	0	3.6	0	0
NH_4Cl	$g \cdot L^{-1}$	0	0	0.6	0.6
NH_4OH (25% NH_3)	mL	5.5	5.5	0	0
NH_4HCO_3	$g \cdot L^{-1}$	6	6	0	0
$NaHCO_3$	$g \cdot L^{-1}$	0	0	0	1.7
$KHCO_3$	$g \cdot L^{-1}$	0	0	2	0
KH_2PO_4	$g \cdot L^{-1}$	0.8	0	0.05	0
$NaH_2PO_4 \cdot 2H_2O$	$g \cdot L^{-1}$	0	0.95	0	0.06

Table S2: Recipe for the trace element solution added to the synthetic influent solutions. A volume of 2 mL of the trace element solution was added to each liter of influent solution in the urine reactors, and 1 mL per liter of influent solution in the wastewater reactors.

$FeSO_4 \cdot 7H_2O$	$mg \cdot L^{-1}$	172
$ZnCl_2$	$mg \cdot L^{-1}$	20
$MnCl_2 \cdot 4H_2O$	$mg \cdot L^{-1}$	47
H_3BO_3	$mg \cdot L^{-1}$	6
$CuSO_4 \cdot 5H_2O$	$mg \cdot L^{-1}$	3
$Na_2MoO_4 \cdot 2H_2O$	$mg \cdot L^{-1}$	2
NaCl	$mg \cdot L^{-1}$	584
KCl	$mg \cdot L^{-1}$	746
$MgSO_4 \cdot 7H_2O$	$mg \cdot L^{-1}$	2465
$CaCl_2 \cdot 2H_2O$	$mg \cdot L^{-1}$	1470

Table S3: Nitrogen mass balances of the urine reactors (UR-K and UR-Na) and wastewater reactors (WWR-K and WWR-Na). Mass balances for the liquid were calculated from the total ammonia input and the total nitrogen output (sum of total ammonia, nitrate and total nitrite). Nitrogen losses from the liquid phase are balanced by gaseous nitrogen emissions (sum of NO, NO_2, N_2O). HNO_2 emissions were not analyzed but estimated using Henry's Law to be below 1.2 and 1.8 $mgN \cdot L^{-1} \cdot d^{-1}$ for UR-K and UR-Na. Indicated precisions were calculated by error propagation of the standard deviations for liquid and gas phase measurements.

		UR-K	UR-Na	WWR-K	WWR-Na	
Liquid phase:						
Input	Total ammonia	17.4 ± 0.7	18.7 ± 0.7	8.4 ± 0.3	8.2 ± 0.3	$mgN \cdot L^{-1} \cdot d^{-1}$
Output	Total ammonia	3.6 ± 0.1	4.2 ± 0.2	0.9 ± 0.0	0.6 ± 0.0	$mgN \cdot L^{-1} \cdot d^{-1}$
Output	Nitrate	4.5 ± 0.2	5.0 ± 0.2	8.0 ± 0.3	7.2 ± 0.3	$mgN \cdot L^{-1} \cdot d^{-1}$
Output	Total nitrite	0.03 ± 0.00	0.04 ± 0.00	0.00 ± 0.00	0.00 ± 0.00	$mgN \cdot L^{-1} \cdot d^{-1}$
Nitrogen mass balance (Input – Output)		**9.2 ± 0.7**	**9.4 ± 0.8**	**-0.5 ± 0.5**	**0.4 ± 0.4**	$mgN \cdot L^{-1} \cdot d^{-1}$
		53	50	-6	5	%
Gas phase:						
Output	NO	8.7 ± 1.3	7.1 ± 1.1	< 0.5	< 0.5	$mgN \cdot L^{-1} \cdot d^{-1}$
Output	NO_2	1.3 ± 0.3	1.6 ± 0.4	< 0.3	< 0.3	$mgN \cdot L^{-1} \cdot d^{-1}$
Output	N_2O	0.4 ± 0.1	0.2 ± 0.0	< 0.1	<0.1	$mgN \cdot L^{-1} \cdot d^{-1}$
Total nitrogen emissions		**10.4 ± 1.3**	**8.9 ± 1.1**	**< 0.9**	**< 0.9**	$mgN \cdot L^{-1} \cdot d^{-1}$

Table S4: Measured concentrations and standard deviations in all four reactors. The urine reactors (UR-K and UR-Na) contained higher total ammonia and total salt concentrations than the wastewater reactors (WWR-K and WWR-Na). UR-K and WWR-K contained high potassium, but low sodium concentrations, whereas UR-Na and WWR-Na contained high sodium, but low potassium concentrations.

		UR-K	UR-Na	WWR-K	WWR-Na
NH_4-N	$mg \cdot L^{-1}$	**875 ± 231**	**842 ± 176**	**15.6 ± 3.2**	**12.3 ± 3.1**
NO_3-N	$mg \cdot L^{-1}$	959 ± 148	916 ± 103	152 ± 8.2	150 ± 8.0
PO4-P	$mg \cdot L^{-1}$	192 ± 19.0	194 ± 12.6	12.1 ± 2.5	13.0 ± 3.2
Cl	$mg \cdot L^{-1}$	2490 ± 234	2250 ± 66.2	459 ± 66.4	459 ± 91.9
Na	$mg \cdot L^{-1}$	**13.2 ± 4.6**	1620 ± 86.5	**6.1 ± 1.4**	524 ±41.9
K	$mg \cdot L^{-1}$	2920 ± 457	**25.8 ±21.3**	887 ±70.1	**13.2 ± 4.4**
COD dissolved	$mg \cdot L^{-1}$	123 ± 39.1	103 ± 34.7	12.2 ± 4.1	11.8 ± 4.2
COD particulate	$mg \cdot L^{-1}$	201 ± 97.6	124 ± 40.5	26.9 ± 28.6	22.2 ± 9.1
Total salts	$mmol \cdot L^{-1}$	**283 ± 46.2**	**266 ± 26.5**	**48.3 ± 4.6**	**48.1 ± 5.4**

Supplementary Figures

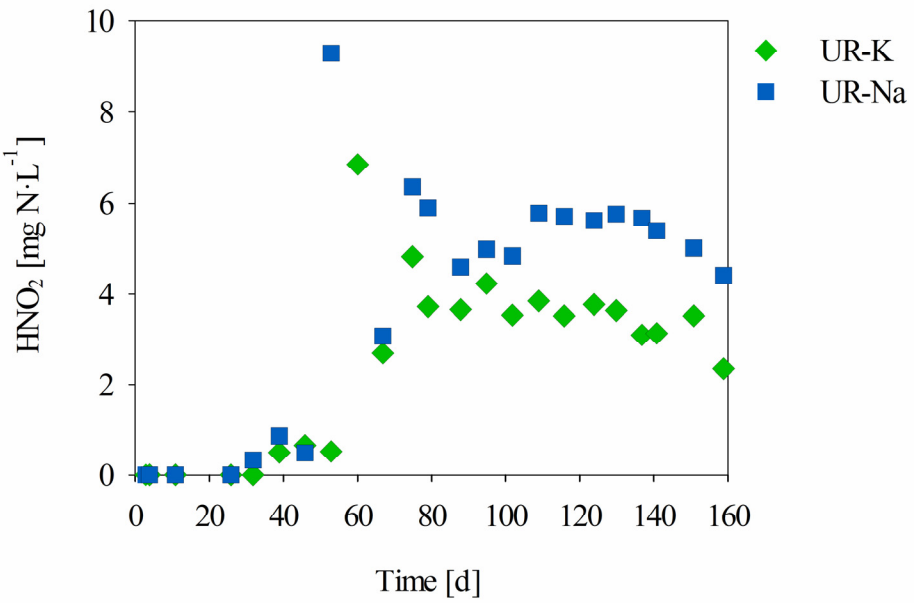

Figure S1: HNO_2 concentrations in both urine reactors (UR-K and UR-Na) calculated from nitrite and pH.

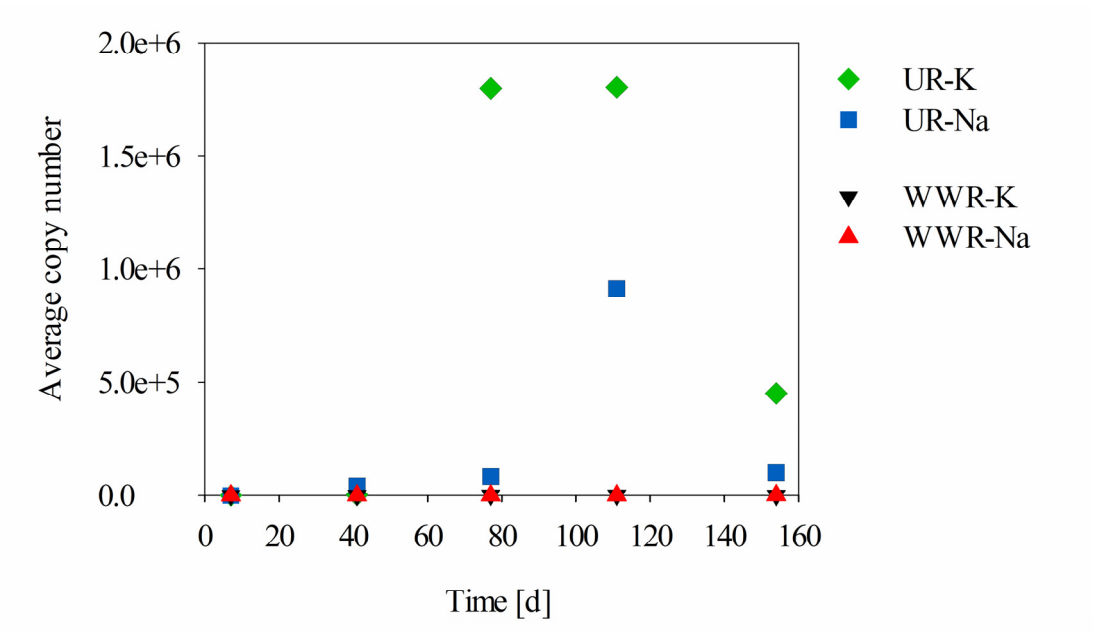

Figure S2: Average copy number of *Nitrosococcus* OTU 1 in the urine reactors (UR-K and UR-Na) and in the wastewater reactors. Copy numbers were below a value of 1000 in all samples of the wastewater reactors (WWR-K and WWR-Na).

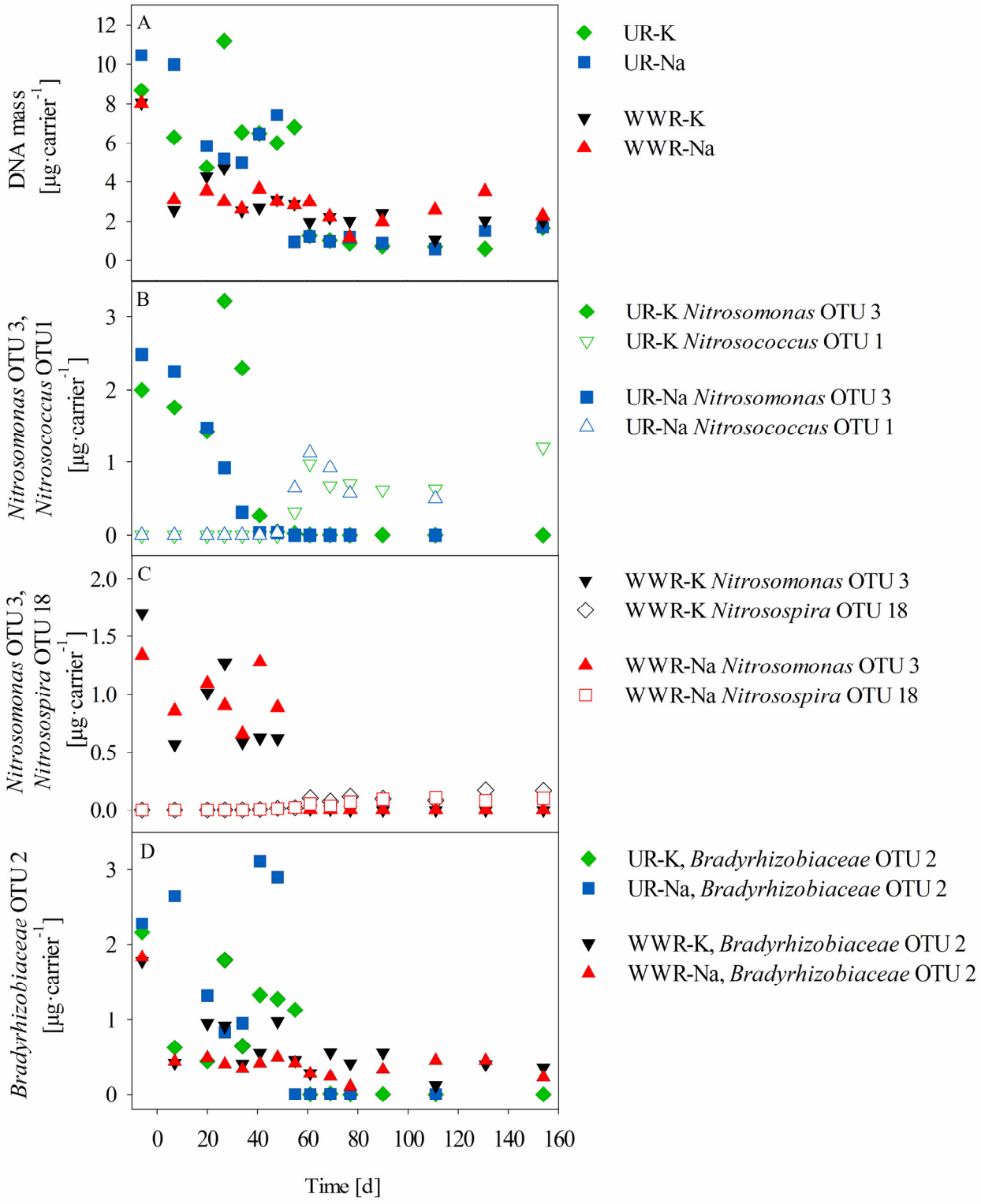

Figure S3: (A) Measured DNA concentrations in all reactors, (B) specific DNA concentrations of *Nitrosomonas* OTU 3 and *Nitrosococcus* OTU 1 in the urine reactors (UR-K and UR-Na), (C) specific DNA concentrations of *Nitrosomonas* OTU 3 and *Nitrosospira* OTU 18 in the wastewater reactors (WWR-K and WWR-Na), as well as (D) specific DNA concentrations of *Bradyrhizobiaceae* OTU 2 comprising the genus *Nitrobacter*.

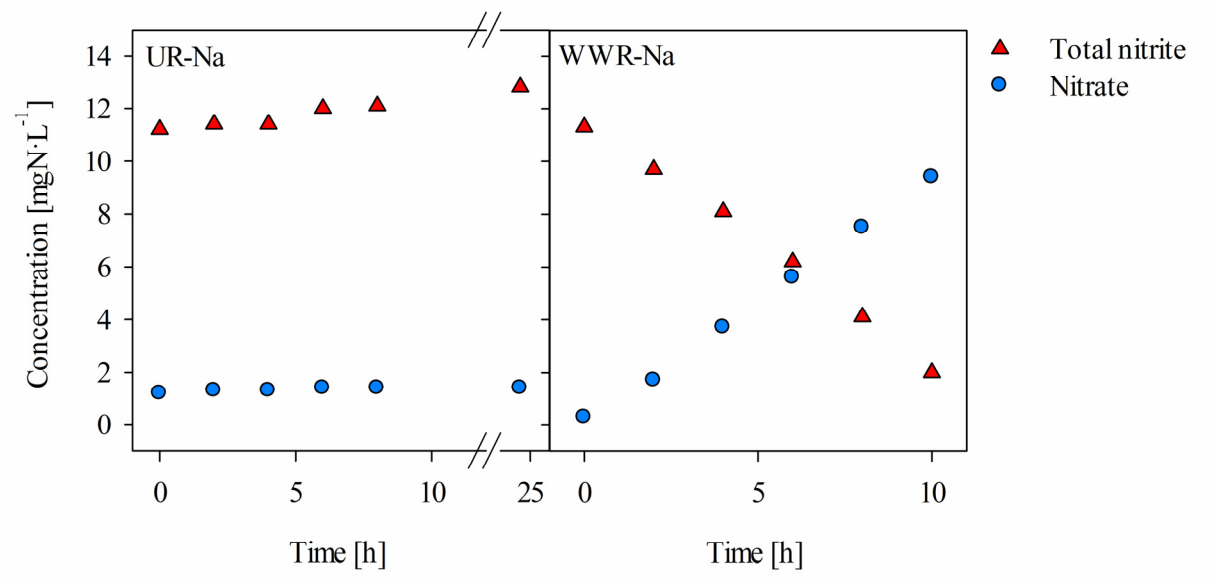

Figure S4: Concentrations of total nitrite and nitrate in two batch experiment performed with biofilm carriers from urine reactor UR-Na (left) and wastewater reactor WWR-Na (right), respectively.

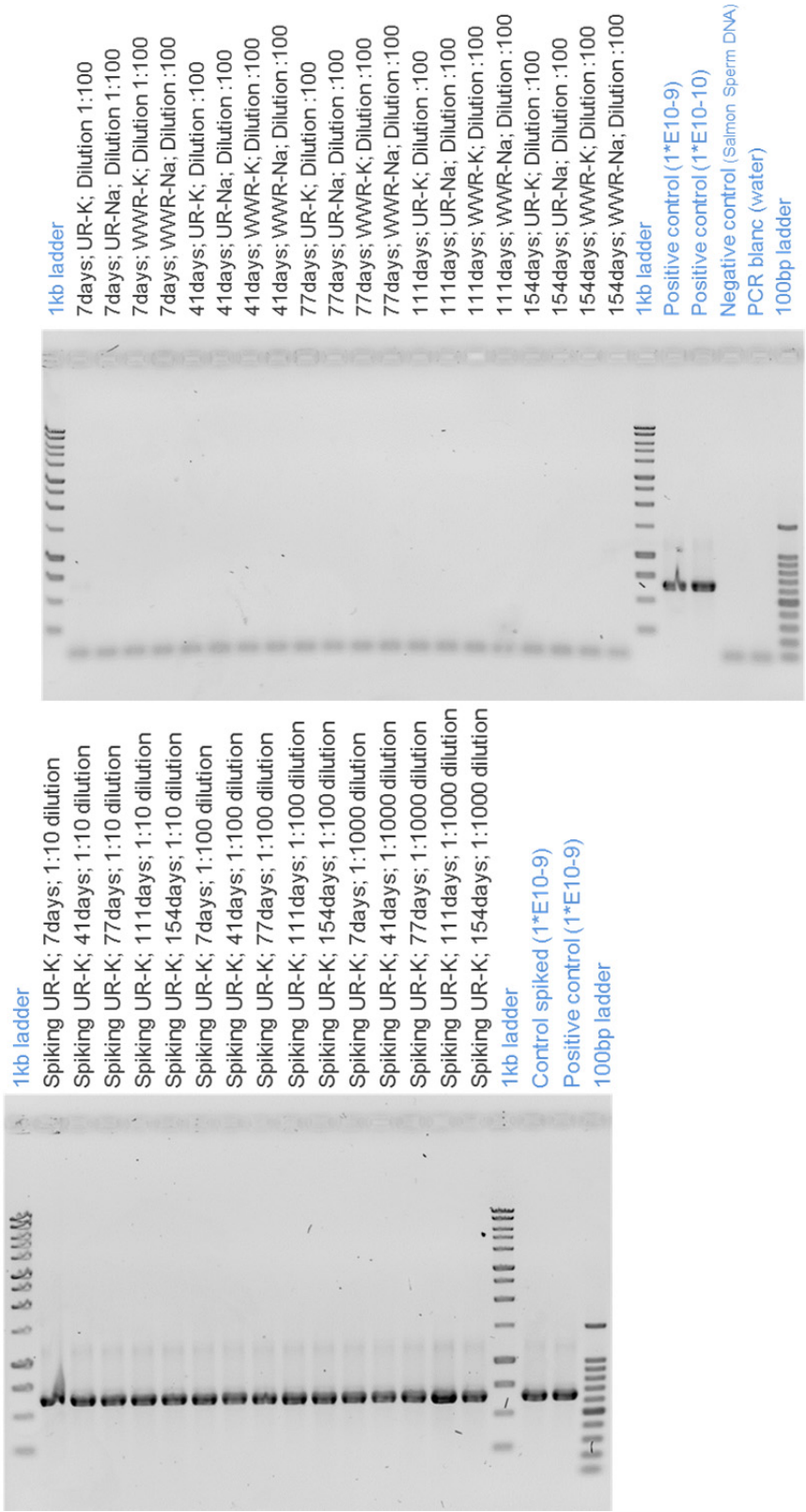

Figure S5: PCR for ammonia oxidizing archaea. 5 samples of each reactor and a positive control were tested. Furthermore samples of urine reactor UR-K at different time points and dilutions were spiked with the positive control. Positive results in the spiked samples show that negative results were not due to PCR inhibition problems.

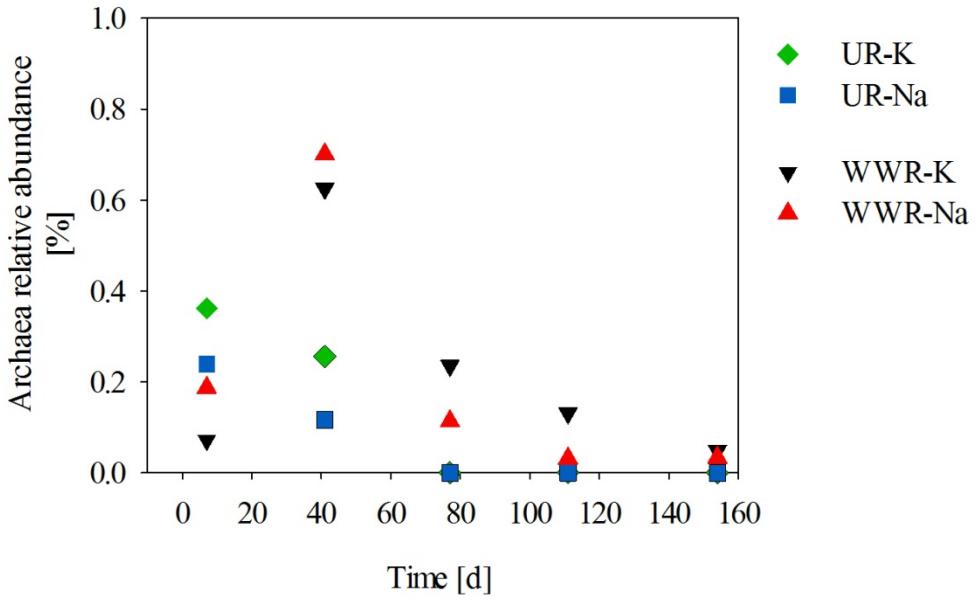

Figure S6: Relative abundance of archaea compared to the total sum of bacteria and archaea in the urine reactors (UR-K and UR-Na) as well as in the wastewater reactors (WWR-K and WWR-Na). Archaea were below the detection limit of 50 gene copies / reaction in the later samples of the urine reactors (days 77, 111 and 154).

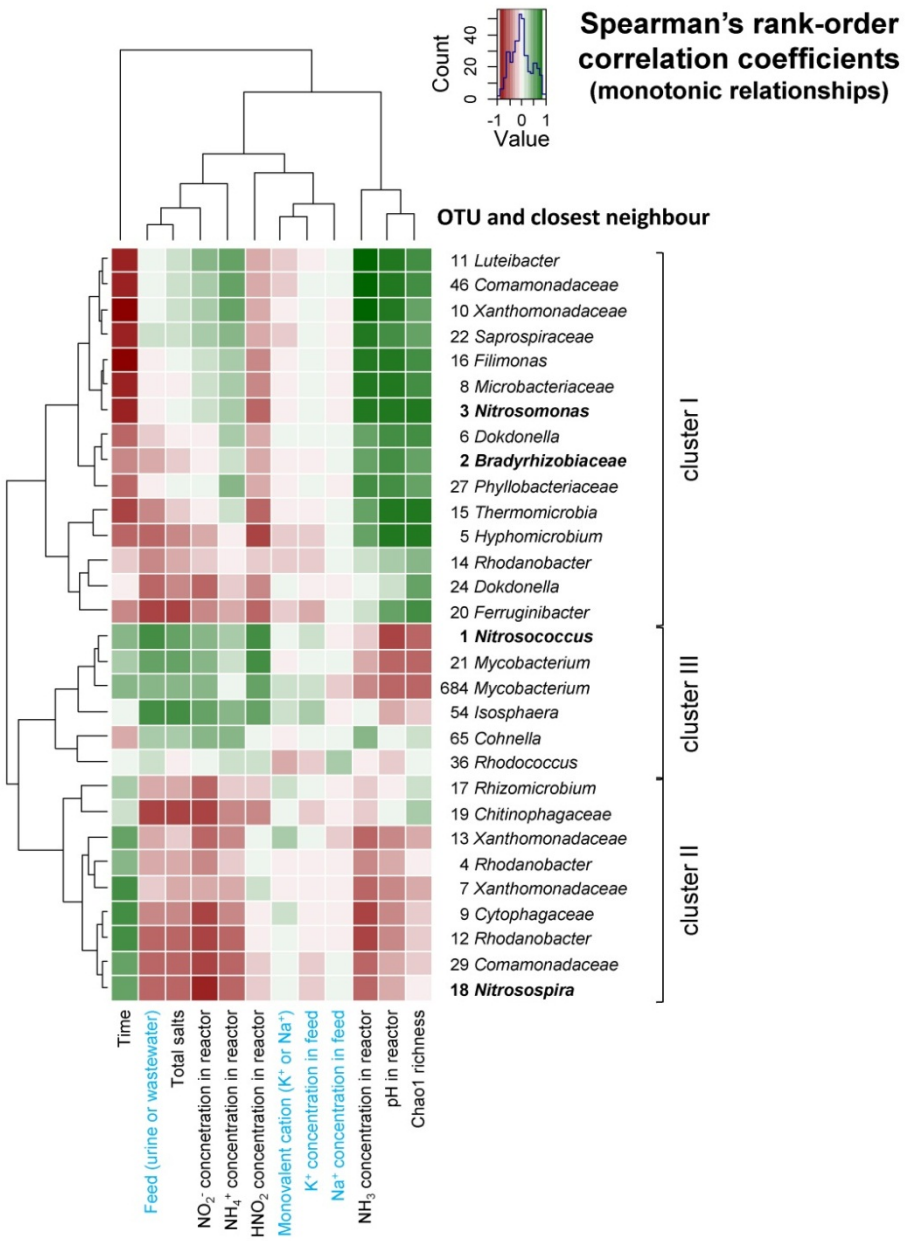

Figure S7: Heatmaps of Spearman's rank-order correlations computed to assess the monotonic relationships between predominant phylotypes (vertical axis) that displayed relative abundance above 5% and that shared similar dynamics in function of environmental conditions (horizontal axis) prevailing in the urine and wastewater reactors. The fixed operational conditions are provided in blue font, while the environmental variables that evolved over the experimental period are provided in black font. Three main clusters of phylotypes were identified in function of positive (green gradient) and inverse (red gradient) correlations. Cluster I is notably composed of *Nitrosomonas* OTU 3 which relative abundance positively correlated with the higher pH conditions that prevailed in the first experimental period. Cluster II notably comprises *Nitrosospira* OTU 3 that was mainly selected by the wastewater matrix under lower pH condition. Cluster III is mainly represented by *Nitrosococcus* OTU 1 and *Mycobacterium* OTUs 21 and 684 that dominated the bacterial community in the urine-based reactors at low pH. Only low correlations were obtained between the dynamics of OTUs and the type of monovalent cation.

Chapter 4

Stable ammonia conversion to nitrate and the prevention of unfavorable system states during nitrification of urine

Alexandra Fumasoli, Eberhard Morgenroth, Kai M. Udert

Submitted

Graphical abstract

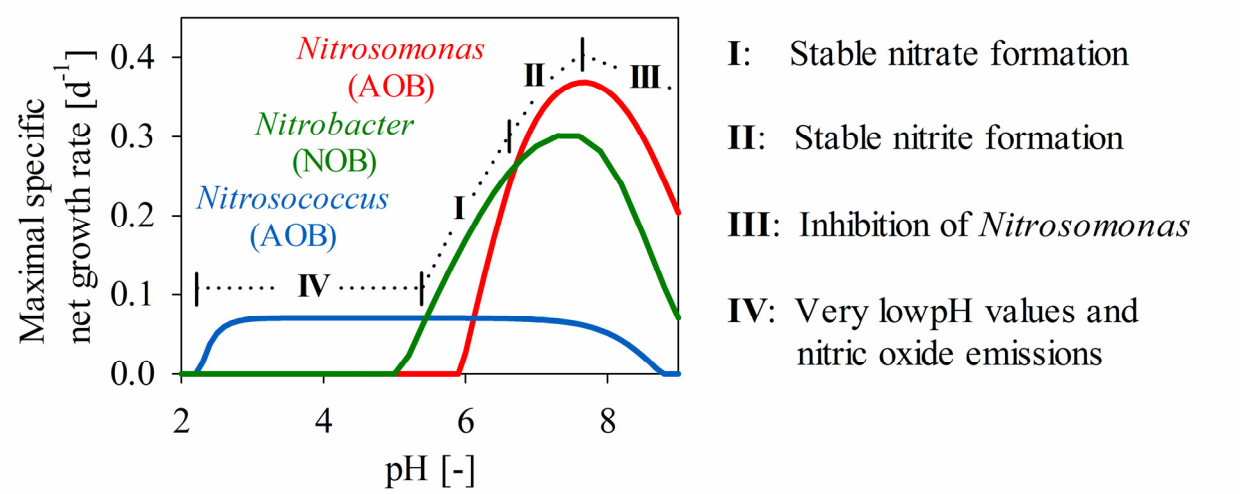

Abstract

Microbial nitrification is a pretreatment step for fertilizer production from human urine. As the molar ratio of alkalinity to total ammonia is approximately one to one in urine, only half of the total ammonia is converted during nitrification. After nitrification, the solution has a very low alkalinity and increases of the inflow rate can lead to strong increases of the pH value and concomitantly of the free ammonia concentration. This can cause two major failures: (1) the production of nitrite instead of nitrate, when nitrite oxidizing bacteria (NOB) are too slow or inhibited and (2) complete cessation of nitrification, when ammonia oxidizing bacteria (AOB) are too slow or inhibited. The third major failure is caused by very low inflow rates: acid-tolerant AOB can grow in, which decrease the pH to very low values. The aim of this study was to use a mechanistic model to determine the conditions enabling stable nitrate production and preventing unfavorable system states. The nitrification model revealed that stable nitrate formation is only possible within a narrow pH range. At increased urine dosage and higher pH values, nitrite accumulates to irreversibly high levels within days. Nitrification ceases completely within short time, when the inflow rate is increased even further. Long-term underloading results in the selection of acid-tolerant AOB and a pH drop to very low values. As a consequence of the pH drop, nitrous acid (HNO_2) is formed, which inhibits NOB. However, at the low pH values, HNO_2 is converted chemically to nitrate, during which the volatile intermediate nitric oxide (NO) is released to the atmosphere. To ensure safe reactor operation, the pH should be controlled within a narrow range by regulating the urine influent. Furthermore, nitrite should be continuously monitored.

Introduction

Biological nitrification followed by distillation is a promising process combination to recover nutrients from urine (Udert and Wächter 2012). Nitrification is a required pretreatment for distillation, particularly to prevent volatilization of free ammonia (NH_3) due to the high pH of around 9 and the high total ammonia concentration in stored urine (Udert et al. 2006). Due to the limited alkalinity compared to the total ammonia concentration ($NH_3 + NH_4^+$), only 50% of the total ammonia is converted to nitrate (NO_3^-). Despite the partial conversion, NH_3 losses are prevented, because the pH drop during nitrification converts NH_3 into stable ammonium (NH_4^+).

The limited alkalinity is thus not a problem per se, but it makes the process susceptible for pH changes leading to process failures. Three major failures have been observed in urine nitrification reactors, whether operated with suspended biomass or with biofilms: (1) complete cessation of nitrification at high pH values, (2) the conversion to nitrite (NO_2^-) instead of nitrate, and (3) low pH values due to the growth of acid-tolerant AOB (Table 1). Ammonium nitrite is an unwanted nitrification product, as it leads to nearly complete nitrogen loss during distillation (Wächter et al. In prep.) and nitrogen should be retained for the use as a fertilizer. The low pH values caused by the growth of acid-tolerant AOB have to be prevented, because nitrogen oxide gases are emitted, which are harmful for humans and the environment (Fumasoli et al. subm., Udert et al. 2005).

Nitrifiers will not grow in untreated stored urine, because the high NH_3 concentrations impede nitrification (Anthonisen et al. 1976). The inhibition by NH_3 can be circumvented, when nitrification reactors are operated as continuous flow stirred tank reactors (CSTR) or as sequencing batch reactors (SBR) with low exchange volumes. However, inhibition by free ammonia will occur, if these reactors are overloaded with stored urine (Table 1).

To prevent inhibition by NH_3, lower pH values must be maintained during urine nitrification. However, under these conditions, another process failure can occur: nitrite accumulation. At a pH of 7 and a temperature of 30°C, nitrite and not nitrate was produced in a CSTR operated with urine (Udert et al. 2003a). Nitrite also accumulated after a pH increase from 6.1 to 6.9 in a membrane aerated biofilm reactor (MABR) (Table 1, Udert and Wächter 2012). The conversion to nitrite at elevated pH and temperatures is due to the selective wash out of NOB. This effect is used intentionally in the SHARON process (Single reactor system for High activity Ammonia Removal Over Nitrite) to produce a nitrite, which is later converted to nitrogen gas (Hellinga et al. 1999). A pH value of 7 ensures high but not inhibitory concentrations of NH_3, which is the actual substrate for AOB (Suzuki et al. 1974). High temperatures between 30 and 40°C are chosen, as the maximal growth rate of AOB exceeds the one of NOB at temperatures above 20°C (Hunik et al. 1994).

Table 1: Example of the three observed process instabilities of complete inhibition of nitrification at high pH values, nitrite production, and the pH drop as a result of acid-tolerant AOB.

	High pH values	**Nitrite**	**Low pH values**
	Own measurements in a pilot-scale **MBBR** in the main building of Eawag (Forum Chriesbach)	Reported in: - **MABR (Udert and Wächter 2012)** - CSTR (Udert et al. 2003a) - SBRs (Sun et al. 2012) (Udert et al. 2003a) - MBR (Sun et al. 2012)	Reported in: - **MBBRs (Fumasoli et al. subm.)** - CSTR (Fumasoli et al. 2016) - MABR (Udert et al. 2005)
	Example MBBR	**Example MABR**	**Example MBBR**
	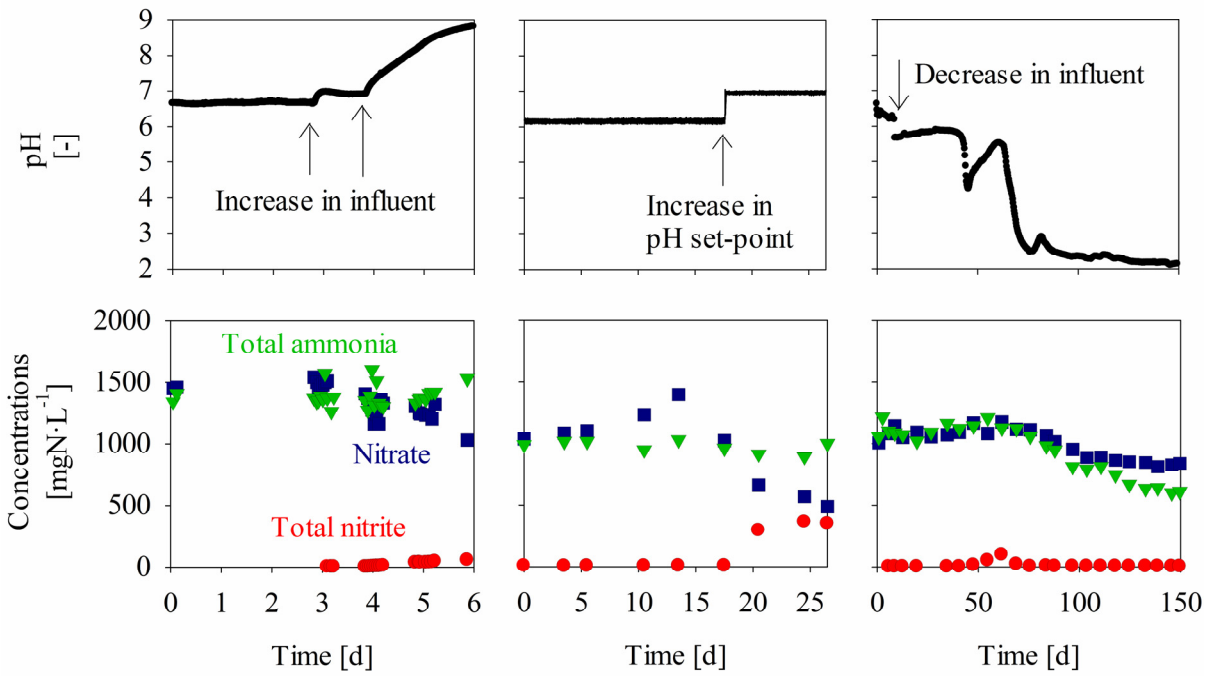		
	Increase in influent rate causes pH to increase Nitrification ceases and pH adjusts to pH of influent urine	Increase in pH setpoint by adding more urine Total nitrite increases, while nitrate decreases	Decrease in influent rate decreases pH to 5.7 The growth of *Nitrosococcus* causes pH drop to 2.2 NOB are lost, but total nitrite is converted chemically (HNO_2 decomposition) to NO and nitrate Nitrate decreases due to stripping of NO

MBBR: Moving bed biofilm reactor, MABR: Membrane aerated biofilm reactor, CSTR: Continuous stirred tank reactor, SBR: Sequencing batch reactor, MBR: Membrane bioreactor

To prevent a selective NOB wash out, the pH should be kept low, which requires low urine dosage. Low pH values decrease the growth rate of the most common AOB in urine nitrification reactors (*Nitrosomonas europaea* lineage), due to the limited availability of NH_3 (Hellinga et al. 1999) and due to energy limitations (Fumasoli et al. 2015). However, low pH values can select for acid-tolerant AOB in urine nitrification reactors (Fumasoli et al. 2016, Fumasoli et al. subm.). In moving bed biofilm reactors (MBBR) operated at a low continuous dosage of synthetic urine, acid-tolerant AOB related with *Nitrosococcus* were selected and decreased the pH to values as low as 2.2 (Table 1 and Fumasoli et al. subm.). NOB (affiliated with *Nitrobacter*) disappeared with the pH drop, but nitrite was converted further to nitrate by the chemical decomposition of nitrous acid (HNO_2). The stripping of the volatile intermediates nitric oxide (NO), nitrogen dioxide (NO_2), and nitrous oxide (N_2O) as well as HNO_2 caused high nitrogen losses. Hence, while pH needs to be kept low in order to keep NOB active, low pH values also pose the risk for the selection of acid-tolerant AOB.

The operational conditions leading to nitrite or nitrate formation have been investigated for the SHARON process by the use of a two-step nitrification model (Volcke et al. 2007a, Volcke et al. 2007b). These studies focused mainly on pH values of 7, while lower pH values are required for urine treatment. To be able to represent the behavior of urine reactors, the nitrification model has to be extended. The most important extensions are the inclusion of acid-tolerant AOB and a pH term, which describes the pH dependency of the *Nitrosomonas europaea* lineage at low pH values.

The aim of this study was to investigate how urine nitrification needs to be operated in order to produce nitrate and to prevent the three unwanted system states of (1) complete cessation of nitrification at high pH values, (2) nitrite accumulation, and (3) low pH nitrification by the selection of acid-tolerant AOB. Furthermore, we evaluated whether and how the change to the three unwanted system states is reversible. For this purpose, we set up a mathematical model based on a literature review and used this model to investigate the behavior of suspended growth systems at different urine dosage patterns.

Nitrification model

Biological processes

Two AOB were included in the nitrification model: an acid-sensitive AOB affiliated with the *Nitrosomonas europaea* lineage (further referred to *Nitrosomonas*), and an acid-tolerant AOB related to *Nitrosococcus* (further referred to *Nitrosococcus*). Furthermore, NOB affiliated with the *Nitrobacter* genus (further referred to *Nitrobacter*) were included. These AOB and NOB were identified in our experiments with synthetic urine (Fumasoli et al. subm.). The stoichiometric matrix for the growth of all nitrifiers is shown in Table S1. The model was implemented in the simulation environment AQUASIM (Reichert 1994) as a mixed reactor compartment.

***Nitrosomonas* (AOB 1)**. To model the growth rate of *Nitrosomonas*, the kinetic approach derived in Fumasoli et al. (2015) was extended by a non-competitive inhibition term for NH_3 (Equation 1). The NH_3 inhibition term was included to being able to model high pH values, which was not the focus in Fumasoli et al. (2015).

$$r_{AOB} = \mu_{max,AOB} \cdot \frac{\{NH_3\}}{\{NH_3\}+K_{NH3,\mathrm{AOB}}} \cdot \frac{K_{I,NH3,AOB}}{\{NH_3\}+K_{I,NH3,\mathrm{AOB}}} \cdot \frac{K_{I,HNO2,\mathrm{AOB}}}{\{HNO_2\}+K_{I,HNO2,\mathrm{AOB}}} \cdot \left(1 - 10^{\left(K_{pH,AOB}\left(pH_{min,AOB}-pH\right)\right)}\right) \cdot X_{AOB} \quad (1)$$

with r_{AOB} the growth rate (g COD·L^{-1}·d^{-1}), μ_{max} the maximum growth rate (d^{-1}), $K_{NH3,AOB}$ the affinity constant for NH_3 (mol·L^{-1}), $K_{I,NH3,AOB}$ the constant for non-competitive inhibition by NH_3 (mol·L^{-1}), $K_{I,HNO2,AOB}$ the constant for non-competitive inhibition by HNO_2 (mol·L^{-1}), pH_{min} the minimal pH for growth (-), K_{pH} a parameter describing how fast the activity ceases as the pH limit is approached (-), and X_{AOB}, the biomass concentration (g COD·L^{-1}). The growth rate in Equation 1 is valid for cases where pH ≥ $pH_{min,AOB}$; for pH < $pH_{min,AOB}$ the growth rate is set to 0. The values in {} brackets mean that we calculated in activities and not concentrations.

***Nitrosococcus* (AOB 2)**. To model the growth rate of *Nitrosococcus*, we used the same kinetic approach as in Equation 1, but we neglected the NH_3 affinity term and the HNO_2 inhibition term: a NH_3 affinity constant was not included, because *Nitrosococcus* would require an extremely low NH_3 affinity constant to grow at a pH of 2.2 (Fumasoli et al. subm.). It is therefore likely that *Nitrosococcus* use an alternative mechanism, which allows the uptake of ammonium instead of ammonia. In our simulations, however, ammonium concentrations are so high that a substrate limitation is unlikely. This assumption is supported by experiments for *Nitrosococcus oceani* (Ward 1987): the author found that the NH_3 affinity constant varied by a factor of 78 within a pH range of 6.3 to 8.6, while the affinity constant calculated for NH_4^+ varied only by a factor of 2. This is different than for *Nitrosomonas europaea*, where the affinity constant remained, within experimental error, unchanged with respect to NH_3 within a pH range between 6.5 and 9.1 (Suzuki et al. 1974). The HNO_2 inhibition term was neglected, as *Nitrosococcus* were experimentally shown to be selected at high HNO_2 concentrations (Fumasoli et al. subm.). They resisted concentrations of above 9 mg HNO_2-N·L^{-1}, values at which *Nitrosomonas* (and also *Nitrobacter*) would be severely inhibited.

***Nitrobacter* (NOB)**. The growth rate of *Nitrobacter* was modeled by assuming that nitrite is the substrate, but HNO_2 the inhibitory compound (Pambrun et al. 2006):

$$r_{NOB} = \mu_{max,NOB} \cdot \frac{\{NO_2^-\}}{\{NO_2^-\}+K_{NO2-,\mathrm{NOB}}} \cdot \frac{K_{I,NH3,\mathrm{NOB}}}{\{NH_3\}+K_{I,NH3,\mathrm{NOB}}} \cdot \frac{K_{I,HNO2,\mathrm{NOB}}}{\{HNO_2\}+K_{I,HNO2,\mathrm{AOB}}} \cdot X_{NOB} \quad (2)$$

with r_{NOB} the growth rate (g COD·L^{-1}·d^{-1}), $\mu_{max,NOB}$ the maximum growth rate (d^{-1}), $K_{NO2-,NOB}$ the affinity constant for NO_2^- (mol·L^{-1}), $K_{I,NH3,NOB}$ the constant for non-competitive inhibition by NH_3 (mol·L^{-1}), $K_{I,HNO2,NOB}$ the constant for non-competitive inhibition by HNO_2 (mol·L^{-1}), and X_{NOB}, the biomass concentration (g COD·L^{-1}). Many nitrification models included HNO_2 as substrate for NOB, as it can pass the cell membrane by diffusion, which is not the case for the ionized form NO_2^- (Wiesmann 1994). However, Pambrun et al. (2006) showed experimentally that the affinity constant determined for nitrite oxidizers at pH 7.5 and 8.5 remained identical in terms of NO_2^- rather than HNO_2. Similar results were obtained for pure cultures of *Nitrobacter agilis*, where the NO_2^- affinity constant only slightly increased within a pH range of 6.5 to 8.5 (Hunik et al. 1993). Nitrite oxidoreductase (NXR) in *Nitrobacter* is oriented towards the cytoplasmic side (Spieck and Bock 2005) with NO_2^- being the substrate. However, NO_2^- transporters are found in all known *Nitrobacter* genomes (Starkenburg et al. 2008), indicating that the uptake of nitrite is not restricted to HNO_2 diffusion.

Biomass decay. The decay for all nitrifiers was modeled according to a conventional activated sludge model (Henze et al. 2000):

$$r_{Decay} = b \cdot X \quad (3)$$

with r_{Decay} the decay rate ($gCOD \cdot L^{-1} \cdot d^{-1}$), and b the decay coefficient (d^{-1}).

Kinetic constants. The model considers a case in which the maximal growth rate of *Nitrosomonas* exceeds the one of *Nitrobacter*, which is in turn higher than the one of *Nitrosococcus* (Table 2). The maximal growth rates of *Nitrosomonas* and *Nitrobacter* of 0.89 and 0.64 d^{-1} were calculated for temperatures of 25°C from the relationship determined by Hunik et al. (1994) for *Nitrobacter agilis* and *Nitrosomonas europaea*, respectively. The maximal growth rates were corrected for the salt concentrations of around 250 $mmol \cdot L^{-1}$ (calculated as the sum of the molar mass of all ions) of the urine solution used for the simulations (Table 3). The maximal specific net growth rate (μ_{max} - b) of *Nitrosomonas* was reduced by 40% and the one of *Nitrobacter* by 20% according to the results presented by Moussa et al. (2006). For the maximal growth rate of *Nitrosococcus* we used the value of 0.34 d^{-1} determined by Glover (1985) for a pure culture of *Nitrosococcus oceani* and a temperature of 20°C as an approximation in lack of literature values for 25°C. Considering that *Nitrosococcus oceani* and *halophilus* have a salt optimum of 500 and 700 $mmol \cdot L^{-1}$, respectively (Koops et al. 1990), the maximal specific net growth rate of *Nitrosococcus* was reduced by 50%. For biomass decay we used the values given for a reactor treating high strength nitrogen wastewaters (Jubany 2007). Growth yields were taken from Jubany (2007) and were assumed to be the same for both AOB.

For *Nitrosomonas*, we used the same kinetic constants as discussed in Fumasoli et al. (2015). The additional NH_3 inhibition constant was estimated based on data by Van Hulle et al. (2007). For *Nitrobacter*, we used the nitrite affinity and HNO_2 inhibition constant determined for *Nitrobacter agilis* (Hunik et al. 1993). The NH_3 inhibition constant was approximated as 250 mg NH_3-$N \cdot L^{-1}$ based on data reported by Blackburne et al. (2007). We assumed that the lower pH limit for growth of *Nitrosococcus* was 2, as continuous ammonium oxidation was still observed at a pH of 2.2 (Fumasoli et al. subm.). K_{pH} was estimated to be 2.3 in the case of *Nitrosomonas eutropha* (Fumasoli et al. 2015). For *Nitrosococcus*, we used the same constant as a first approach. In reality this value is likely to differ from the one of *Nitrosomonas eutropha* due to the distinct capabilities of controlling the intracellular pH (Fumasoli et al. 2015). For simplicity, we used the same NH_3 inhibition constant for *Nitrosococcus* as for *Nitrosomonas*. All kinetic parameters are summarized in Table 2.

Table 2: Kinetic parameters for microbial growth and decay of *Nitrosomonas* (AOB 1), *Nitrosococcus* (AOB 2) as well as *Nitrobacter* (NOB).

Parameter	Maximal growth rate μ_{max}	Decay rate b	Growth yield Y	NH_3 affinity constant K_{NH3}	NO_2^- affinity constant K_{NO2-}	NH_3 inhibition constant $K_{I,NH3}$	HNO_2 inhibition constant $K_{I,HNO2}$	Minimal pH pH_{min}	Fitting parameter K_{pH}
	d^{-1}	d^{-1}	g COD· mol N^{-1}	$mol \cdot L^{-1}$	$mol \cdot L^{-1}$	$mol \cdot L^{-1}$	$mol \cdot L^{-1}$	-	-
Nitrosomonas (AOB 1)	0.61 [a]	0.20 [c]	2.52 [c]	$5.4 \cdot 10^{-5}$ [d]	-	0.043 [d]	$1.5 \cdot 10^{-4}$ [d]	5.4 [h]	2.3 [h]
Nitrosococcus (AOB 2)	0.27 [b]	0.20 [c]	2.52 [c]	-	-	0.043 [d]		2.0 [g]	2.3 [h]
Nitrobacter (NOB)	0.55 [a]	0.17 [c]	1.12 [c]	-	$4.8 \cdot 10^{-4}$ [e]	0.018 [f]	$1.4 \cdot 10^{-5}$ [e]	-	

[a] estimated from Hunik et al. (1994) for a temperature of 25°C and corrected for the salt concentration according to Moussa et al. (2006)

[b] value from Glover (1985) corrected for salt concentrations according to Koops et al. (1990)

[c] Jubany (2007)

[d] estimated from Van Hulle et al. (2007)

[e] Hunik et al. (1993)

[f] estimated from Blackburne et al. (2007)

[g] assumed based on Fumasoli et al. (subm.)

[h] Fumasoli et al. (2015)

Modeling pH

The effects of ionic strength were considered for charged species by calculating in activities. Activity factors were calculated by using the Davis approach according to Stumm and Morgan (1996). Acid-base equilibria and complex formation reactions were considered according to Fumasoli et al. (2015) and are specified in Table S2 and S3.

Chemical reactions at low pH values

Chemical reactions for nitrogen transformation and rate constants were considered according to Udert et al. (2005) and are summarized in Table S2 and S3. In short, these reactions include (1) the chemical conversion of HNO_2 to NO_3^- via the intermediates NO and NO_2, and (2) the chemical oxidation of NH_3 with dinitrogen trioxide (N_2O_3) to N_2. N_2O_3 is in an equilibrium with the NO and NO_2 concentration. The chemical processes are important at low pH values (< pH 4).

Gas exchange

Gas exchange rates to model stripping by bubble aeration were included for CO_2, NO, NO_2,O_2, HNO_2 and NH_3. The gas exchange of CO_2 is given in Equation 4. The stripping of NO, NO_2, and O_2 was modeled accordingly.

$$r_{CO_2} = H_{CO_2} \cdot (\{CO_2\} - \{CO_{2,Sat}\}) \cdot \frac{Q_{gas}}{V} \cdot (1 - e^{\frac{-KLa_{CO2} \cdot V}{Q_{gas} \cdot H_{CO2}}}) \quad (4)$$

with r_{CO2} the rate of CO_2 volatilization (mol·L^{-1}·d^{-1}), H_{CO2} the Henry coefficient for CO_2 (1.2 mol(g)·mol(aq)$^{-1}$, Stumm and Morgan 1996), $CO_{2,sat}$ the CO_2 concentration in water at equilibrium with air (mol·L^{-1}, supplementary information), Q_{gas} the controlled gas flow (L·d^{-1}), V the liquid volume (L), and K_La_{CO2} the gas exchange coefficient for CO_2 (d^{-1}). The Henry coefficients of all gases are listed in Table S3. The NO and NO_2 concentrations in water at equilibrium with air were assumed to be zero. The K_La values for CO_2, NO and NO_2 were estimated via the diffusion coefficients from the K_La_{O2} based on the penetration theory (Supplementary information). For K_La_{O2}, we used a value of 200 d^{-1}, which was experimentally determined in our laboratory MBBR with a volume of 2 L and a volumetric filling ratio with Kaldnes® K1 carriers of 40%. For Q_{gas}, we used a value of 840 L·d^{-1}, measured for the same reactor set-up.

For HNO_2 and NH_3, we used a simplified formula to calculate stripping that does not require a K_La term (Equation 5). This simplification is justified for highly soluble gases.

$$r_{HNO_2} = H_{HNO_2} \cdot \{HNO_2\} \cdot \frac{Q_{gas}}{V} \quad (5)$$

Calculation of specific net growth rates

The specific net growth rate μ_{net}, e.g. in case of *Nitrobacter*, is expressed as follows:

$$\mu_{NOB,net} = \mu_{max,NOB} \cdot \frac{\{NO_2^-\}}{\{NO_2^-\} + K_{NO2-,NOB}} \cdot \frac{K_{I,HNO2,NOB}}{\{HNO_2\} + K_{I,HNO2,AOB}} - b_{NOB} \quad (6)$$

Specific net growth rates were estimated for a temperature of 25°C (except the growth rate of *Nitrosococcus*, see above), for a total salt concentration of 250 mmol·L^{-1}, and for the total ammonia concentration of 1100 mg N·L^{-1}, which is the expected total ammonia concentration in the reactor for the influent composition given in Table 3. Specific net growth rates were also estimated for a total ammonia concentration of 50 mg N·L^{-1}, which is a typical concentration, if total ammonia is completely converted to nitrate by the addition of a base (Oosterhuis and van Loosdrecht 2009).

Model simulations

Model simulations were performed to investigate the influence of different urine dosage rates. All simulations started with steady state conditions for a given dilution rate, which was determined by running the model until the steady state was reached. As not all species were present at the simulated steady states, low concentrations of all bacterial populations (0.0001 g°COD·L^{-1}) were continuously added with the influent in all simulations. As influent we used urine with a composition similar to women's urine from Eawag's NoMix collection system (Table 3). The simulations assumed that oxygen was not limiting.

Table 3: Average urine influent composition for the simulations. The composition corresponds to observed concentrations in Eawag's NoMix collection system for women's urine (Fumasoli et al. 2016).

pH	8.9	-
NH_4	1990	mg $N \cdot L^{-1}$
TIC	1020	mg $C \cdot L^{-1}$
PO_4	106	mg $P \cdot L^{-1}$
SO_4	308	mg $SO_4 \cdot L^{-1}$
Cl	1630	$mg \cdot L^{-1}$
K	854	$mg \cdot L^{-1}$
Na	881	$mg \cdot L^{-1}$

Results

Specific net growth rates

The pH and the nitrite concentration in the reactor strongly influence the specific net growth rate of *Nitrosomonas*, *Nitrobacter* and *Nitrosococcus* (Figure 1). The specific net growth rate of *Nitrobacter* increases with the substrate nitrite, but subsequently decreases due to the inhibition by HNO_2 (Figure 1A). *Nitrobacter* grow slower the lower the pH values, as the inhibitory effect of HNO_2 increases with decreasing pH value. The growth of *Nitrobacter* is also inhibited at high pH due to the inhibition by NH_3. The specific net growth rate of *Nitrosomonas* reveals a maximum at a pH of 7.7, and decreases at higher pH values due to the inhibition by NH_3 (Figure 2), and at lower pH values due to the limitation by NH_3 and a direct pH effect. *Nitrosomonas* are also inhibited by HNO_2, but at much higher HNO_2 concentrations than *Nitrobacter*. The model assumes that the specific net growth rate of *Nitrosococcus* is constant within a wide pH range, but decreases at high pH values due to the inhibition by NH_3 and at pH values below 3 due to a direct pH effect. The growth of *Nitrosococcus* is assumed to be independent of the nitrite concentration.

Each of the three bacterial populations grows faster than the other two populations at particular pH values and nitrite concentrations: *Nitrosomonas* at high pH and high nitrite concentrations, *Nitrosococcus* at low pH and high nitrite concentrations, and *Nitrobacter* within a limited pH range between 5.4 and 6.8 and up to maximal nitrite concentrations of 280 mg $N \cdot L^{-1}$.

In addition to pH and nitrite, several other factors influence the specific net growth rates, particularly the urine composition (total ammonia and salt concentration) and temperature. The pH and nitrite range, where the specific net growth of *Nitrobacter* exceeds the ones of both AOB, is much larger when the total ammonia concentrations is only 50 mg $N \cdot L^{-1}$ (Figure 1B). This is a typical case when nitrate production from urine is increased by dosing a base (Oosterhuis and van Loosdrecht 2009).

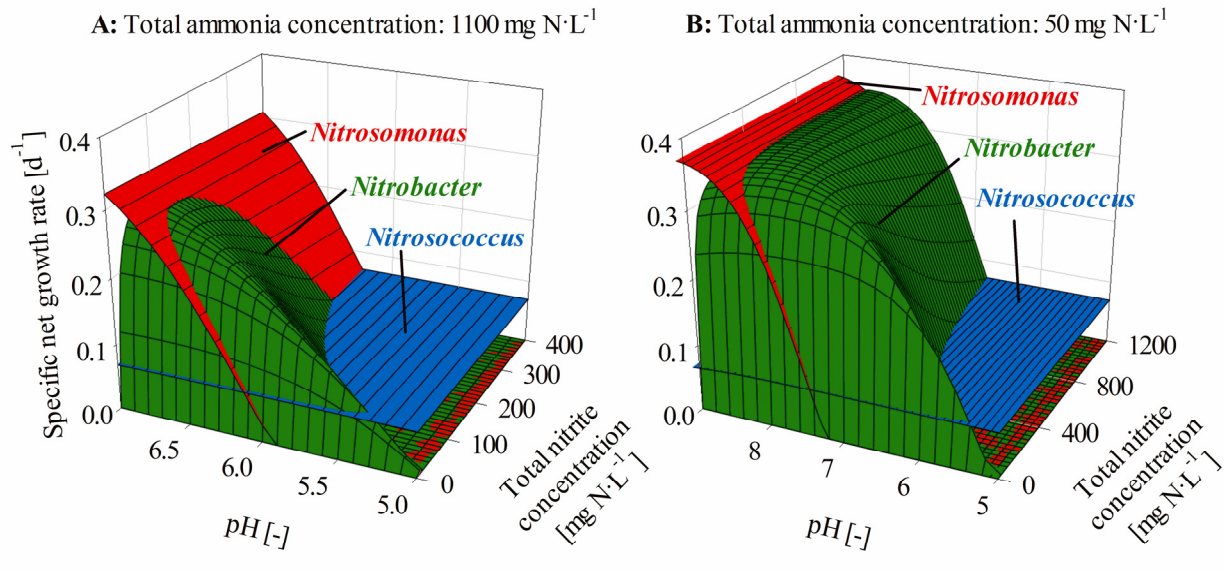

Figure 1: Specific net growth rates of *Nitrobacter* (NOB), *Nitrosomonas* (AOB 1), and *Nitrosococcus* (AOB 2) as a function of pH and the total nitrite concentrations. Specific net growth rates were calculated for a total ammonia concentration of 1100 mg $N \cdot L^{-1}$ (A) and 50 mg $N \cdot L^{-1}$ (B), a total salt concentration of 250 $mmol \cdot L^{-1}$, and a temperature of 25°C. Oxygen was assumed to be not limiting.

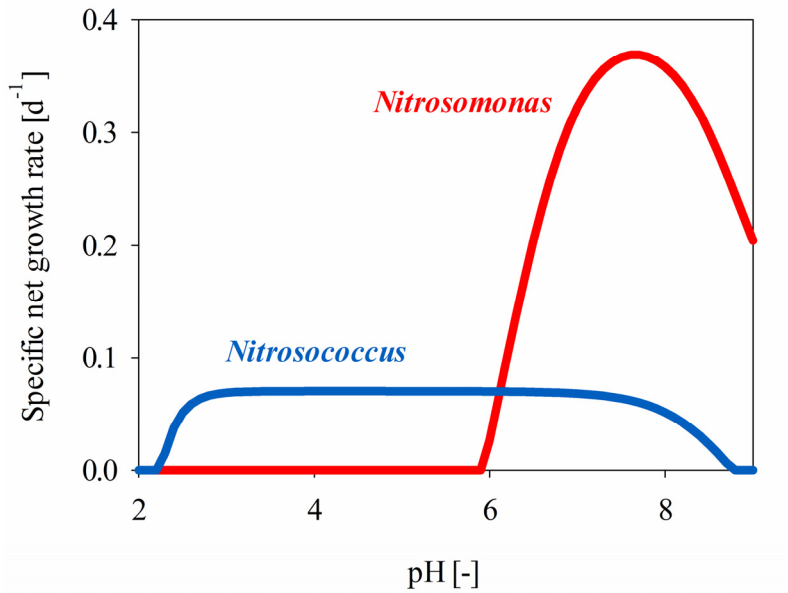

Figure 2: Specific net growth rates of the modeled AOB *Nitrosomonas* and *Nitrosococcus* over a pH range of 2 to 9. The specific net growth rates were calculated for a total ammonia concentration of 1100 mg $N \cdot L^{-1}$, a total nitrite concentration of 0 mg $N \cdot L^{-1}$, a temperature of 25°C, a total salt concentration of 250 $mmol \cdot L^{-1}$, and under the assumption that oxygen is not limiting.

Steady state considerations

Bacteria are washed out in a CSTR, if the dilution rate is above a critical value (D_c), which corresponds to the specific net growth rate (Equation 7). The critical dilution rate for all

simulated populations depends on the pH value, as the specific net growth rates are pH dependent. The critical dilution rates for *Nitrosomonas* and *Nitrobacter*, for instance, decrease within the pH range of 7 to 5 (Figure 1).

The actual dilution rate and the growth rate of the AOB determine the pH in the reactor (Figure 3). High actual dilution rates lead to higher pH values and a faster *Nitrosomonas* growth rate, while low actual dilution rates allow more time for the proton release by the AOB and result in lower pH levels. Due to the feedback-loop between pH and AOB growth, pH will adjust as long as the specific net growth rate of AOB corresponds to the critical dilution rate at equilibrium conditions (Equation 8). *Nitrobacter* will be washed out from a CSTR, as soon as the specific net growth rate is slower than the one of AOB (Equation 9). This criterion is true for all suspended growth systems with sludge retention, if the solids retention time is the same for all bacteria. The pH and total nitrite range outlined in Figure 1, where the specific net growth rate of *Nitrobacter* exceeds the one of the AOB is thus the range in which nitrate is produced.

Wash out in CSTR: $D_c > \mu_{net}$ (7)

Steady state in urine nitrification: $D_c = \mu_{AOB,net}$ (8)

Wash out of NOB: $\mu_{AOB,net} > \mu_{NOB,net}$ (9)

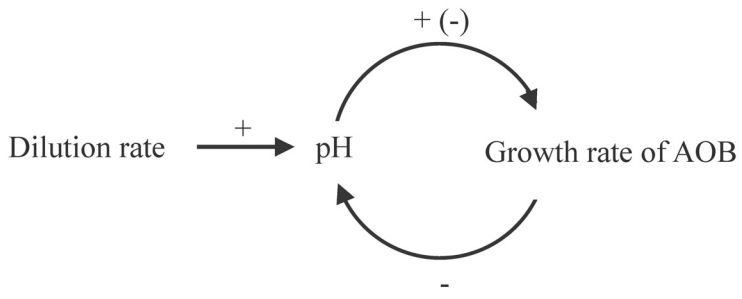

Figure 3: The dilution rate and the growth rate of AOB act as the increasing and decreasing force on pH. AOB do not only influence the pH but are also influenced by it. The pH has a positive feedback on the growth rate of AOB, except if NH_3 concentrations increase so far that AOB are inhibited.

Dynamic urine dosage

Simulations of a dynamic urine influent regime (Figure 4, left) confirm experimental observations (Table 1) showing that:

- Continuous, moderately low dilution rates result in a constant pH and stable nitrate formation (Scenario 1)
- Moderate increases in the urine dosage rate result in a pH increase and a complete change in the nitrification product from nitrate to nitrite (Scenario 2)
- Strong increases in the urine dosage rate lead to the cessation of nitrification and a pH increase up to the values in stored urine (Scenario 3)

- Strong influent decreases lead initially to a small pH decrease, followed by a strong decrease in pH when *Nitrosococcus* grow in (Scenario 4)

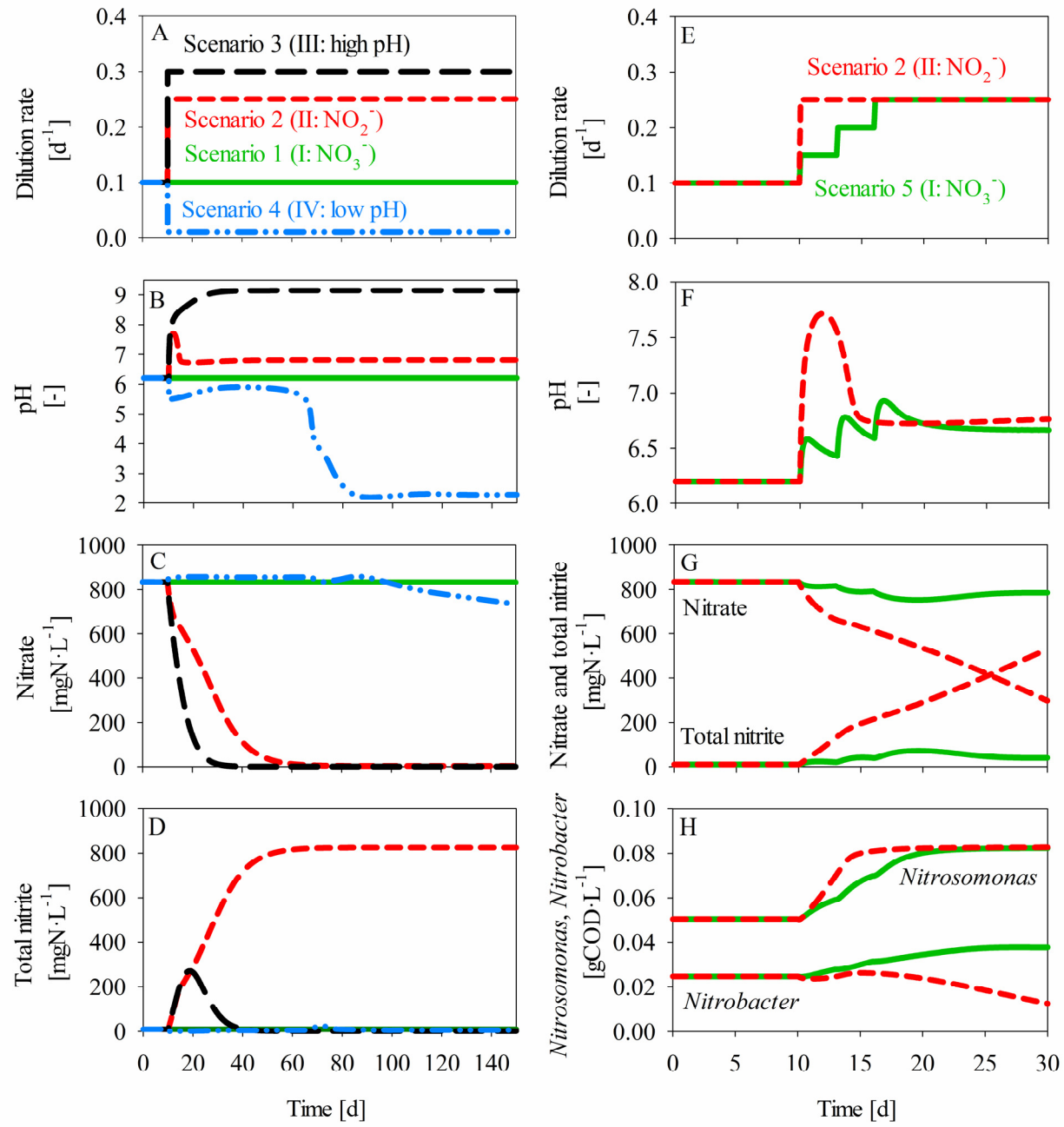

Figure 4: Dilution rates (A, E), pH values in the reactor (B, F), nitrate concentrations (C, G), and total nitrite concentrations (D, G), and biomass concentrations (H), for five scenarios leading to nitrate formation (I: NO_3^-), nitrite formation (II: NO_2^-), cessation of nitrification (III: high pH), and selection of acid-tolerant AOB (IV: low pH). All case scenarios were simulated for a CSTR without sludge retention. All simulations started with steady state conditions allowing for nitrate production.

According to the model simulations, stable nitrate formation is achieved (Scenario 1), when low NH_3 concentrations limit the specific growth rate of *Nitrosomonas*, while *Nitrobacter* are hardly inhibited by the HNO_2 concentrations. Nitrite accumulates (Scenario 2), when high NH_3

concentrations allow high growth rates of *Nitrosomonas*, while they inhibit the specific growth rate of *Nitrobacter*, in the case of Scenario 2 by up to 11%. Once nitrite starts to form, *Nitrobacter* are increasingly inhibited by HNO_2. The inhibition of *Nitrosomonas* and *Nitrobacter* by NH_3 explains the wash out of the nitrifiers and the cessation of nitrification at higher pH values (Scenario 3). During strong underdosage (Scenario 4), the pH initially drops to a value of 5.7, as *Nitrosomonas* are abundant, but impeded by the direct pH effect (61% inhibition of specific growth rate) and the low NH_3 concentrations (83% reduction of specific growth rate due to substrate limitation). Due to the biomass decay of *Nitrosomonas*, the pH value increases subsequently to values of 5.9, but starts to decrease to very low values, when the *Nitrosococcus* concentration has increased sufficiently. With and after the pH drop, *Nitrobacter* are inhibited by HNO_2, but total nitrite remains low, because HNO_2 is decomposed chemically to nitrate. The nitrate concentration decreases due to the stripping of HNO_2 as well as NO and NO_2, both volatile intermediates of the HNO_2 decomposition reaction. The simulated emissions consist mainly of NO (72%), followed by HNO_2 (27%), while the ones of NO_2 are minor.

The dynamic simulations confirm the general expectations for the steady state considerations (Figure 1); however, they add important information about time scales. The influent decrease has a direct influence on pH, but it does not immediately result in a process failure. The reactor failure occurs only, when acid-tolerant AOB grow in, which can be several weeks after the influent decrease. The accumulation of nitrite and the cessation of nitrification are, however, the immediate response of the influent increase. Nitrite accumulates, if the pH is only temporarily increased to high values, but subsequently decreases again due to the increased biomass concentrations of *Nitrosomonas*: the excess nitrite produced at high pH values is sufficient to inhibit *Nitrobacter* by HNO_2 as the pH decreases (Scenario 2, Figure 4 right). The same is true for the complete cessation of nitrification: the strong pH increase inhibits *Nitrosomonas* by NH_3 and causes their wash out, even if they would generally be able to grow at a dilution rate of 0.3 d^{-1}. A temporal increase to very high pH values and subsequent NOB wash out can be prevented, by increasing the influent rate in smaller steps (Scenario 5).

Reversibility of system states

Depending on the initial conditions in the reactor different system states are reached even if the same dilution rate is applied (Table 4). Starting with the initial conditions of nitrate production by *Nitrosomonas* and *Nitrobacter* (I: NO_3^-), the system state can change to all other system states (Table 4 and Figure 4). However, none of these secondary system states are reversible, but some unwanted system states can change into another.

A urine reactor with the initial system state of nitrite production by *Nitrosomonas* (II: NO_2^-), e.g. at a dilution rate of 0.3 d^{-1}, cannot switch back to nitrate production even if the dilution rate has decreased. *Nitrobacter* cannot grow sufficiently fast at the high nitrite concentrations due to their inhibition by HNO_2. The system state of nitrite production by *Nitrosomonas* can, however, still change to low pH nitrification (IV: low pH), if the dilution rate is decreased to 0.05 d^{-1} and presupposed that *Nitrosococcus* species are present.

If the pH is initially at very low values, the increase to higher dilution rates causes the wash out of *Nitrosococcus*. The pH increase to very high pH values also inhibits *Nitrosomonas* and

Nitrobacter by the accumulated NH_3 and leads to the complete cessation of nitrification (III: high pH).

Table 4: Simulated system states after the change in the dilution rate within a range of 0.05 to 0.30 d^{-1}. The simulations started at steady state conditions for the initial dilution rate, and were run until a new steady state was reached after a change in the dilution rate. Four system states are differentiated: I nitrate production (NO_3^-, ■), II nitrite production (NO_2^-, ■), III no nitrification due to high pH values (High pH, ■), IV growth of *Nitrosococcus* and chemical nitrite oxidation processes at low pH values (Low pH, ■).

Initial dilution rate [d^{-1}]: \ Change to [d^{-1}]:	0.05	0.10	0.15	0.20	0.25	0.30
0.05	IV: Low pH		III: High pH			
0.10	*					
0.15	*					
0.20	*IV: Low pH		I: NO_3^-			II: NO_2^-
0.25	*					
0.30	*					

* if any *Nitrosococcus* present

Discussion

Operation of urine nitrification reactors

Continuous, moderately low loading rates result at steady state in pH values, which allow for nitrate formation (Scenario 1, Figure 4). Operational strategies resulting in large pH fluctuations, such as SBRs with large exchange volumes, are to be prevented, as the excess nitrite produced by *Nitrosomonas* at high pH values leads to the inhibition of NOB by HNO_2 at low pH values (in analogy to Scenario 2, Figure 4). Nitrite and hardly any nitrate was therefore produced in a SBR operated with urine between pH 8.8 and 6 (Udert et al. 2003a). Instead of keeping the influent constant, the pH can also be controlled directly by regulating the urine influent within tight pH setpoints (Udert and Wächter 2012). This strategy has the advantage that it prevents too high or too low pH values.

Nitrite may still accumulate by choosing too high setpoints or after strong changes in temperature or urine composition (e.g., due to higher total ammonia concentrations). Nitrite should therefore be monitored regularly. The nitrite measurement is particularly important after strong environmental or operational changes, due to which nitrite can accumulate as a fast and direct response (Scenario 2, Figure 4). An online nitrite sensor would help to better control reactor operation. However, reliable nitrite sensors are currently not available for the high nitrite and nitrate concentrations in urine, though recent studies with a ultraviolet sensor are promising (Mašić et al. 2015).

The quantitative data produced with the model in this study (such as the exact pH and nitrite boundaries) have not been validated in this study. The results should therefore be used to draw qualitative, but not quantitative interpretations.

Prevent acid-tolerant AOB

High biomass concentrations of acid-tolerant AOB alone are not a problem, as long as the pH is controlled at a value, where NOB still grow faster than acid-tolerant AOB (Figure 1). Stable nitrate production from urine was thus observed in a CSTR by keeping the pH between of 5.80 and 5.85, despite the presence of acid-tolerant AOB affiliated with *Nitrosospira* (Fumasoli et al. 2016). The risk of highly abundant acid-tolerant AOB is, though, that the pH drops immediately at a failure of the influent pump, which causes a durable inhibition of NOB by HNO_2.

A short term underdosage is, however, not critical, if the acid-sensitive *Nitrosomonas europaea* lineage is abundant: the *Nitrosomonas europaea* lineage decreases the pH to a minimal value of 5.4 only (Fumasoli et al. 2015), at which NOB remain active (Figure 1). Hence, only long-, but not short-term influent decreases must be prevented in reactors with high abundance of the acid-sensitive *Nitrosomonas europaea* lineage. The pH should thus be set sufficiently high to select for the *Nitrosomonas europaea* lineage.

Nitrite removal

As urine is a very concentrated solution, nitrite concentrations of up to 830 mg $N \cdot L^{-1}$ were reached in the simulations (Figure 4). Once nitrite has accumulated to such high values, a change back to nitrate formation is not possible anymore due to the strong inhibition of NOB by HNO_2 (Table 4). Consequently, the nitrite concentration needs to be decreased by other measures, e.g., by denitrification (Udert and Wächter 2012) or by dilution.

The removal of the excess nitrite by NOB is only possible, if nitrite is detected and removed at an early stage. To decrease the rate of nitrite production by the *Nitrosomonas europaea* lineage the pH needs to be decreased by providing less urine. The influent can also be switched off completely, which causes a pH drop to a minimal value of 5.4, where the activity of the *Nitrosomonas europaea* lineage and nitrite production ceases. However, as a result to the lower pH values, NOB are more strongly inhibited by HNO_2. Hence, a decrease in pH is only suitable to remove nitrite, if the concentrations are not yet very high.

The return from nitrite to nitrate production is more likely in urine nitrification reactors, where total ammonia is completely converted by the addition of a base. NOB will be able to degrade even high concentrations of nitrite, as the *Nitrosomonas europaea* lineage is more strongly impeded by NH_3 limitation than *Nitrobacter* by HNO_2 inhibition (Figure 1). Accordingly,

Oosterhuis and van Loosdrecht (2009) observed in a CSTR for complete ammonia oxidation from urine that nitrite concentrations of above 1200 mg $N \cdot L^{-1}$ were removed at pH 7. High nitrite levels of 3900 or 1200 mg $N \cdot L^{-1}$ could in turn not be degraded during partial ammonia oxidation from urine in a CSTR at pH 7 or in a SBR at pH 6, respectively (Udert et al. 2003a). Hence, reactors for complete ammonia oxidation may be less susceptible for irreversible nitrite accumulation.

Biofilm vs. suspended growth reactors

In suspended urine nitrification reactors, NOB are lost as soon as their specific net growth rate is slower than the one of the AOB population (Equation 9). This criterion is valid, as long as the solids retention time (SRT) is the same for all bacteria. This condition is not given in a biofilm, where the local cell retention time varies over the thickness of the biofilm (Morgenroth and Wilderer 2000). The possible pH window for nitrate formation in urine depends thus on the stratification of bacteria in the biofilm and may be very distinct to suspended sludge systems.

Depending on their location in the biofilm, bacteria can be limited by oxygen. AOB have a higher affinity for oxygen and outcompete NOB at low oxygen concentrations (Guisasola et al. 2005, Jubany et al. 2009). The slower growth of NOB due to oxygen limitation is thus an additional potential mechanism leading to the accumulation of nitrite in a biofilm reactor. Oxygen limitation of NOB will be particularly critical after an increase in pH due to the faster growth and oxygen consumption of AOB. Keeping pH constant and measuring nitrite after a change in operational conditions, as proposed for suspended growth systems (see above), is thus also a well-suited strategy for the operation of biofilm reactors.

Conclusion

- Partial ammonia oxidation to nitrate is only possible, if pH is sufficiently low to limit the growth of the *Nitrosomonas europaea* lineage by NH_3, and sufficiently high to prevent the selection of acid-tolerant AOB. The pH should therefore be controlled within a narrow range by regulating the urine influent. The pH range depends on the total ammonia and total salt concentration as well as the temperature and will have to be determined for particular cases.
- The selection of acid-tolerant AOB must be prevented, as acid-tolerant *Nitrosococcus* decrease the pH to very low values, as soon as not sufficient urine is provided. Low pH values inhibit NOB durably by HNO_2 and cause substantial NO emissions due to the chemical decomposition of HNO_2. The acid-sensitive *Nitrosomonas europaea* lineage, in turn, can decease the pH to a minimal value of 5.4 only, where NOB remain active.
- High pH values, e.g. after an increase in the influent rate, can result in the accumulation of nitrite. As HNO_2 inhibits NOB, a return from nitrite back to nitrate formation is only possible, if accumulating nitrite is detected at an early stage (within days). Nitrite must therefore be monitored regularly, particularly after process or environmental changes where the risk for nitrite formation is increased. An online nitrite sensor would greatly facilitate reactor operation and should be developed as a next step.

Acknowledgement

This study was funded by the Bill and Melinda Gates Foundation and was conducted as part of the VUNA project (www.vuna.ch, Grant No. OPP1011603). The authors like to thank Kris Villez for helpful discussions.

Supporting Information for Chapter 4

Stable ammonia conversion to nitrate and the prevention of unfavorable system states during nitrification of urine

Alexandra Fumasoli, Eberhard Morgenroth, Kai M. Udert

Submitted

Supplementary information on nitrification model

The saturation concentration of CO_2 was calculated as follows:

$$CO_{2,Sat} = \frac{p_{CO_2}}{R \cdot T \cdot H_{CO_2}}$$

With $CO_{2,sat}$ the saturation concentration of CO_2 ($mol \cdot L^{-1}$), p_{CO2} the CO_2 partial pressure (0.00039 bar), R the gas constant ($8.314 \cdot 10^{-2}$ $L \cdot bar \cdot K^{-1} \cdot mol^{-1}$), T the temperature (K), and H_{CO2} the Henry constant for CO_2 (1.2 $mol(g) \cdot mol(aq)^{-1}$, Stumm and Morgan 1996).

The K_La_{CO2} was not determined experimentally, but was calculated from the K_La_{O2}.

Diffusion coefficients in water (25°C) are:

$D_{CO2} = 1.91 \cdot 10^{-5}$ $cm^2 \cdot s^{-1}$ (Lide 2009)

$D_{NO} = 2.21 \cdot 10–5$ $cm^2 \cdot s^{-1}$ (Zacharia and Deen 2005)

$D_{NO2} = 1.4 \cdot 10^{-5}$ $cm^2 \cdot s^{-1}$ (Lide 2009)

$D_{O2} = 2.42 \cdot 10^{-5}$ $cm^2 \cdot s^{-1}$ (Lide 2009)

Or:

$D_{CO2} = 0.79 \cdot D_{O2}$

$D_{NO} = 0.91 \cdot D_{O2}$

$D_{NO2} = 0.58 \cdot D_{O2}$

According to the penetration theory (Higbie 1935), the gas exchange coefficient K_La is a function of the square root of the diffusion coefficient:

$K_La_{O2} = f(D_{O2}^{0.5})$

$K_La_{CO2} = f(D_{CO2}^{0.5}) = f((0.79 \cdot D_{O2})^{0.5}) = f(0.89 \cdot D_{O2}^{0.5})$

$K_La_{CO2} = 0.89 \cdot K_La_{O2}$

$K_La_{NO} = 0.96 \cdot K_La_{O2}$

$K_La_{NO2} = 0.76 \cdot K_La_{O2}$

Supplementary Tables

Table S1: Stoichiometric matrix for bacterial growth and decay of the AOB *Nitrosomonas* and *Nitrosococcus*, as well as the NOB *Nitrobacter*. i_N and i_C were calculated as 0.00625 and 0.03125 mol·gCOD^{-1} based on the assumed biomass composition of $C_5H_7O_2N$.

Parameter	$X_{Nitrosomonas}$	$X_{Nitrosococcus}$	$X_{Nitrobacter}$	O_2	NH_3	HNO_2	NO_3	CO_2	H^+
	g COD	g COD	g COD	mol	mol	mol	mol	mol	mol
Nitrosomonas									
Aerobic growth	1			$(1-48/Y_{Nitrosomonas})/32$	$-1/Y_{Nitrosomonas} - i_N$	$1/Y_{Nitrosomonas}$		$-i_C$	
Decay	-1			-1/32	i_N			i_C	
Nitrosococcus									
Aerobic growth		1		$(1-48/Y_{Nitrosococcus})/32$	$-1/Y_{Nitrosococcus} - i_N$	$1/Y_{Nitrosococcus}$		$-i_C$	
Decay		-1		-1/32	i_N			i_C	
Nitrobacter									
Aerobic growth			1	$(1-16/Y_{Nitrobacter})/32$	$-i_N$	$-1/Y_{Nitrobacter}$	$1/Y_{Nitrobacter}$	$-i_C$	$1/Y_{Nitrobacter}$
Decay			-1	-1/32	i_N			i_C	

Table S2: Process rates of chemical reactions, acid-base equilibria, complex formation reactions, and gas exchange reactions included in the computer model. For all equilibrium rate constants (k) a value of 10^6 L·mol^{-1}·d^{-1} was used. Chemical processes were modeled according to Udert et al. (2005), acid-base and complex formation reactions according to Fumasoli et al. (2015).

Equation	Process rate
Nitrogen compounds equilibria	
$NO + NO_2 + H_2O \rightharpoonup 2\ HNO_2$	$k\_NO\_back \cdot [NO] \cdot [NO_2]$
$2\ HNO_2 \rightharpoonup NO + NO_2 + H_2O$	$k\_NO\_for \cdot [HNO_2]^2$
$HNO_2 + NO_3^- + H^+ \rightharpoonup 2\ NO_2 + H_2O$	$k\_nitrate\_back \cdot [HNO_2] \cdot [NO_3^-] \cdot f_{A1} \cdot [H^+] \cdot f_{A1}$
$2\ NO_2 + H_2O \rightharpoonup HNO_2 + NO_3^- + H^+$	$k\_nitrate\_for \cdot [NO_2]^2$
$N_2O_3 \rightharpoonup NO + NO_2$	$k\_N_2O_3\_for \cdot 10^{pK\_N2O3} \cdot [N_2O_3]$
$NO + NO_2 \rightharpoonup N_2O_3$	$k\_N_2O_3\_for \cdot [NO] \cdot [NO_2]$
Chemical nitrite conversion	
$N_2O_3 + NH_3 \rightharpoonup N_2 + HNO_2 + H_2O$	$k\_NH_3\_nitro \cdot [NH_3] \cdot [N_2O_3]$
$2\ NO + O_2 \rightharpoonup 2\ NO_2$	$k\_NO\_ox \cdot [NO]^2 \cdot [O_2]$
Acid-Base equilibria	
$HCO_3^- \rightleftharpoons CO_3^{2-} + H^+$	$k \cdot ([HCO_3^-] \cdot f_{A1} - [CO_3^{2-}] \cdot f_{A2} \cdot [H^+] \cdot f_{A1} \cdot 10^{pK\_CO3})$
$H_2CO_3 \rightleftharpoons HCO_3^- + H^+$	$k \cdot ([CO_2] - [HCO_3^-] \cdot f_{A1} \cdot [H^+] \cdot f_{A1} \cdot 10^{pK\_HCO3})$
$NH_4^+ \rightleftharpoons NH_3 + H^+$	$k \cdot ([NH_4^+] \cdot f_{A1} - [NH_3] \cdot [H^+] \cdot f_{A1} \cdot 10^{pK\_NH3})$
$HNO_2 \rightleftharpoons NO_2^- + H^+$	$k \cdot ([HNO_2] - [NO_2^-] \cdot f_{A1} \cdot [H^+] \cdot f_{A1} \cdot 10^{pK\_nitrite})$
$H_3PO_4 \rightleftharpoons H_2PO_4^- + H^+$	$k \cdot ([H_3PO_4] - [H_2PO_4^-] \cdot f_{A1} \cdot [H^+] \cdot f_{A1} \cdot 10^{pK\_H2PO4})$
$H_2PO_4^- \rightleftharpoons HPO_4^{2-} + H^+$	$k \cdot ([H_2PO_4^-] \cdot f_{A1} - [HPO_4^{2-}] \cdot f_{A2} \cdot [H^+] \cdot f_{A1} \cdot 10^{pK\_HPO4})$
$HPO_4^{2-} \rightleftharpoons PO_4^{3-} + H^+$	$k \cdot ([HPO_4^{2-}] \cdot f_{A2} - [PO_4^{3-}] \cdot f_{A3} \cdot [H^+] \cdot f_{A1} \cdot 10^{pK\_PO4})$
$HSO_4^- \rightleftharpoons SO_4^{2-} + H^+$	$k \cdot ([HSO_4^-] \cdot f_{A1} - [SO_4^{2-}] \cdot f_{A2} \cdot [H^+] \cdot f_{A1} \cdot 10^{pK\_SO4})$
Complex formation	
$K^+ + H_2PO_4^- \rightleftharpoons KH_2PO_4$	$k \cdot ([K^+] \cdot f_{A1} \cdot [H_2PO_4^-] \cdot f_{A1} - [KH_2PO_4] \cdot 10^{pK\_KH2PO4})$
$K^+ + H_2PO_4^- \rightleftharpoons KHPO_4^- + H^+$	$k \cdot ([K^+] \cdot f_{A1} \cdot [H_2PO_4^-] \cdot f_{A1} - [KHPO_4^-] \cdot f_{A1} \cdot [H^+] \cdot f_{A1} \cdot 10^{pK\_KHPO4})$
$2\ K^+ + H_2PO_4^- \rightleftharpoons K_2HPO_4 + H^+$	$k \cdot ([K^+]^2 \cdot f_{A1}^2 \cdot [H_2PO_4^-] \cdot f_{A1} - [K_2HPO_4]\ [H^+] \cdot f_{A1} \cdot 10^{pK\_K2HPO4})$
$K^+ + SO_4^{2-} \rightleftharpoons KSO_4^-$	$k \cdot ([K^+] \cdot f_{A1} \cdot [SO_4^{2-}] \cdot f_{A2} - [KSO_4^-] \cdot f_{A1} \cdot 10^{pK\_KSO4})$
$Na^+ + H_2PO_4^- \rightleftharpoons NaH_2PO_4$	$k \cdot ([Na^+] \cdot f_{A1} \cdot [H_2PO_4^-] \cdot f_{A1} - [NaH_2PO_4] \cdot 10^{pK\_NaH2PO4})$
$Na^+ + H_2PO_4^- \rightleftharpoons NaHPO_4^- + H^+$	$k \cdot ([Na^+] \cdot f_{A1} \cdot [H_2PO_4^-] \cdot f_{A1} - [NaHPO_4^-] \cdot f_{A1} \cdot [H^+] \cdot f_{A1} \cdot 10^{pK\_NaHPO4})$
$2\ Na^+ + H_2PO_4^- \rightleftharpoons Na_2HPO_4 + H^+$	$k \cdot ([Na^+]^2 \cdot f_{A1}^2 \cdot [H_2PO_4^-] \cdot f_{A1} - [Na_2HPO_4]\ [H^+] \cdot f_{A1} \cdot 10^{pK\_Na2HPO4})$
$Na^+ + SO_4^{2-} \rightleftharpoons NaSO_4^-$	$k \cdot ([Na^+] \cdot f_{A1} \cdot [SO_4^{2-}] \cdot f_{A2} - [NaSO_4^-] \cdot f_{A1} \cdot 10^{pK\_NaSO4})$
$NH_4^+ + H_2PO_4^- \rightleftharpoons NH_4H_2PO_4$	$k \cdot ([NH_4^+] \cdot f_{A1} \cdot [H_2PO_4^-] \cdot f_{A1} - [NH_4H_2PO_4] \cdot 10^{pK\_NH4H2PO4})$
$NH_4^+ + HPO_4^{2-} \rightleftharpoons NH_4HPO_4^-$	$k \cdot ([NH_4^+] \cdot f_{A1} \cdot [HPO_4^{2-}] \cdot f_{A2} - [NH_4HPO_4^-] \cdot f_{A1} \cdot 10^{pK\_NH4HPO4})$
$NH_4^+ + SO_4^{2-} \rightleftharpoons NH_4SO_4^-$	$k \cdot ([NH_4^+] \cdot f_{A1} \cdot [SO_4^{2-}] \cdot f_{A2} - [NH_4SO_4^-] \cdot f_{A1} \cdot 10^{pK\_NH4SO4})$
Gas exchange	
$CO_2(aq) \rightarrow CO_2(g)$	$H\_CO_2 \cdot ([CO_2] - [CO_{2,sat}]) \cdot Q\_gas/V \cdot (1 - exp^{-KLa\_CO2 \cdot V/H\_CO2/Q\_gas})$
$NO\ (aq) \rightarrow NO\ (g)$	$H\_NO \cdot [NO] \cdot Q\_gas/V \cdot (1 - exp^{-KLa\_NO \cdot V/H\_NO/Q\_gas})$
$NO_2\ (aq) \rightarrow NO_2\ (g)$	$H\_NO_2 \cdot [NO_2] \cdot Q\_gas/V \cdot (1 - exp^{-KLa\_NO2 \cdot V/H\_NO2/Q\_gas})$
$HNO_2(aq) \rightarrow HNO_2\ (g)$	$H\_HNO_2 \cdot [HNO_2] \cdot Q\_gas/V$
$NH_3\ (aq) \rightarrow NH_3\ (g)$	$H\_NH_3 \cdot [NH_3] \cdot Q\_gas/V$
$O_2(g) \rightarrow O_2(aq)$	$H\_O_2 \cdot ([O_2] - [O_{2,sat}]) \cdot Q\_gas/V \cdot (1 - exp^{-KLa\_O2 \cdot V/H\_O2/Q\_gas})$

All concentrations in [mol·L^{-1}]. f_{A1}, f_{A2}, f_{A3}: activity coefficients

Table S3: Rate constants, pK_a values and Henry coefficients for the processes included in Table S2. Constants were taken from Udert et al. (2005) (nitrogen compounds equilibria, chemical nitrite conversion) and Fumasoli et al. (2015) (acid-base, complex formation).

	Rate constant *k*, pK_a value, Henry coefficient H	Unit	Reference
Nitrogen compounds equilibria			
*k*_NO_back	$1.4 \cdot 10^{13}$	1/M/d	(Park and Lee 1988)
*k*_NO_for	$1.6 \cdot 10^{6}$	1/M/d	(Park and Lee 1988)
*k*_nitrate_back	730	$1/M^2/d$	(Schwartz and White 1983)
*k*_nitrate_for	$6.9 \cdot 10^{12}$	1/M/d	(Park and Lee 1988)
*k*_N_2O_3_for	$9.5 \cdot 10^{13}$	1/M/d	(Grätzel et al. 1970)
pK_N_2O_3	-4.5	-	(Schwartz and White 1983)
Chemical nitrite conversion			
*k*_NH_3_nitro	$7.7 \cdot 10^{10}$	1/M/d	(Harrison et al. 1996)
*k*_NO_ox	$1.8 \cdot 10^{11}$	$1/M^2/d$	(Awad and Stanbury 1993)
Acid-Base equilibria			
pK_CO_3	10.33	-	(Gustafsson 2012)*
pK_HCO_3	6.35	-	(Gustafsson 2012)
pK_NH_3	9.24	-	(Gustafsson 2012)
pK_nitrite	3.25	-	(Lide 2009)
pK_H_2PO_4	2.15	-	(Gustafsson 2012)
pK_HPO_4	7.20	-	(Gustafsson 2012)
pK_PO_4	12.38	-	(Gustafsson 2012)
pK_SO_4	1.99	-	(Gustafsson 2012)
Complex formation		-	
pK_KH_2PO_4	-0.30	-	(Gustafsson 2012)
pK_$KHPO_4$	6.30	-	(Gustafsson 2012)
pK_K_2HPO_4	6.07	-	(Gustafsson 2012)
pK_KSO_4	-0.85	-	(Gustafsson 2012)
pK_NaH_2PO_4	-0.30	-	(Gustafsson 2012)
pK_$NaHPO_4$	6.13	-	(Gustafsson 2012)
pK_Na_2HPO_4	6.25	-	(Gustafsson 2012)
pK_$NaSO_4$	-0.74	-	(Gustafsson 2012)
pK_$NH_4H_2PO_4$	-0.10	-	(Martell et al. 1997)
pK_NH_4HPO_4	-1.30	-	(Martell et al. 1997)
pK_NH_4SO_4	-1.03	-	(Gustafsson 2012)
Gas exchange			
H_HNO_2	$8.3 \cdot 10^{-4}$	M(g)/M(aq)	(Schwartz and White 1981)
H_NH_3	$7.2 \cdot 10^{-4}$	M(g)/M(aq)	(Stumm and Morgan 1996)
H_NO_2	4.1	M(g)/M(aq)	(Schwartz and White 1981)
H_NO	21	M(g)/M(aq)	(Schwartz and White 1981)
H_O_2	32.4	M(g)/M(aq)	(Stumm and Morgan 1996)
H_CO_2	1.2	M(g)/M(aq)	(Stumm and Morgan 1996)

*thermo_minteq.dat, standard database in Visual MINTEQ (Gustafsson 2012)

Conclusion and Outlook

Conclusion

This thesis revealed that urine nitrification can be applied successfully under dynamic conditions such as the reactor start-up as well as at different scales. The challenge is, though, the possible process destabilization due to nitrite accumulation or low pH values.

Nitrite accumulates mainly at high pH values, as under these conditions AOB affiliated with the *Nitrosomonas europaea* lineage – abundant in most urine nitrification reactors – grow faster than NOB. Once nitrite accumulates, HNO_2 acts as an inhibitor for NOB and leads to further nitrite accumulation. A return from nitrite back to nitrate production is only possible, if accumulating nitrite is detected at an early stage (within days): excess nitrite can then be removed biologically by decreasing the influent rate or by switching off the influent completely. In a later stage, nitrite needs to be removed either by dilution or denitrification, which is labor-intensive and time-consuming.

To prevent the accumulation of nitrite, pH needs to be kept low. The low pH values decrease the growth rate of the *Nitrosomonas europaea* lineage and even lead to a complete cessation of activity at pH 5.5, allowing NOB to keep up converting nitrite into nitrate. The decrease in activity between pH 7 to 6 of the *Nitrosomonas europaea* lineage can be attributed to substrate limitation of NH_3 and product inhibition by HNO_2. The cessation of activity at pH 5.5, however, is caused by an energy limitation: the low pH values likely impede the energy conservation of *Nitrosomonas europaea* by preventing NADH production. The activity or inhibition of a single enzyme thus influences the growth rate, but the energy conservation determines the limit of activity. To model the growth rate of the *Nitrosomonas europaea* lineage close to the pH limit, conventional Monod-type kinetics need to be extended with an exponential pH term. This term might not only be suitable to model the low pH limit of the *Nitrosomonas europaea* lineage, but for many other bacteria growing close to their thermodynamic pH limits.

Low pH values, though, pose the risk that acid-tolerant AOB are selected over the acid-sensitive *Nitrosomonas europaea* lineage. The growth of acid-tolerant *Nitrosococcus* decreases the pH in urine nitrification reactors to values as low as 2.2. During and after such a pH drop, NOB are inhibited and the overall bacterial richness declines strongly. While nitrite is still converted chemically to nitrate, large nitrogen losses occur due to stripping of NO, HNO_2, N_2O, and NO_2. Not only *Nitrosococcus*, but also *Nitrosospira* can thrive in low pH environments. The salt concentration is the most likely criterion for the selection of *Nitrosococcus*- and *Nitrosospira*-type AOB, respectively. Salt-tolerant *Nitrosococcus* are very likely to be the key players in concentrated wastewaters such as urine, whereas *Nitrosospira* seem to be more important in less concentrated wastewaters.

A high biomass concentration of acid-tolerant AOB is not critical per se, as long as the pH is controlled sufficiently high. However, as soon as not sufficient urine is provided, acid-tolerant AOB will decrease the pH to low values, inhibiting NOB durably. The acid-sensitive *Nitrosomonas europaea* lineage, in turn, decreases the pH to a minimal value of 5.5 only, at which NOB remain active. Hence, the acid-sensitive *Nitrosomonas europaea* lineage rather than acid-tolerant AOB should be selected by keeping the pH sufficiently high. In cases, where not enough urine is produced to keep the pH high, e.g. during holidays, the reactor should rather

be switched off completely (no aeration, no urine addition) than constantly underloaded with urine.

Stable urine nitrification is thus only possible if the pH is sufficiently low to limit the growth of the *Nitrosomonas europaea* lineage by NH_3, but sufficiently high to prevent the selection of acid-tolerant AOB. The feasible pH range depends on the temperature and the urine composition, but may lie approximately between pH 6.0 and 6.5. The pH value is maintained within this pH range by dosing urine continuously and at an appropriate rate or by controlling pH within a tight interval by regulating the influent. The latter strategy has the advantage that it prevents too high and too low pH values at any time and that it can be applied even if the biomass concentrations are far away for steady state, such as during reactor start-up.

By keeping the pH at an appropriate value, reactor failures can be reduced to a minimum. However, a frequent manual nitrite monitoring is still recommended, particularly after environmental or operational changes where the risk for nitrite formation is increased. This promising technology for urine stabilization is, thus, currently limited to an application in centralized or semi-decentralized locations, where a regular surveillance is possible.

Outlook

Real-time nitrite sensor

Transport of urine from the urine-diverting toilet to a centralized or semi-decentralized treatment site may be expensive. The urine treatment would thus ideally take place as close to the toilet as possible. Such a decentralized urine nitrification requires, however, a real-time control of pH as well as the nitrite concentration. The real-time control of these two factors would also be very beneficial in more centralized reactors, as it allows maximizing nitrification rates resulting in lower infrastructure and operational costs.

While pH sensors are common in wastewater treatment plants, real-time nitrite sensors for the high nitrite and nitrate concentrations in urine are not available yet. Future reactor optimization should thus focus on the development of new technologies to measure nitrite online. An ultraviolet spectral probe is currently being tested for its application to measure nitrite in urine and recent results have been promising (Mašić et al. 2015).

Distribution and characteristics of *Nitrosococcus*

The *Nitrosococcus*-related AOB revealed an extraordinary tolerance to low pH values and high HNO_2 concentrations. These traits even allowed this AOB to drive the reactor into pH regions, where HNO_2 decomposes chemically and harmful off-gases are emitted. *Nitrosococcus*-related AOB have also been detected in strongly acidic agricultural field receiving large amounts of nitrogen fertilizers (Hayatsu 1993). It remains thus to be elucidated whether *Nitrosococcus* are more widespread than currently thought. They may particularly play an important role in very acidic soils, where the same HNO_2 decomposition reactions as in the urine reactors take place (Van Cleemput and Baert 1984).

The *Nitrosococcus*-related AOB observed at pH 2.2 in the urine reactors belong possibly to a so far undescribed specie or even a new genus. Further studies should thus determine key growth

parameters, e.g. the maximal growth rate and the ammonium affinity constant, for their later use in mathematical models. Additionally, the *Nitrosococcus* genome could be sequenced and compared with other, so far sequenced AOB and AOA genomes. Particularly the comparison of the *Nitrosococcus* genome with the one of the obligate acidophile AOA *Nitrosotalea devanaterra* may allow identifying common features among acid-tolerant ammonia oxidizing organisms.

References

Altschul, S.F., Madden, T.L., Schaffer, A.A., Zhang, J., Zhang, Z., Miller, W. and Lipman, D.J. (1997) Gapped BLAST and PSI-BLAST: a new generation of protein database search programs. Nucleic Acids Research 25(17), 3389-3402.

Anthonisen, A.C., Loehr, R.C., Prakasam, T.B. and Srinath, E.G. (1976) Inhibition of nitrification by ammonia and nitrous acid. Journal of the Water Pollution Control Federation 48(5), 835-852.

Antoniou, P., Hamilton, J., Koopman, B., Jain, R., Holloway, B., Lyberatos, G. and Svoronos, S.A. (1990) Effect of temperature and pH on the effective maximum specific growth rate of nitrifying bacteria. Water Research 24(1), 97-101.

Awad, H.H. and Stanbury, D.M. (1993) Autoxidation of NO in aqueous solution. International Journal of Chemical Kinetics 25(5), 375-381.

Baker-Austin, C. and Dopson, M. (2007) Life in acid: pH homeostasis in acidophiles. Trends in Microbiology 15(4), 165-171.

Batstone, D.J., Amerlinck, Y., Ekama, G., Goel, R., Grau, P., Johnson, B., Kaya, I., Steyer, J.P., Tait, S., Takács, I., Vanrolleghem, P.A., Brouckaert, C.J. and Volcke, E. (2012) Towards a generalized physicochemical framework. Water Science and Technology 66(6), 1147-1161.

Bekker, M., Kramer, G., Hartog, A.F., Wagner, M.J., de Koster, C.G., Hellingwerf, K.J. and Teixeira de Mattos, M.J. (2007) Changes in the redox state and composition of the quinone pool of *Escherichia coli* during aerobic batch-culture growth. Microbiology 153(6), 1974-1980.

Blackburne, R., Vadivelu, V.M., Yuan, Z. and Keller, J. (2007) Kinetic characterisation of an enriched *Nitrospira* culture with comparison to *Nitrobacter*. Water Research 41(14), 3033-3042.

Bonvin, C., Etter, B., Udert, K.M., Frossard, E., Nanzer, S., Tamburini, F. and Oberson, A. (2015) Plant uptake of phosphorus and nitrogen recycled from synthetic source-separated urine. AMBIO 44(2), 217-227.

Clarke, K.R. and Ainsworth, M. (1993) A method of linking multivariate community structure to environmental variables. Marine Ecology-progress Series 92, 205-219.

Claros, J., Jiménez, E., Aguado, D., Ferrer, J., Seco, A. and Serralta, J. (2013) Effect of pH and HNO_2 concentration on the activity of ammonia-oxidizing bacteria in a partial nitritation reactor. Water Science and Technology 67(11), 2587-2594.

Council Regulation (EEC) (1991) No 2092/91 on organic production of agricultural products and indications referring thereto on agricultural products and foodstuffs.

Daims, H., Lücker, S., Le Paslier, D. and Wagner, M. (2011) Diversity, environmental genomics, and ecophysiology of nitrite-oxidizing bacteria. In: Ward, B.B., Arp, D.J. and Klotz, M.G. (eds) Nitrification, ASM Press, Washington, DC.

De Boer, W. and Kowalchuk, G.A. (2001) Nitrification in acid soils: micro-organisms and mechanisms. Soil Biology and Biochemistry 33(7-8), 853-866.

DeSantis, T.Z., Hugenholtz, P., Larsen, N., Rojas, M., Brodie, E.L., Keller, K., Huber, T., Dalevi, D., Hu, P. and Andersen, G.L. (2006) Greengenes, a Chimera-Checked 16S rRNA Gene Database and Workbench Compatible with ARB. Applied and environmental microbiology 72(7), 5069-5072.

Eggimann, S., Truffer, B. and Maurer, M. (2015) To connect or not to connect? Modelling the optimal degree of centralisation for wastewater infrastructures. Water Research 84, 218-231.

Etter, B., Tilley, E., Khadka, R. and Udert, K.M. (2011) Low-cost struvite production using source-separated urine in Nepal. Water Research 45(2), 852-862.

Etter, B., Hug, A. and Udert, K.M. (2013) Total Nutrient Recovery from Urine – Operation of a Pilot-Scale Nitrification Reactor, WEF/IWA Conference on Nutrient Removal and Recovery Vancouver, Canada.

Ferguson, S.J., Richardson, D.J. and van Spanning, R.J.M. (2007) Chapter 14 - Biochemistry and Molecular Biology of Nitrification. In: Hermann, B., Ferguson, S.J. and William, E.N. (eds) Biology of the Nitrogen Cycle, pp. 209-222, Elsevier, Amsterdam.

Fierer, N. and Jackson, R.B. (2006) The diversity and biogeography of soil bacterial communities. Proceedings of the National Academy of Sciences of the United States of America 103(3), 626-631.

Francis, C.A., Roberts, K.J., Beman, J.M., Santoro, A.E. and Oakley, B.B. (2005) Ubiquity and diversity of ammonia-oxidizing archaea in water columns and sediments of the ocean. Proceedings of the National Academy of Sciences of the United States of America 102(41), 14683-14688.

Fumasoli, A., Morgenroth, E. and Udert, K.M. (2015) Modeling the low pH limit of *Nitrosomonas eutropha* in high-strength nitrogen wastewaters. Water Research 83, 161-170.

Fumasoli, A., Etter, B., Sterkele, B., Morgenroth, E. and Udert, K.M. (2016) Operating a pilot-scale nitrification/distillation plant for complete nutrient recovery from urine. Water Science & Technology 73(1), 215-222.

Fumasoli, A., Bürgmann, H., Weissbrodt, D.G., Wells, G.F., Beck, K., Mohn, J., Morgenroth, E. and Udert, K.M. (subm.) The growth of *Nitrosococcus*-related ammonia oxidizing bacteria causes strong acidification in high strength nitrogen wastewater.

Gieseke, A., Tarre, S., Green, M. and de Beer, D. (2006) Nitrification in a biofilm at low pH values: role of in situ microenvironments and acid tolerance. Applied and environmental microbiology 72(6), 4283-4292.

Glover, H.E. (1985) The relationship between inorganic nitrogen oxidation and organic carbon production in batch and chemostat cultures of marine nitrifying bacteria. Archives of Microbiology 142(1), 45-50.

Goosse, P., Steiner, M., Udert, K.M. and Neuenschwander, W. (2009) NoMix-Anlage. Erste Monitoringergebnisse im Forum Chriesbach (NoMix Toilet System. First monitoring results in Forum Chriesbach, in German, English summary). Gas Wasser Abwasser 7, 567-574.

Grätzel, M., Taniguchi, S. and Henglein, A. (1970) Pulsradiolytische Untersuchung der NO-Oxydation und des Gleichgewichts N_2O_3 □ NO + NO_2 in wäßriger Lösung. Berichte der Bunsengesellschaft für physikalische Chemie 74(5), 488-492.

Grau, M.G.P., Rhoton, S.L., Brouckaert, C.J. and Buckley, C.A. (2015) Evaluation of an automated struvite reactor to recover phosphorus from source-separated urine collected at urine diversion toilets in eThekwini. Water SA 41(3), 383-389.

Groeneweg, J., Sellner, B. and Tappe, W. (1994) Ammonia oxidation in *Nitrosomonas* at NH_3 concentrations near k_m: Effects of pH and temperature. Water Research 28(12), 2561-2566.

Guisasola, A., Jubany, I., Baeza, J.A., Carrera, J. and Lafuente, J. (2005) Respirometric estimation of the oxygen affinity constants for biological ammonium and nitrite oxidation. Journal of Chemical Technology & Biotechnology 80(4), 388-396.

Gustafsson, J.P. (2012) Visual MINTEQ version 3.0, Royal Institute of Technology, Stockholm, Sweden, Department of Land and Water Resources Engineering.

Harrison, C., Malati, M. and Smetham, N. (1996) Solvent and deuterium isotope effects on the decomposition of ammonium nitrite solutions. Journal of Solution Chemistry 25(5), 505-514.

Hayatsu, M. (1993) The lowest limit of pH for nitrification in tea soil and isolation of an acidophilic ammonia oxidizing bacterium. Soil Science and Plant Nutrition 39(2), 219-226.

Hellinga, C., Van Loosdrecht, M.C.M. and Heijnen, J.J. (1999) Model based design of a novel process for nitrogen removal from concentrated flows. Mathematical and Computer Modelling of Dynamical Systems 5(4), 351-371.

Hem, L.J., Rusten, B. and Ødegaard, H. (1994) Nitrification in a moving bed biofilm reactor. Water Research 28(6), 1425-1433.

Henze, M., Gujer, W., Mino, T. and van Loosdrecht, M.C.M. (2000) Activated Sludge Models ASM1, ASM2, ASM2D and ASM3, IWA Publishing, London.

Herlemann, D.P.R., Labrenz, M., Jürgens, K., Bertilsson, S., Waniek, J.J. and Andersson, A.F. (2011) Transitions in bacterial communities along the 2000 km salinity gradient of the Baltic Sea. The ISME Journal 5(10), 1571-1579.

Higbie, R. (1935) The rate of absorption of a pure gas into a still liquid during short periods of exposure. Transactions of the American Institution of Chemical Engineers 31, 365-389.

Hug, A. and Udert, K.M. (2013) Struvite precipitation from urine with electrochemical magnesium dosage. Water Research 47(1), 289-299.

Hunik, J.H., Meijer, H.J.G. and Tramper, J. (1992) Kinetics of *Nitrosomonas europaea* at extreme substrate, product and salt concentrations. Applied Microbiology and Biotechnology 37, 802-807.

Hunik, J.H., Meijer, H.J.G. and Tramper, J. (1993) Kinetics of *Nitrobacter agilis* at extreme substrate, product and salt concentrations. Applied Microbiology and Biotechnology 40(2-3), 442-448.

Hunik, J.H., Tramper, J. and Wijffels, R.H. (1994) A strategy to scale up nitrification processes with immobilized cells of *Nitrosomonas europaea* and *Nitrobacter agilis*. Bioprocess Engineering 11(2), 73-82.

Ishii, S.K.L. and Boyer, T.H. (2015) Life cycle comparison of centralized wastewater treatment and urine source separation with struvite precipitation: Focus on urine nutrient management. Water Research 79, 88-103.

Jeschke, C., Falagán, C., Knöller, K., Schultze, M. and Koschorreck, M. (2013) No nitrification in lakes below pH 3. Environmental Science and Technology 47(24), 14018-14023.

Jiang, F., Chen, Y., Mackey, H.R., Chen, G.H. and van Loosdrecht, M.C.M. (2011) Urine nitrification and sewer discharge to realize in-sewer denitrification to simplify sewage treatment in Hong Kong. Water Science & Technology 64(3), 618-626.

Jiang, Q.Q. and Bakken, L.R. (1999) Comparison of *Nitrosospira* strains isolated from terrestrial environments. FEMS Microbiology Ecology 30, 171-186.

Jin, Q. and Bethke, C.M. (2002) Kinetics of Electron Transfer through the Respiratory Chain. Biophysical Journal 83(4), 1797-1808.

Jin, Q. and Bethke, C.M. (2007) The thermodynamics and kinetics of microbial metabolism. American Journal of Science 307(4), 643-677.

Jönsson, H. and Vinnerås, B. (2013) Closing the loop: Recycling nutrients to agriculture. In: Larsen, T.A., Udert, K.M. and Lienert, J. (eds) Source separation and decentralization for wastewater management, IWA Publishing, London.

Jubany, I. (2007) Operation, modeling and automatic control of complete and partial nitrification of highly concentrated ammonium wastewaters, Universitat Autónoma de Barcelona, Bellaterra.

Jubany, I., Lafuente, J., Baeza, J.A. and Carrera, J. (2009) Total and stable washout of nitrite oxidizing bacteria from a nitrifying continuous activated sludge system using automatic control based on Oxygen Uptake Rate measurements. Water Research 43(11), 2761-2772.

Klindworth, A., Pruesse, E., Schweer, T., Peplies, J., Quast, C., Horn, M. and Glöckner, F.O. (2013) Evaluation of general 16S ribosomal RNA gene PCR primers for classical and next-generation sequencing-based diversity studies. Nucleic Acids Research 41(1).

Koops, H.-P. and Pommerening-Röser, A. (2001) Distribution and ecophysiology of the nitrifying bacteria emphasizing cultured species. FEMS Microbiology Ecology 37(1), 1-9.

Koops, H.-P., Purkhold, U., Pommerening-Röser, A., Timmermann, G. and Wagner, M. (2006) The Lithoautotrophic Ammonia-Oxidizing Bacteria. In: Dworkin, M., Falkow, S., Rosenberg, E., Schleifer, K.-H. and Stackebrandt, E. (eds) The Prokaryotes, pp. 778-811, Springer New York.

Koops, H.P., Böttcher, B., Möller, U.C., Pommerening-Röser, A. and Stehr, G. (1990) Description of a new species of *Nitrosococcus*. Archives of Microbiology 154(3), 244-248.

Kumar, S. and Nicholas, D.J.D. (1983) Proton Electrochemical Gradients in Washed Cells of *Nitrosomonas europaea* and *Nitrobacter agilis*. Journal of Bacteriology 154(1), 65-71.

Lan, Y., Wang, Q., Cole, J.R. and Rosen, G.L. (2012) Using the RDP Classifier to Predict Taxonomic Novelty and Reduce the Search Space for Finding Novel Organisms. PLoS ONE 7(3), e32491.

Larsen, T.A. and Gujer, W. (1996) Separate management of anthropogenic nutrient solutions (human urine). Water Science and Technology 34(3–4), 87-94.

Larsen, T.A., Udert, K.M. and Lienert, J. (2013) Source separation and decentralization for wastewater management, IWA Publishing, London.

LeConte, J. (1962) Instructions for the Manufacture of Saltpetre, Published by authority of the executive council under direction of Col. James Chestnut, Jr., chief of Military Department. Charles P. Pelham, State Printer, Columbia, South Carolina.

Lide, D.R. (2009) CRC Handbook of Chemistry and Physics, 89th Edition (Internet Version 2009), CRC Press/Taylor and Francis, Boca Raton, FL.

Lin, S.-J. and Guarente, L. (2003) Nicotinamide adenine dinucleotide, a metabolic regulator of transcription, longevity and disease. Current Opinion in Cell Biology 15(2), 241-246.

Lund, P., Tramonti, A. and De Biase, D. (2014) Coping with low pH: molecular strategies in neutralophilic bacteria. FEMS Microbiology Reviews 38(6), 1091-1125.

Martell, A.E., Smith, R.M. and Motekaitis, R.J. (1997) Critical Selected Stability Constants of Metal Complexes, Version 4.0, NIST standard reference data, Maryland, Gaithersburg.

Mašić, A., Santos, A.T.L., Etter, B., Udert, K.M. and Villez, K. (2015) Estimation of nitrite in source-separated nitrified urine with UV spectrophotometry. Water Research 85, 244-254.

Maurer, M., Schwegler, P. and Larsen, T.A. (2003) Nutrients in urine: energetic aspects of removal and recovery. Water Science and Technology 48(1), 37-46.

Maurer, M., Rothenberger, D. and Larsen, T.A. (2006) Decentralised wastewater treatment technologies from a national perspective: at what cost are they competitive? Water Science and Technology 5(6), 145-154.

McIlroy, S.J., Saunders, A.M., Albertsen, M., Nierychlo, M., McIlroy, B., Hansen, A.A., Karst, S.M., Nielsen, J.L. and Nielsen, P.H. (2015) MiDAS: the field guide to the microbes of activated sludge. Database 27(10).

McKenney, D.J., Lazar, C. and Findlay, W.J. (1990) Kinetics of the Nitrite to Nitric Oxide Reaction in Peat. Soil Science Society of America Journal 54(1), 106-112.

McMurdie, P.J. and Holmes, S. (2013) phyloseq: An R Package for Reproducible Interactive Analysis and Graphics of Microbiome Census Data. PLoS ONE 8(4), e61217.

Medinets, S., Skiba, U., Rennenberg, H. and Butterbach-Bahl, K. (2015) A review of soil NO transformation: Associated processes and possible physiological significance on organisms. Soil Biology and Biochemistry 80(0), 92-117.

Mohn, J., Zeeman, M.J., Werner, R.A., Eugster, W. and Emmenegger, L. (2008) Continuous field measurements of $\delta^{13}C–CO_2$ and trace gases by FTIR spectroscopy. Isotopes in Environmental and Health Studies 44(3), 241-251.

Morgenroth, E. and Wilderer, P.A. (2000) Influence of detachment mechanisms on competition in biofilms. Water Research 34(2), 417-426.

Mortensen, H.D., Jacobsen, T., Koch, A.G. and Arneborg, N. (2008) Intracellular pH Homeostasis Plays a Role in the Tolerance of *Debaryomyces hansenii* and *Candida zeylanoides* to Acidified Nitrite. Applied and environmental microbiology 74(15), 4835-4840.

Moussa, M.S., Sumanasekera, D.U., Ibrahim, S.H., Lubberding, H.J., Hooijmans, C.M., Gijzen, H.J. and van Loosdrecht, M.C.M. (2006) Long term effects of salt on activity, population structure and floc characteristics in enriched bacterial cultures of nitrifiers. Water Research 40(7), 1377-1388.

Nicholls, D.G. and Ferguson, S.J. (1997) Bioenergetics 2, Academic Press Limited, London.

Nicol, G.W., Leininger, S., Schleper, C. and Prosser, J.I. (2008) The influence of soil pH on the diversity, abundance and transcriptional activity of ammonia oxidizing archaea and bacteria. Environmental Microbiology 10(11), 2966-2978.

Nielsen, P.H., Daims, H. and Lemmer, H. (2009) FISH Handbook for Biological Wastewater Treatment: Identification and Quantification of Microorganisms in Activated Sludge and Biofilms by FISH, New York.

Nowka, B., Daims, H. and Spieck, E. (2015) Comparison of oxidation kinetics of nitrite-oxidizing bacteria: nitrite availability as a key factor in niche differentiation. Applied Environmental Microbiology 81(2), 745-753.

O'Neal, J.A. and Boyer, T.H. (2013) Phosphate recovery using hybrid anion exchange: Applications to source-separated urine and combined wastewater streams. Water Research 47(14), 5003-5017.

Oezel Duygan, B.D., Udert, K.M., Remmele, A. and McArdell, C.S. (in prep.) Fate of pharmaceuticals in source-separated urine during storage, biological treatment and powdered activated carbon adsorption.

Oksanen, J., Blanchet, F.G., Kindt, R., Legendre, P., Minchin, P.R., O'Hara, R.B., Simpson, G.L., Solymos, P., Henry, M., Stevens, H. and Wagner, H. (2015) vegan: Community Ecology Package. R package version 2.2-1. http://CRAN.R-project.org/package=vegan.

Oosterhuis, M. and van Loosdrecht, M.C.M. (2009) Nitrification of urine for H_2S control in pressure sewers. Water Practice & Technology 4(3).

Painter, H.A. and Loveless, J.E. (1983) Effect of temperature and pH value on the growth-rate constants of nitrifying bacteria in the activated-sludge process. Water Research 17(3), 237-248.

Painter, H.A. (1986) Nitrification in the treatment of sewage and waste-waters. In: Prosser, J.I. (ed) Nitrification, pp. 185-211, IRL Press, Oxford.

Pambrun, V., Paul, E. and Spérandio, M. (2006) Modeling the partial nitrification in sequencing batch reactor for biomass adapted to high ammonia concentrations. Biotechnology and Bioengineering 95(1), 120-131.

Park, J.Y. and Lee, Y.N. (1988) Solubility and decomposition kinetics of nitrous acid in aqueous solution. The Journal of Physical Chemistry 92(22), 6294-6302.

Parkhurst, D.L. and Appelo, C.A.J. (1999) User's Guide to PHREEQC (Version 2) - a computer program for speciation, batch-reaction, one-dimensional transport, and inverse geochemical calculations, Water-Resources Investigations Report 99-4259, US Geological Survey, Denver CO, USA.

Poughon, L., Dussap, C.-G. and Gros, J.-B. (2001) Energy model and metabolic flux analysis for autrotrophic nitrifiers. Biotechnology and Bioengineering 72(4), 416-433.

Prakasam, T.B.S. and Loehr, R.C. (1972) Microbial nitrification and denitrification in concentrated wastes. Water Research 6(7), 859-869.

Presser, K.A., Ratkowsky, D.A. and Ross, T. (1997) Modelling the growth rate of *Escherichia coli* as a function of pH and lactic acid concentration. Applied and environmental microbiology 63(6), 2355-2360.

Purkhold, U., Pommerening-Röser, A., Juretschko, S., Schmid, M.C., Koops, H.-P. and Wagner, M. (2000) Phylogeny of all recognized species of ammonia oxidizers based on comparative 16S rRNA and amoA sequence analysis: Implications for molecular diversity surveys. Applied and environmental microbiology 66(12), 5368-5382.

Quast, C., Pruesse, E., Yilmaz, P., Gerken, J., Schweer, T., Yarza, P., Peplies, J. and Glockner, F.O. (2013) The SILVA ribosomal RNA gene database project: improved data processing and web-based tools. Nucleic Acids Research 41(28).

Ratkowsky, D.A. (2002) Some examples of, and some problems with, the use of nonlinear logistic regression in predictive food microbiology. International Journal of Food Microbiology 73(2-3), 119-125.

Reichert, P. (1994) Aquasim - a tool for simulation and data-analysis of aquatic systems. Water Science and Technology 30(2), 21-30.

Ronteltap, M., Maurer, M. and Gujer, W. (2007) The behaviour of pharmaceuticals and heavy metals during struvite precipitation in urine. Water Research 41(9), 1859-1868.

Rusten, B., Eikebrokk, B., Ulgenes, Y. and Lygren, E. (2006) Design and operations of the Kaldnes moving bed biofilm reactors. Aquacultural Engineering 34(3), 322-331.

Sanchez, P.A. (2002) Soil Fertility and Hunger in Africa. Science 295(5562), 2019-2020.

Schielke, S. (2015) Decentralised urine treatment with the nitritation/anammox process. Ph.D thesis, Swiss Federal Institute of Technology Zurich, Switzerland.

Scholz, R.W., Roy, A.H., Brand, F.S., Hellums, D.T. and Ulrich, A.E. (2014) Sustainable Phosphorus Management. A Global Transdisciplinary Roadmap, Springer, Dordrecht.

Schwartz, S.E. and White, W.H. (1981) Solubility equilibria of the nitrogen oxides and oxyacids in dilute aqueous solution. Advances in Enviornmental Science and Engineering 4.

Schwartz, S.E. and White, W.H. (1983) Kinetics of reactive dissolution of nitrogen oxides into aqueous solution. Advances in Environiromental Science and Technology 12(1).

Shimadzu Corporation (2010) Shimadzu TOC-L CSH/CSN User's Manual, Analytical & Measuring Instruments Division, Kyoto, Japan.

Slonczewski, J.L., Fujisawa, M., Dopson, M. and Krulwich, T.A. (2009) Cytoplasmic pH measurement and homeostasis in bacteria and archaea. Advances in Microbial Physiology 55, 1-317.

Spieck, E. and Bock, E. (2005) The Lithoautotrophic Nitrite-Oxidizing Bacteria. In: Brenner, D.J., Krieg, N.R., Staley, J.T. and Garrity, G.M. (eds) Bergey's Manual® of Systematic Bacteriology, pp. 149-153, Springer US.

Starkenburg, S.R., Larimer, F.W., Stein, L.Y., Klotz, M.G., Chain, P.S., Sayavedra-Soto, L.A., Poret-Peterson, A.T., Gentry, M.E., Arp, D.J., Ward, B. and Bottomley, P.J. (2008) Complete genome sequence of *Nitrobacter hamburgensis* X14 and comparative genomic analysis of species within the genus *Nitrobacter*. Applied Environmental Microbiology 74(9), 2852-2863.

Stumm, W. and Morgan, J.J. (1996) Aquatic Chemistry: Chemical Equilibria and Rates in Natural Waters, John Wiley & Sons Inc., New York.

Sun, F.Y., Dong, W.Y., Shao, M.F., Li, J. and Peng, L.Y. (2012) Stabilization of source-separated urine by biological nitrification process: treatment performance and nitrite accumulation. Water Science and Technology 66(7), 1491-1497.

Sun, Y., Wolcott, R. and Dowd, S. (2011) Tag-Encoded FLX Amplicon Pyrosequencing for the Elucidation of Microbial and Functional Gene Diversity in Any Environment. In: Kwon, Y.M. and Ricke, S.C. (eds) High-Throughput Next Generation Sequencing, pp. 129-141, Humana Press.

Suzuki, I., Dular, U. and Kwok, S.C. (1974) Ammonia or ammonium ion as substrate for oxidation by *Nitrosomonas europaea* cells and extracts. Journal of Bacteriology 120(1), 556-558.

Suzuki, I., Lee, D., Mackay, B., Harahuc, L. and Oh, J.K. (1999) Effect of Various Ions, pH, and Osmotic Pressure on Oxidation of Elemental Sulfur by *Thiobacillus thiooxidans*. Applied and environmental microbiology 65(11), 5163-5168.

Takai, K. and Horikoshi, K. (2000) Rapid Detection and Quantification of Members of the Archaeal Community by Quantitative PCR Using Fluorogenic Probes. Applied and environmental microbiology 66(11), 5066-5072.

Tamura, K., Stecher, G., Peterson, D., Filipski, A. and Kumar, S. (2013) MEGA6: Molecular Evolutionary Genetics Analysis version 6.0. Molecular Biology and Evolution 30, 2725-2729.

Tarre, S., Beliavski, M., Denekamp, N., Gieseke, A., de Beer, D. and Green, M. (2004) High nitrification rate at low pH in a fluidized bed reactor with chalk as the biofilm carrier. Water Science and Technology 49(11-12), 99-105.

Tarre, S. and Green, M. (2004) High-rate nitrification at low pH in suspended- and attached-biomass reactors. Applied and environmental microbiology 70(11), 6481-6487.

Tarre, S., Shlafman, E., Beliavski, M. and Green, M. (2007) Changes in ammonia oxidiser population during transition to low pH in a biofilm reactor starting with *Nitrosomonas europaea*. Water Science and Technology 55(8-9), 363-368.

Tchobanoglous, G., Burton, F.L., Stensel, H.D., Metcalf and Eddy (2003) Wastewater engineering : treatment and reuse, McGraw-Hill, Boston.

Tettenborn, F., Behrendt, J. and Otterpohl, R. (2007) Resource recovery and removal of pharmaceutical residues. Treatment of separate collected urine, Institute of Wastewater Management and Water Protection, Hamburg University of Technology, Hamburg.

The World Bank (2015) World DataBank, World Development Indicators. http://databank.worldbank.org (accessed on 1 April 2015).

Troccaz, M., Niclass, Y., Anziani, P. and Starkenmann, C. (2013) The influence of thermal reaction and microbial transformation on the odour of human urine. Flavour and Fragrance Journal 28(4), 200-211.

UCPTE (1994) Yearly Report 1993, Union pour la coordination de la production et du transport de l'électricité, Vienna, Austria.

Udert, K.M., Fux, C., Münster, M., Larsen, T.A., Siegrist, H. and Gujer, W. (2003a) Nitrification and autotrophic denitrification of source-separated urine. Water Science and Technology 48(1), 119-130.

Udert, K.M., Larsen, T.A., Biebow, M. and Gujer, W. (2003b) Urea hydrolysis and precipitation dynamics in a urine-collecting system. Water Research 37(11), 2571-2582.

Udert, K.M., Larsen, T.A. and Gujer, W. (2003c) Estimating the precipitation potential in urine-collecting systems. Water Research 37(11), 2667-2677.

Udert, K.M., Larsen, T.A. and Gujer, W. (2005) Chemical nitrite oxidation in acid solutions as a consequence of microbial ammonium oxidation. Environmental Science and Technology 39(11), 4066-4075.

Udert, K.M., Larsen, T.A. and Gujer, W. (2006) Fate of major compounds in sourceseparated urine. Water Science and Technology: Water Supply 54(11-12), 413-420.

Udert, K.M. and Wächter, M. (2012) Complete nutrient recovery from source-separated urine by nitrification and distillation. Water Research 46(2), 453-464.

Udert, K.M., Buckley, C.A., Wächter, M., McArdell, C.S., Kohn, T., Strande, L., Zöllig, H., Fumasoli, A., Oberson, A. and Etter, B. (2015) Technologies for the treatment of source-separated urine in the eThekwini Municipality. Water SA 41, 212-221.

Uhlmann, C. (2014) Complete nitrification of urine, MSc thesis, ETH Zürich: Swiss Federal Institute of Technology, Zürich, Switzerland.

United Nations (2014) The Millennium Development Goals Report 2014, United Nations, New York.

United Nations Development Programme (2006) Human Development Report. Beyond scarcity: Power, poverty and the global water crisis, New York, USA.

Van Cleemput, O. and Baert, L. (1984) Nitrite: a key compound in N loss processes under acid conditions? Plant and Soil 76(1-3), 233-241.

Van Hulle, S.W.H., Volcke, E.I.P., Teruel, J.L., Donckels, B., Van Loosdrecht, M.C.M. and Vanrolleghem, P.A. (2007) Influence of temperature and pH on the kinetics of the Sharon nitritation process. Journal of Chemical Technology and Biotechnology 82, 471-480.

van Vooren, L. (2000) Buffer capacity based multipurpose hard- and software sensor for environmental applications, Universiteit Gent.

Vandal, O.H., Nathan, C.F. and Ehrt, S. (2009) Acid Resistance in *Mycobacterium tuberculosis*. Journal of Bacteriology 191(15), 4714-4721.

Vieillard, P. and Tardy, Y. (1984) Thermodynamic Properties of Phosphates. In: Nriagu, J.O. and Moore, P.B. (eds) Phosphate Minerals, Springer, Berlin.

Volcke, E.I., Loccufier, M., Noldus, E.J. and Vanrolleghem, P.A. (2007a) Operation of a SHARON nitritation reactor: practical implications from a theoretical study. Water Science & Technology 56(6), 145-154.

Volcke, E.I., Sbarciog, M., Loccufier, M., Vanrolleghem, P.A. and Noldus, E.J. (2007b) Influence of microbial growth kinetics on steady state multiplicity and stability of a two-step nitrification (SHARON) model. Biotechnology and Bioengineering 98(4), 882-893.

Wächter, M., Schwaninger, M., Gmeinwieser, T. and Udert, K.M. (In prep.) Safety assessment for production and storage of nitrified and concentrated fertilizer from human urine. in prep. for Water Research.

Wang, Q., Garrity, G.M., Tiedje, J.M. and Cole, J.R. (2007) Naïve Bayesian Classifier for Rapid Assignment of rRNA Sequences into the New Bacterial Taxonomy. Applied and environmental microbiology 73(16), 5261-5267.

Wang, Q., Ye, L., Jiang, G. and Yuan, Z. (2013) A free nitrous acid (FNA)-based technology for reducing sludge production. Water Research 47(11), 3663-3672.

Ward, B.B. (1987) Kinetic studies on ammonia and methane oxidation by *Nitrosococcus oceanus*. Archives of Microbiology 147(2), 126-133.

Ward, B.B. and O'Mullan, G.D. (2002) Worldwide distribution of *Nitrosococcus oceani*, a marine ammonia-oxidizing gamma-proteobacterium, detected by PCR and sequencing of 16S rRNA and amoA genes. Applied and environmental microbiology 68(8), 4153-4157.

Weissbrodt, D.G., Shani, N., Sinclair, L., Lefebvre, G., Rossi, P., Maillard, J., Rougemont, J. and Holliger, C. (2012) PyroTRF-ID: a novel bioinformatics methodology for the affiliation of terminal-restriction fragments using 16S rRNA gene pyrosequencing data. Bmc Microbiology 12.

Weissbrodt, D.G., Schneiter, G.S., Fürbringer, J.-M. and Holliger, C. (2013) Identification of trigger factors selecting for polyphosphate- and glycogen-accumulating organisms in aerobic granular sludge sequencing batch reactors. Water Research 47(19), 7006-7018.

Weissbrodt, D.G., Shani, N. and Holliger, C. (2014) Linking bacterial population dynamics and nutrient removal in the granular sludge biofilm ecosystem engineered for wastewater treatment. FEMS Microbiology Ecology 88(3), 579-595.

Weissbrodt, D.G., Wells, G.F., Goel, R.K., Laureni, M., Bürgmann, H., Johnson, D.R., Men, Y., Fischer, S., Minder, A., Aluri, S., Harhangi, H.R., Kipf, M., Joss, A., Christensson, M., Nielsen, J.L. and Morgenroth, E. (2015) A process engineering vista in the ecogenomics of aerobic-anaerobic ammonium oxidation, Proceedings of the IWA Nutrient Removal and Recovery 2015: Moving Innovation into Practice, Gdansk, Poland.

Wells, G.F., Park, H.-D., Yeung, C.-H., Eggleston, B., Francis, C.A. and Criddle, C.S. (2009) Ammonia-oxidizing communities in a highly aerated full-scale activated sludge bioreactor: betaproteobacterial dynamics and low relative abundance of Crenarchaea. Environmental Microbiology 11(9), 2310-2328.

Westergreen, S., Brouckaert, C.J. and Foxon, K.M. (2012) Modelling of ionic interactions with wastewater treatment biomass. Water Science and Technology 65(6), 1014-1020.

Wett, B. and Rauch, W. (2003) The role of inorganic carbon limitation in biological nitrogen removal of extremely ammonia concentrated wastewater. Water Research 37(5), 1100-1110.

Wiesmann, U. (1994) Biological nitrogen removal from wastewater. Biotechnics/Wastewater, pp. 113-154, Springer Berlin Heidelberg.

Wiesmann, U., Choi, I.S. and Dombrowski, E.-M. (2006) Biological Nutrient Removal. Fundamentals of Biological Wastewater Treatment, pp. 223-265, Wiley-VCH Verlag GmbH & Co. KGaA.

Wrage, N., Velthof, G.L., van Beusichem, M.L. and Oenema, O. (2001) Role of nitrifier denitrification in the production of nitrous oxide. Soil Biology and Biochemistry 33(12–13), 1723-1732.

Zacharia, I.G. and Deen, W.M. (2005) Diffusivity and Solubility of Nitric Oxide in Water and Saline. Annals of Biomedical Engineering 33(2), 214-222.

Zhang, L.-M., Hu, H.-W., Shen, J.-P. and He, J.-Z. (2012) Ammonia-oxidizing archaea have more important role than ammonia-oxidizing bacteria in ammonia oxidation of strongly acidic soils. ISME Journal 6(5), 1032-1045.

Zhang, Q., Piston, D.W. and Goodman, R.H. (2002) Regulation of Corepressor Function by Nuclear NADH. Science 295(5561), 1895-1897.

Zhou, Y., Oehmen, A., Lim, M., Vadivelu, V. and Ng, W.J. (2011) The role of nitrite and free nitrous acid (FNA) in wastewater treatment plants. Water Research 45(15), 4672-4682.

Zumft, W.G. (1993) The biological role of nitric oxide in bacteria. Archives of Microbiology 160(4), 253-264.